UNIVERSITY OF LIVERPOOL

Molecular Insights into Pharmaceutical Amorphous Solid Dispersions from Solid State Nuclear Magnetic Resonance Spectroscopy

Thesis submitted in accordance with the requirements of the University of Liverpool for the degree of Doctor in Philosophy

by

Andrea Pugliese

Department of Chemistry

July 2022

Table of the Contents

Molecular Insights into Pharmaceutical Amorphous Solid Dispersions from Solid State Nuclear Magnetic Resonance Spectroscopy

Andrea Pugliese

Abstract

Crystalline active pharmaceutical ingredients (APIs) or drugs exhibit low solubility, hence low bioavailability. This represents one of the major issues that pharmaceutical companies have to deal with during the development process of new medicaments. However, thermodynamically unstable amorphous APIs show high solubility and bioavailability. A promising strategy to make bioavailable APIs, is the amorphous solid dispersions (ASDs) technology, in which a crystalline API is converted in its amorphous counterpart and dispersed into a polymer. The polymer effectively stabilises the ASD through the anti-plasticiser effect and by the formation of specific drug-polymer interactions. The understanding of these interactions and the monitoring of the API-polymer miscibility represent an exciting field of research in which solid-state NMR (NMR) is a unique method of investigation providing information at atomic level. In this thesis NMR techniques have been employed for the characterisation of a widely used polymer (HPMC-AS) in ASDs and to spot API-polymer interactions in acetaminophen-HPMC-AS solid dispersions. Finally, a recent developed method based on the time domain (TD) NMMR relaxometry measurements have been tested for the quantification of amorphous/crystalline species ratio in amorphous or crystalline API and amorphous polymer mixtures.

Thesis Overview

Chapter 1 provides a concise introduction to the basic concept around the amorphous solid dispersion technology and to the fundamental ideas of NMR and solid-state NMR. Moreover, the NMR experiments used throughout this thesis are described.

Chapter 2 comprises of a manuscript which has recently been sent for publication entitled “New Development in Understanding Drug-Polymer Interactions in Pharmaceutical Amorphous Solid Dispersions from Solid-State Nuclear Magnetic Resonance”. This section exploits the most advanced and recent approaches and NMR methods to identify API-polymer interactions in solidi dispersions.

Chapter 3 is based on the paper entitled “Solid State Nuclear Magnetic Resonance Studies of HydroxyPropylMethylCellulose Acetyl Succinate polymer, a Useful Carrier in Pharmaceutical Solid Dispersions”, in which the comprehensive understanding of the chemical structure and a definitive spectral assignment of the ^{13}C NMR spectra of this polymer are reported.

Chapter 4 consists of the published manuscript entitled “Drug−Polymer Interactions in Acetaminophen/Hydroxypropylmethylcellulose Acetyl Succinate Amorphous Solid Dispersions Revealed by Multidimensional Multinuclear Solid-State NMR Spectroscopy”. Here is demonstrated as one- and two-dimensional experiments (e.g., HETCOR and HMQC) can be employed to highlight the stabilising molecular interactions in pharmaceutical amorphous dispersions.

Chapter 5 is focused on the use of a recently developed TD NMR based method allowing the quantification of the amorphous/crystalline species ratio in amorphous or crystalline API and amorphous polymer mixtures.

Note: Chapters which have been based on publication have been amended to include the supporting information into the main text, when available.

Acknowledgements

Completing a PhD is a long and tiring process, and despite all efforts one can put in, it wouldn't be possible if there weren't amazing people around to help and support you.

Firstly, I would like to express my gratitude to my primary supervisor, prof. Frédéric Blanc, for guided me throughout this project over the last 5 years. Thanks for your time, being patient and extremely enlightening. Thanks for your suggestions and advice.

It is also my duty to thank Dr Lucy E. Hawarden and Dr Mike Tobyn my co-supervisors from Bristol-Myers Squibb (BMS) for their continue support, encouragement, assistance and for introducing me to the exciting world of amorphous solid dispersions. Also thank for the great time spent during my placement at Moreton (UK).

I can not fail to mention Dr Anuji Abraham and Dr Daniel McNamara. They made my visit at the BMS laboratories in New Brunswick (New Jersey, US) an amazing opportunity to hugely improve my knowledge of the pharmaceutical dispersions.

I would like to acknowledge the University of Liverpool and the Engineering and Physical Sciences Research Council (EPSRC) for a Doctoral Training Studentship, as well as the BMS to have founded my doctorate and the EPSRC NPIF Innovation Placement scheme for founding my placement. The 800 MHz spectrometer at the University of Liverpool used in this research was funded by EPRSEC. The UK 850 MHz solid-state NMR Facility used in this research was funded by the EPSRC and Biotechnology and Biological Sciences Research Council (BBSRC), as well as the University of Warwick including via part funding through the Birmingham Science

City Advanced Materials Project 1 and 2 supported by Advantage West Midlands (AWM) and the European Regional Development Fund (ERDF).

The 850 MHz facility manger, Dr Dinu Iuga is also a acknowledge for his precious assistance and help.

I would like also to thank the numerous people who I have meet and helped me in over the last years at the chemistry department.

Thank to Dr Konstantin Luzyanin, friend and esteemed colleague, for the time spent together discussing about of science, politics, philosophy, and all the coffee breaks.

Thanks to all the people from the solid-state NMR laboratory I have spent more time and shared experience with: Dr Ashlea Hughes, Dr Stuart J. Elliott, Aine Black Lucia Corti and Ben Duff. To this list I have also to include Dr George Schenck, from the liquid-state NMR group. Thanks to you all for being around at any time for help, support, and advise me. My stay in Liverpool was more pleasant thanks to you.

I want also thanks to my parent Francesca and Michel Jean, and my brother Gian Luca. Thank you for always giving me the opportunity to follow my ambitions. Thank for being a constant daily presence during my stay in Liverpool and thank you for always supporting and advising me especially during the most difficult moments. What I am I owe it to you.

Awards, Presentation and Publications

Awards

2020 EPSRC NPIF Innovation Placement Award – Placement at Moreton (UK) and New Brunswick (US) Bristol-Myers Squibb facilities.

2019 Runner-up prize for poster presentation at RSC Annual NMR Discussion Group Postgraduate Meeting.

Presentation

2021 Poster/short talk presentation at RSC Annual NMR Discussion Group Postgraduate Meeting.

2021 Oral presentation at the UK 850 MHz solid-state NMR facility annual symposium.

2021 Poster/short talk presentation at the Experimental Nuclear Magnetic Resonance (ENC) Conference.

2021 Oral presentation at the University of Liverpool PGR Symposium 2021.

2021 Oral presentation at the FORGE: Characterisation of Pharmaceutical Formulations.

2020 Poster presentation at the University of Liverpool PGR Symposium 2020.

2019 Poster presentation at RSC Annual NMR Discussion Group Postgraduate Meeting (*runner-up best poster prize*).

2019 Poster presentation at the Faculty Poster Day – University of Liverpool.

Publications

"Solid-state nuclear magnetic resonance studies of hydroxypropylmethylcellulose acetyl succinate polymer, a useful carrier in pharmaceutical solid dispersions". **Andrea Pugliese**, Lucy E Hawarden, Anuji Abraham, Michael Tobyn, and Frédéric Blanc, *Magn. Reson. Chem.* **2020**, *58,* 1036- 1048 (**Chapter 3** of this thesis).

"Drug–Polymer Interactions in Acetaminophen/Hydroxypropylmethylcellulose Acetyl Succinate Amorphous Solid Dispersions Revealed by Multidimensional Multinuclear Solid-State NMR Spectroscopy". **Andrea Pugliese**, Michael Toresco, Daniel McNamara, Dinu Iuga, Anuji Abraham, Michael Tobyn, Lucy E. Hawarden, and Frédéric Blanc, *Mol. Pharmaceutics*, **2021**, *18*, 3519–3531 (**Chapter 4** of this thesis).

"Li^+ Dynamics of Liquid Electrolytes Nanoconfined in Metal–Organic Frameworks". Marco Farina, Benjamin B. Duff, Cristina Tealdi, **Andrea Pugliese**, Frédéric Blanc, and Eliana Quartarone, *ACS Appl. Mater. Interfaces* **2021**, *13*, 53986–53995.

"Melting of hybrid organic–inorganic perovskites". Bikash Kumar Shaw, Ashlea R. Hughes, Maxime Ducamp, Stephen Moss, Anup Debnath, Adam F. Sapnik, Michael F. Thorne, Lauren N. McHugh, **Andrea Pugliese**, Dean S. Keeble, Philip

Chater, Juan M. Bermudez-Garcia, Xavier Moya, Shyamal K. Saha, David A. Keen, François-Xavier Coudert, Frédéric Blanc & Thomas D. Bennett, *Nature Chemistry* **2021**, *13*, 778–785.

List of Abbreviations

1D	One-dimensional
2D	Two-dimensional
3D	Three-dimensional
A	Acetyl
API	Active pharmaceutical ingredient
ASD	Amorphous solid dispersion
B_0	Static magnetic field
BABA	Back-to-back
BCS	Biopharmaceutical classificiation
CBZ	Carbamazepine
CLF	Clofazimine
CNT	Classic nucleation theory
CP	Cross polarisation
CPPI	Cross polarisation phase inversion
CSA	Chemical shift anisotropy
δ	Chemical shift
ΔG	Gibbs free energy
DNP	Dynamic nuclear polarisation
DQ	Double quantum
DS	Degree of substitution
DSC	Differentail scanning calorimetry
EE	Methylacrylate copolymer Eudragit ® E
FEL	Felodipine
FID	Free induction signal/decay
FT	Fourier transformation

FT-IR	Fourier-transformation infrared
FWHM	Full width at half maximum
GB	Gefitinib
GI	Gastrointestinal
GT	Gordon Taylor's model
H-bond	Hydrogen bond
HETCOR	Heteronuclear correlation
HME	Hot melt extrusions
HMQC	Heteronuclear multiple quantum coherence
HPMC	Hydroxypropylmethylcellulose
HPMC-AS	Hydroxypropylmethylcellulose acetyl succinate
HPMC-P	Hydroxypropylmethylcellulose phthalate
IBU	Ibuprofen
IMC	Indomethacin
ITR	Itraconazole
KTZ	Ketaconazole
LB	Lapatinib
M	Methyl
m.p.	melting point
M_0	Bulk magnetisation
MAS	Magic angle spinning
NCE	New chemical entitie
NIF	Nifedipine
NMR	Nuclear magnetic resonance
P	Hydroxylpropyl
PAA	poly(acrylic acid)

PEG	poly(ethylen glycol)
PEO	poly(ethylene oxide)
PHEMA	poly(2-hydroxyethylmethacrylate)
PHPA	α,β-poly(*N*-5-hydroxylpentyl)-L-aspartamide
POSA	Posaconazole
ppm	parts per milion
PSSA	polystyrene sulfonic acid
PVAc	poly(vinyl acetate)
PVP	poly(vinyl pyrrolidone)
PVP-VA	poly(vinyl pyrrolidone)-co-vynlacetate
PXRD	Powder X-Ray diffraction
qSRC	Quantitative saturation recovery curve
r*	Critical crystal nuclation size
RAF	Rafoxamide
rf	radio frequency
RFDR	radio frequency driven recoupling
RH	Relative humidity
RT	Room temperature
Rutin-G	α-glycosyl rutin
S	Succinoyl
SCL	Supercooled liquid
SD	Spray dry
SRC	Saturation recovery curve
T_1	Spin-lattice relaxation time
$T_{1\rho}$	Spin-lattice relaxation time in the rotating frame
T_2	Spin-spin relaxation time

TD	Time domain
Tg	Glass transition temperature
TK	Kauzmann temperature
Tm	melting point temperature
UV	Ultraviolet

Chapter 1: Introduction to Amorphous Solid Dispersions and Nuclear Magnetic Resonance Spectroscopy

1.1 Overview

This introductory chapter consists of two sections. The first one is a concise introduction to the fundamental concepts to understand the needs of pharmaceutical amorphous solid dispersions (ASD), along with some general essential insight of drug delivery. The second section is a brief overview to general ideas behind nuclear magnetic resonance (NMR), with particular emphasis on the nuclear spin interactions that govern solid state NMR experiments. Some general NMR techniques and pulse sequences which were applied to study the material investigated throughout the results chapters of this thesis are described.

1.2 Introduction to amorphous solid dispersions

1.2.1 Drug solubility

Pharmaceutical companies screen thousands of new chemical entities (NCEs) every year in the hope to find cures for diseases. Relatively few of these reach the market.

Due to the nature of the targets being investigated for treatment and the mechanisms for discovering NCE's an increasing proportion of these molecules show poor aqueous solubility. Main reasons for the poor aqueous solubility includes:

1. The complexity of the molecules being developed now. Developments in chemistry and the need to access novel molecules outside the known intellectual property space mean that molecules now often have a higher molecular weight and/or a complex structure with, for instance, fused heterocyclic rings. These molecules more frequently break the "Rules of 5"[1,2], to indicate how "developable" a drug will be. These larger molecules have lower aqueous solubility, and the large number of hydrogen bonding sites makes them challenging to develop.
2. The targets themselves are evolving. Many previous molecules were targeted at receptors in the blood or other body cavity accessible by the blood. Many of these targets were receptors for endogenous amines and were often amines themselves. Many of these amine drugs could form salts to increase their solubility. Many current targets for drugs are located intracellularly and/or in less accessible body cavities (e.g., the brain or central nervous system). Such drugs often have to be uncharged to reach

their targets. The absence of charged groups in the molecule means that they are not candidates for salt formation, and thus have no help in forming water soluble species. When combined with point 1 it means that larger, more lipophilic drugs are now in development.

Indeed, drugs or active pharmaceutical ingredients (APIs) with poor aqueous solubility represent a major challenge to pharmaceutical scientists because they exhibit low oral bioavailability. It has been estimated that up to the 70% of the compound in the pipeline have poor aqueous solubility as synthesised in their crystalline form.[3] While poor aqueous solubility is a challenge in drug development, both the pharmaceutical Industry and academia have come up with many novel ways to deal with the challenge. These face some of the challenges of development, at a cost of increased complexity of development.

For an orally administered drug to have a therapeutic effect, the drug molecules must be dissolved in the gastrointestinal (GI) fluids, pass through GI membrane to the circulatory system, and reach the target in sufficient quantity. That is, drug molecules must be soluble enough in the aqueous-based GI fluids to have any therapeutic effect. If the solubility of the drug in GI fluids is not enough, the bioavailability will be compromised as the absorption will be “solubility limited.”

In 1995, the biopharmaceutical classification system (BCS)[4-6] was introduced to facilitate drug development, classifying drug molecules according the to their solubility and permeability (**Figure 1.1**).

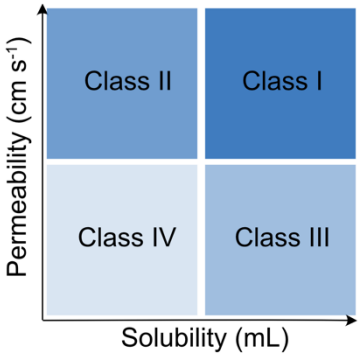

Figure 1.1. Biopharmaceutical classification system (BSC). Drugs are classified in four different classes as function of their ability to permeate the biological membrane and water solubility.

The BCS system was initially developed to identify those drugs for which it would be more difficult to develop generic versions of patented drugs. For those molecules with high solubility and high permeability (BCS I) this job would be relatively easy, as the drug is readily soluble and absorbed quickly. For BCS II, in which drugs show low solubility but exhibit high absorption, a dosage form that can match the dissolution characteristics should be equivalent. For BCS III, compounds are characterised by high solubility and low absorption. In these cases, the rate limiting step is not defined by the dosage form. Finally, BCS class IV agents, which are limited by both solubility and absorption, matching any performance of an available dosage form represents a huge challenge. These designations are now used for new drugs as well as existing ones as they provide a convenient way for assessing the difficulties in developing an effective dosage form.

One way to enhance the oral bioavailability is to increase the concentration of the dissolved drug in the GI fluids. This can be achieved by increasing the dissolution rate, increasing the drug solubility, or the combination of both. In practice the solubility of the molecule depends by the properties of the molecule in its crystalline form. The solubility is set by the equilibrium between the crystal form and the drug

in solution. The formation of crystalline drug salts represents a simple way to enhance the solubility proprieties of a drug. However, this apparent solubility can be lost if the drug salt has the possibility to evolve to a more energetic stable form. This form is likely to have different bioavailability from the metastable form, and thus require all the clinical work to be redone whilst the product is off the market, or delayed from the market. This process can take years.[7,8]

Generally, an amorphous form of a drug exhibits greater dissolution route than a crystalline material of the same drug, although there is a thermodynamic tendency for this system to crystallise in the solid state, and crystallisation from solution in the GI tract (prior to absorption occurring, making it unavailable to the body). Nevertheless, an increasing number of pharmaceuticals are now being formulated as amorphous systems.

1.2.2 Amorphous and crystalline state

An amorphous material can be defined as a disordered non-crystalline solid which lacks the long-range three-dimensional order of the crystalline form.[9-11] However, molecules in amorphous materials have some short-range chemical and topological order with nearest neighbours, but overall demonstrate a more randomly disordered molecular structure with respect the crystalline form. This disorder in crystal lattice introduced as crystal defects can serve to increase dissolution rate from the amorphous materials relative to crystalline material with few crystal defects. An amorphous solid, at the molecular level, has properties similar to a liquid; but at the macroscopic level (bulk viscosity), it has solid-like properties.

By contrast a crystalline solid is defined as a solid showing a high ordered internal structure based on symmetrically arranged plane surfaces, intersecting at definite and characteristic angles. Therefore, crystalline APIs exhibit well organised three-dimensional structures, with repeated unit cells providing long-range order and high physical stability. This high internal lattice energy, as often reflected at high melting point temperature (Tm) can serve as a barrier to reaching appreciable aqueous solubility or dissolution rate.[12,13]

From the thermodynamic perspective, compared to the crystalline form of a drug, the amorphous form is in a state of higher energy. This denotes that the amorphous state has inherent physical and chemical instabilities. Compared to their crystalline counterparts, amorphous materials possess excess thermodynamic properties such as enthalpy, entropy, Gibbs free energy[14,17], and mobility.[18] **Figure 1.2** shows the relationship of the thermodynamic properties and temperature for the amorphous (or glass) and crystalline state. When a melted crystalline material is

cooled rapidly, recrystallisation may be avoided and the slope of the equilibrium liquid curve may be followed below the Tm resulting in a gradual decrease of thermodynamic properties below Tm. This is known as the supercooled liquid (SCL) state, in which viscosity is low and mobility of the molecules is high as is typically expected in a liquid. Upon further cooling, at the glass transition temperature (Tg) the molecules cannot follow the decrease in temperature any longer and the system solidifies or vitrifies, forming a solid glass. This is represented by the change of the slope of the curve in **Figure 1.2(a).** Below the Tg, the solid is in the amorphous state, exhibiting high solid-like viscosity.

If the solid did not vitrify at Tg, the SCL line could be extrapolated (now as an equilibrium glass) and it would intersect the equilibrium crystal line at the Kauzmann temperature (T_K). At T_K, the SCL amorphous system would have comparable entropy and enthalpy as the crystalline state, which is against the laws of thermodynamics. Hence, the occurrence of the Tg has two implications for amorphous systems: glasses are in a non-equilibrium state and the physical-chemical properties of amorphous systems above and below the Tg are different. **Figure 1.2(b)** reports the Gibbs free energy diagrams for the amorphous, supercooled liquid, and crystalline states. While the amorphous and crystalline correspond to a high unstable (high energy) and high stable (low energy) states, respectively, due to its position in a free energy minimum the configuration corresponding to the SCL, can persist over infinitely large time scales.[19] However, the energetical jump from the supercooled liquid state to the crystalline is observed when the temperature of system goes below Tg.

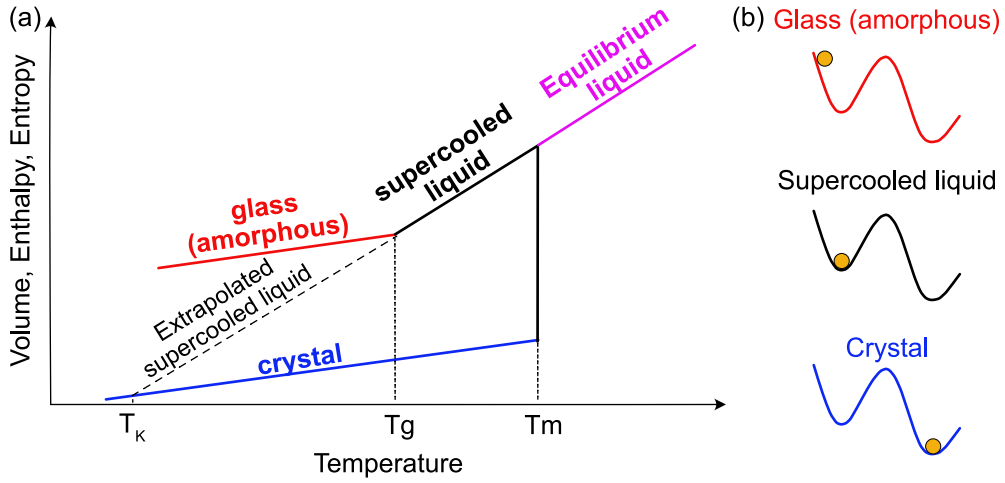

Figure 1.2. (a) Thermodynamic relationship of crystalline and amorphous state as a function of temperature. T_K, Tg and Tm are the Kauzmann temperature, glass transition temperature and the melting temperature, respectively. (b) Stability plots for the glass (red), metastable supercooled liquid (black), and the stable crystal (blue). Adapted from [19].

The benefit of non-equilibrium highly energetic amorphous materials is that they exhibit higher aqueous solubility and bioavailability; however, the liability is that they may lose their energetic surplus, crystallise and return to the more stable crystalline state.

1.2.3 Amorphous active pharmaceutical ingredients and amorphous solid dispersions

Common laboratory methods such as vapour deposition, milling/compaction of crystals, solvent evaporation, precipitation from solution, and melt/quench are used to prepare amorphous APIs using crystalline API as starting materials.

However, neat amorphous API can potentially be physically unstable due to its high amount of internal energy as mentioned above. The physical instability of neat amorphous API is a complex problem and the major limitation which precludes the wider application of amorphous pharmaceutical products which require expiry periods of years in usual practice. The metastable nature, together with the Tg values which may be close to room temperature suggest high molecular mobility of API amorphous systems. In particularly highly molecularly mobile systems, molecules can diffuse, collide, and aggregate with each other forming molecular "seeds" or nuclei where the process of recrystallisation, initially at a local level, can promote the growth of crystals to macroscopic dimensions, leading to catastrophic scenarios in which the all the amorphous sample recrystallises.[20,21]

An approximative qualitative description of the inexorable recrystallisation process of a neat amorphous API through its crystalline counterpart is described, both from the kinetic and thermodynamic point of view, by the classic nucleation theory (CNT). According to this model, the recrystallisation process can be essentially divided in two stages. The first one starts when an assembly of a few crystalline molecules is spontaneously formed making a thin interface between a solid and a liquid phase (**Figure 1.3**). While at the beginning the growth of this assembly is slow and thermodynamically unfavourable, the process became irreversible when

the critical nucleus size, r*, is reached and goes through to the complete recrystallisation of the whole sample.[22]

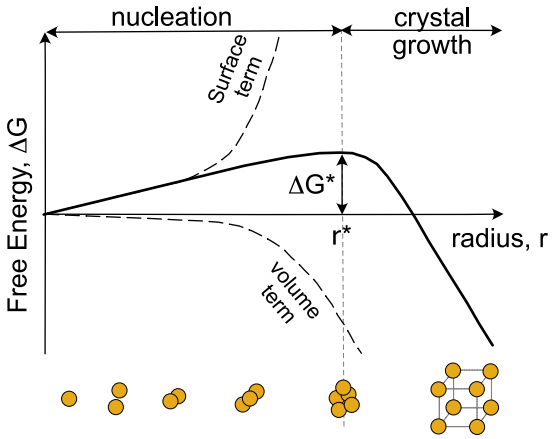

Figure 1.3. The reconversion of an amorphous species into its crystalline counterpart is described by the two steps classic nucleation theory (CNT). During the nucleation step, particles can assembly together forming gradually larger aggregates up to a critical radius, r*, in which a catastrophic irreversible macroscopic recrystallisation occurs (second step, crystal growth). The solid black line represents the variation of the total free energy during the process as function of the nucleus radius. The shape of the ΔG curve depends by the surface and volume terms. The maximum of ΔG(r) corresponds to a free energy barrier for nucleation that needs to be overcame to produce a critical nucleus and promote the crystal growth. Adapted from [11].

The solid curve in **Figure 1.3** represents the free energy variation as function of the radius, r, during the process. According to the CNT the shape of free energy of nucleation curve, ΔG, depends essentially on a negative term, lowering the total free energy, due to the formation of the stable crystalline phase (volume term) and

by a positive surface contribution (surface term) arising from the free energy costs needed to form the liquid-crystalline interface.[22]

In the nucleation stage, the ΔG increases as the size of the aggregates increase up to the critical nucleus size. It has been reported that the nucleation phenomena rate strongly depends on the molecular mobility of the system and by the presence of water, moisture or other impurities and it starts preferentially in particular regions of the systems like on the container walls, where both the wall itself and the particles surrounding the small nucleation “seeds” can play a role as catalysts, speeding up and reducing the energy barrier of the process.[23]

At r*, the ΔG function shows a sudden change in slope. From this point forward, the critical nucleus increases in size leading to the continuous development of crystalline phase, hence going towards a low energy, stable thermodynamic state. Three models have been proposed to describe the crystal growing known as continuous growth model, screw-dislocation model, and surface nucleation growth model.[24,25] However, the understanding of these models is beyond the limit of this concise introduction.

Thermodynamics portends that every metastable amorphous material is destined to eventually crystallise. However, the kinetics associated with crystallisation, can be slowed down and controlled or managed to accommodate expiry periods consistent with manageable shelf life. It has been extensively demonstrated that the shelf life of neat amorphous API can be extended when the API is dispersed in a polymer and an amorphous solid dispersion (ASD) is formed.[10,11,13,26,27]

Amorphous solid dispersions (ASDs) are the most promising technique used to take benefit of the useful bioavailability properties of amorphous API by combining the API with a polymer. ASDs are defined as dispersions of one or more APIs in an inert and hydrophilic excipient (polymer) in the solid state.[13,28-30] In these

ASD formulations, the initially crystalline API (hydrophobic, hence poor bioavailability) is transformed into its high energy amorphous state, and combined with a polymer to produce a miscible homogeneous material with small particle size, high wettability, and high apparent solubility and dissolution rate.[29,31,32] The long term physical stability of this ASD derives from the role played by the polymer. The high polymer viscosity (in terms of high Tg) can decrease the mobility of the system, lowering the probability of collisions between API molecules, thus reducing the probability of the formation of molecular aggregates, hence, overall reducing the rate of the nucleation process as described by the CNT[33,34], and enhancing the stability of the amorphous API towards the irreversible catastrophic recrystallisation process.[35,36] Furthermore, the polymer not only plays an essential role in stabilising the API in its amorphous state, as described above, it is found to be crucial in generating and maintaining supersaturated aqueous solutions once the ASD dissolves *in-vivo*.[10,13,30,37]

Beyond these aspects, another extra, potentially beneficial way that the polymer has to effectively stabilise an ASD is the ability to promote the formation of intermolecular API-polymer (e.g., hydrogen bonding, ionic forces, π–π, or electrostatic interactions), thus inhibiting the formation of API-API intermolecular interactions capable of promoting the API recrystallisation.[10,13,29,33,38,39] The understanding and the identification of these API-polymer intermolecular interactions, represent an exciting field of research, where nuclear magnetic resonance (NMR) has shown itself to be an invaluable, unique toolkit[40-50], as it will be demonstrated in the next chapters of this thesis.

Common formulation methods include solvent evaporation, spray drying (SD), cryo-milling, hot melt extrusion (HME), nano-solid suspension formation via controlled precipitation and solvent-free supercritical fluid processing. SD and hot melt extrusion HME are the most mature and used in the pharmaceutical industry.

The advantages of these two techniques over other methods, technical details of the two processes, as well as their direct comparison are reported and discussed in Chapter 2.

At the moment, the pharmaceutical industry has a limited number of polymers which are approved for oral pharmaceutical use.[51]

Before to be officially admitted as an approved excipient, a pharmaceutical polymer has to undergo a long (and expensive) development and acceptance process. The bar for approval as an acceptable pharmaceutical excipient ingredient is high, and in many ways the palette of approved materials is shrinking, rather than growing.

A desirable polymer that can be used as excipient in an ASD should:

1. be inert both chemically and pharmacologically,
2. have a high Tg,
3. have high viscosity,
4. have high aqueous solubility and in term of *in-vivo* performance,
5. be able to inhibit the precipitation of drugs in GI milieu into their respective crystalline form.[52]

However, this list could not be exhaustive and in practice, the choice of the most suitable polymer is selected empirically and the ASD prepared is extensively studied.

To date no polymer has been developed only for use as an excipient in amorphous solid dispersions. All materials were selected from the already approved list of excipients, in use for other purposes within pharmaceuticals.

Widely used polymer examples include poly(ethylene glycol) (PEG), poly(vinyl pyrrolidone) (PVP), poly(vinyl pyrrolidone)-co-vinylacetate (PVP-VA), and hydroxylpropylmethylcellulose (HPMC).

Derived as a chemical modification from HPMC, hydroxypropylmethylcellulose acetyl succinate (HMPC-AS) have been recently described as an excellent solid

matrix to make ASDs as of its high Tg value (around 120 ºC), its high solubility in volatile organic solvents (like methanol and acetone), and its amphiphilic nature. The amphiphilic nature of HPMC-AS allows insoluble drug molecules to interact with the hydrophobic regions of the polymer, whereas the hydrophilic regions allow these structures to remain as stable colloids in aqueous solution.[53,54] HPMC-AS was initially developed as a pH dependent “enteric” coating for tablets[55] (an “enteric” coating prevents the break up and dissolution of the tablet in the low pH environment of the stomach, where either the drug needs to be protected from the acid, or the patient’s stomach needs to be protected from the drug). The availability of the polymer as an approved excipient for another purpose made it a ready choice for evaluation in the amorphous solid dosage form arena.

The knowledge about API-polymer solubility is of great importance for a rational development of ASDs, as the selection of polymer and the applied API-polymer ratio will determine whether at particular condition the amorphous composition will be kinetically and thermodynamic stable or not. The crystallisation tendency at certain conditions of an ASD will be indicated by the so-called solubility and glass transition line of the phase-diagram of an API-polymer system (**Figure 1.4**). The solubility (dashed line) and the glass transition (solid line) curves indicate the specify conditions where the system is thermodynamically stable, and the frontier between the dynamically distinct glass and the liquid regions, respectively.

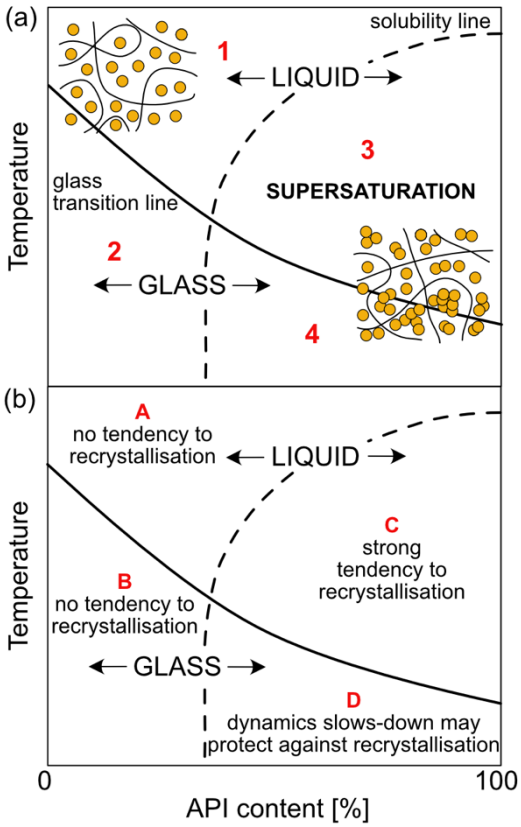

Figure 1.4. The phase-diagram of API-polymer system. (a) The four areas delimited by the solubility and glass transition lines correspond to the four (1 - 4) possible thermodynamic conditions to which correspond (b) the four (A - D) possible scenarios of recrystallisation behaviour. Adapted from[11].

Depending on the temperature and the API concentration four possible scenario are possible. In the scenario (**1**) the system is in a thermodynamically stable liquid condition, in which recrystallisation phenomena do not occur (**A**). All the possible API concentration/temperature combinations into the area (**2**) correspond to stable thermodynamically conditions in which the API-polymer system is completely amorphous. No crystallisation phenomena are expected (**B**). Systems in the area (**3**) and (**4**) are thermodynamically unstable liquids and glass, respectively. Therefore, conditions (**C**) and (**D**) correspond to scenario in which the compositions

are physically unstable, and the API is prone to crystallisation which may be prevented by the reduction of molecular mobility.[56]

1.2.4 Drug delivery

The aim of any drug delivery system is to solubilise and to transport a sufficient quantity of API to the desidered site in the body, thus generating a timely pharmaceutical response. The system should remain stable under the different extreme conditions it will find along the body (pH variations, penetration into biological barriers, etc.)[30,57], having already survived the rigours of packaging, transport, and administration to the patient.

Oral administration is the preferred route of administration for the patient. However, poor bioavailability is one of the major issues associated with this route of administration. It have been demonstrated that the any technique capable of generating a supersaturation state of API in the GI fluid can be substantially helpful in raising the oral bioavailability of that drug.[58,59]

ASDs represent a good example of super saturated API solution, and then they are good candidate for the drug oral administration.

1.3 Introduction to nuclear magnetic resonance spectroscopy

A spectroscopy technique is usually defined by the observation of a phenomenon that involves a transition of some physical entities (e.g., photons) from a lower energy level state, E_1, to a higher energy level, E_2.[60] The gap in energy between these two energy levels states is given by the follow fundamental **Equation 1.1**, where h is a Planck's constant and ν is the frequencies:

$$\Delta E = E_2 - E_1 = h\nu \qquad \textbf{Eq. 1.1}$$

As a spectroscopy technique, NMR signal arises from the transition between energy levels that correspond to the values of magnetic moment or nuclear spin quantum number. Only the nuclei with nuclear spin quantum number (or spin) $I \neq 0$, defined as "NMR active nuclei", possess a magnetic moment μ, and can generate a NMR signals. The magnetic moment of a nucleus, μ, is proportional to its spin angular momentum I with γ, that is a constant of proportionality, called the gyromagnetic ratio.

Due to the Zeeman's effect, when these nuclei are placed in a static magnetic field, B_0, there is an energetic preference for the spins to be aligned either with or against the magnetic field, resulting in (2I+1) spin states at different energy levels (**Figure 1.5(a)**). Nuclear spins also precess within a magnetic field. The frequency rate of precession is known as the Larmor frequency and depends on B_0, and γ, as reported in **Equation 1.2**

$$\nu_0 = \frac{\gamma B_0}{2\pi} \qquad \textbf{Eq. 1.2}$$

For spins with I = 1/2 (e.g., ^{1}H, ^{13}C, ^{15}N, ^{19}F) there are two possible orientations or spins states (defined as “upper” or “β” and “lower” or “α”). As shown in **Figure 1.5(b)**, the energy gap between these states is describe by **Equation 1.3.**

$$\Delta E = E_2 - E_1 = h\nu = \frac{h\,\gamma\,B_0}{2\pi} \qquad \textbf{Eq .1.3}$$

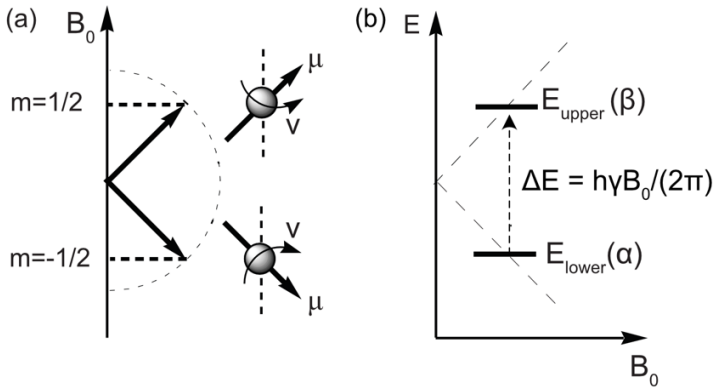

Figure 1.5. (a) The splitting of the spins states in a static magnetic field, B_0. I_z is parallel to B_0. The spins align either with or against the magnetic field. (b) Energy level diagram showing the possible transitions for a I = 1/2 nucleus. Figure adapted from[60]

The intensity of signal in NMR depends on the population difference between energy levels. At thermal equilibrium, the population of the energy levels of identical, non-interacting spins in B_0 is given by the Boltzmann distribution **Equation 1.4**, where ΔE is from **Eq. 1.3**, k_B is Boltzmann’s constant and T is the temperature.

$$\frac{n_{upper}}{n_{lower}} = \exp\left(-\frac{\Delta E}{k_B T}\right) \qquad \textbf{Eq. 1.4}$$

Consider ^{1}H nucleus in a 9.4 T field at a temperature T = 300 K, the ratio of the population is 1 in 20000. Therefore, NMR signal is inherently weak. For this reason, the use of high magnetic field, and/or lower temperatures are often employed to maximises the energy difference, resulting in a higher ratio of n_{upper}/n_{lower}.

The NMR frequency of a nucleus depends mainly on its gyromagnetic ratio and the strength of B_0. Mathematically this relationship can be expressed by **Eq. 1.2**. Therefore, NMR spectroscopy can distinguish one magnetic nucleus from another. While this is useful, the main reason for widespread application of NMR spectroscopy lies in the sensitivity of the NMR frequency to the local electronic environment of a particular chemical site. The effects of electron density surrounding a nucleus generates a small magnetic field, B_{ind}, which is oriented against B_0**.** The intensity of this localised magnetic field, B_{loc}, can be estimated by **Equation 1.5**:

$$B_{loc} = B_0 (1 - \sigma) \qquad \textbf{Eq. 1.5}$$

Where σ is the chemical shielding constant, which gives information regarding the surrounding electron density and electronic structure. This phenomenon is well known as “chemical shift”.

Practically, the effect of the B_{loc} alters the frequency at which a nucleus will appear on an NMR spectrum. Hence the resonance condition becomes (**Equation 1.6):**

$$\nu = \frac{\gamma B_0}{2\pi}(1 - \sigma) \qquad \textbf{Eq. 1.6}$$

For nuclei at different chemical environments, they suffer from different chemical shielding effects, resulting in the difference of the frequency of their NMR signals.

Usually, the frequencies are quoted relative to an agreed reference compound. The chemical shift (δ) is thus defined by the **Equation 1.7** and is measured into parts per million (ppm) as the differences between sample and reference compounds are usually very small and do not depend on the external static magnetic field.

$$\delta = 10^6 \frac{\nu - \nu_{ref}}{\nu_{ref}} \qquad \textbf{Eq. 1.7}$$

1.3.1 The vector model

The interaction between the nuclear magnetic moment and B_0 leads the spins to aligning either with (α-state) or against the magnetic field (β-state).

Using the Boltzmann distribution equation (**Eq. 1.4**) to estimate the ratio α/β population it can be found that there is a small excess of spins in the α-state. This excess leads to a net magnetisation in parallel alignment along the field B_0, named bulk magnetisation M_0 (**Figure 1.6(a)).**

Bulk magnetisation is the key concept to understand the vector model. Although not exempt from limitation, this model is a simple pictorial model to explore how NMR experiment works.[61]

In general, a NMR experiment consists in a series of consecutive acts over time (pulse sequence) in which the bulk magnetisation is manipulated and tilts into a reference system called “laboratory frame of reference” (**Figure 1.6(b)**). This x, y, and z geometric reference system can be found in a Cartesian coordinate system, in which conventionally M_0 lies along the z-axis.[61]

Figure 1.7(c) describes the simplest NMR experiment. Considering the rotating frame system, the M_0 vector is tilted by a π/2 radio frequency (rf) applied on the x-axis. The amplitude of the magnetic field of the applied rf field is called B_1 and it is applied via a coil. As result, M_0 moves from +z-axis to –y-axis through the yz-plane as it executes a motion of precession around the B_1 field axis. When the effect of the rf is finished, the nuclei take time to relax back to the z-axis releasing energy. Spin–lattice relaxation is the mechanism by which the longitudinal component relaxes to thermodynamic equilibrium with its surroundings (the "lattice"). This mechanism is characterised by the spin–lattice relaxation time, a time constant known as T_1.

At the same time, when the magnetisation vector processes about the direction of the magnetic field, inducing a current in the coil placed in the xy-plane. This current is then recorded in the time domain as free induction signal/decay (FID) and transformed in the frequency domain by applying the Fourier transformation.

Figure 1.7(d) summarises an NMR experiment in terms of pulse sequence. The horizontal line represents the electrical channel tuned to the observed nucleus, X, in order to record the signal close to the Larmor frequency of X. The rectangle represents a rf pulse, of strength and time such that the nuclear magnetic moment is transformed through the space (e.g., π/2 pulse). The oscillating line is the FID. This line showing a strongest signal at the beginning that gradually decaying to noise.

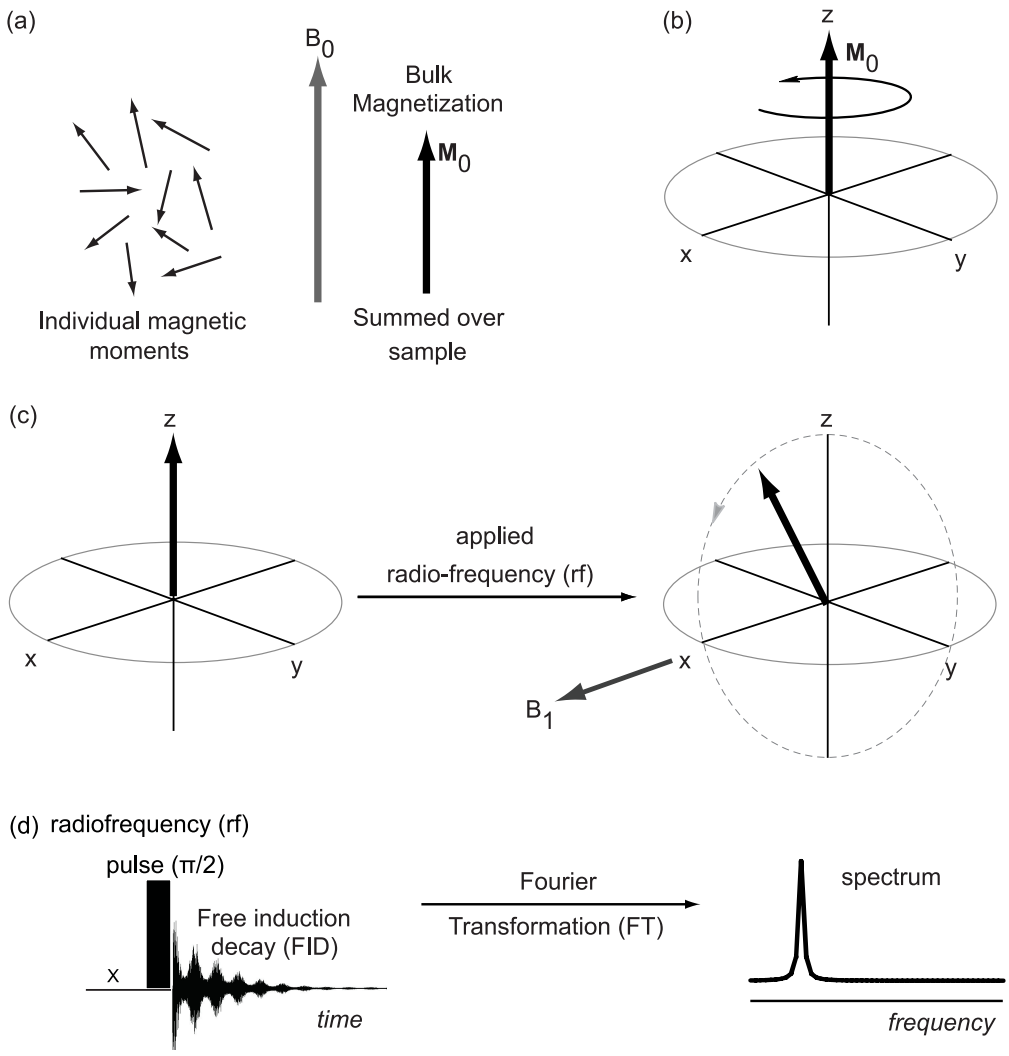

Figure 1.6. (a) In the presence of a B_0, the random oriented individual magnetic moments align either with (α-state) or against the magnetic field (β-state), differently populated. The bulk magnetisation vector, M_0 arises from the excess of spin in the α -state (b) M_0 conventionally lies on the z-axis of the laboratory frame. (c) The effect of a radiofrequency (rf) is to tilt the M_0. d) A pulse sequence of the simples NMR experiment. The horizontal line is the channel tuned on the nuclei X, the rectangular block outlines the rf pulse and, finally the oscillating line represents the FID. The figure is adapted from[61]

1.4. Introduction to solid-state nuclear magnetic resonance

The NMR signals depend on the sum of several interactions.[63] The quantum mechanics describes each of these interactions by appropriate nuclear spin Hamiltonians as reported in **Equation 1.8.**

$$\hat{H} = \hat{H}_Z + \hat{H}_{CS} + \hat{H}_D + \hat{H}_J + \hat{H}_Q + (\hat{H}_{para}) \qquad \textbf{Eq.1.8}$$

In **Eq. 1.8**, from left to right, the Hamiltonians are corresponding to Zeeman effect, isotropic chemical shift, dipolar coupling, scalar coupling, quadrupolar coupling (only for nuclei with $I > 1/2$), and paramagnetic coupling (only for paramagnetic nuclei). respectively. **Table 1.1** reports the equation of the main Hamiltonians and a brief explanation of them.

Interactions like anisotropic chemical shielding, dipolar and quadrupolar interaction are orientation dependent.[62,63] In the liquid state, such orientation dependent component is averaged out by the fast molecular motions.

In contrast, in solid state, atoms and molecules are more likely to be rigid, therefore do not experience random rapid tumbling. This particular molecular scenario leads to broadening lines within the solid-state spectrum.

In the next paragraphs, some of this observed interaction in solid-state NMR will be described.

Table 1.1. List of many NMR interactions with the corresponding equations, magnitudes and a brief explanation.

Type of interaction	Equation[62,63]	Magnitude	Description
Zeeman splitting	$\hat{H}_Z = -\gamma B_o \hat{I}_z$	MHz	It refers to the energy level difference between two spin states when spins interact with B_0.
Chemical shift	$\hat{H}_{CS} = -\gamma \hat{I}_z B_0 \left[\sigma_{iso} + \frac{1}{2}\sigma_{aniso}\left(3\cos^2\vartheta - 1\right)\right]$	kHz	It relates the indirect magnetic interaction of the B_0 with the nuclear spins, through the involvement of the electron.
Dipolar coupling	$\hat{H}_{D_{Hetero}} = d_{ij}\left(3\cos^2\vartheta - 1\right)\hat{I}_z\hat{S}_z$ $\hat{H}_{D_{Homo}} = -\frac{d_{ij}}{2}\left(3\cos^2\vartheta - 1\right)\left(3\hat{I}_{1z}\hat{I}_{2z} - \hat{I}_1\cdot\hat{I}_2\right)$ with $d_{ij} = \hbar\left(\frac{\mu_0}{4\pi}\right)\frac{\gamma_i\gamma_j}{r_{ij}^3}$	kHz	It represents the direct magnetic interactions of nuclear spins with each and depend by the intermolecular distance, r.
j-coupling	$\hat{H}_J = -J_{12}\hat{I}_{1z}\hat{I}_{2z}$	Hz	It describes the interactions between two spins when interacting through a chemical bond.
Quadrupolar coupling	$\hat{H}_Q = f\hat{I}_z\hat{S}_z\left[\frac{g^{iso}}{\omega_0} + h^{aniso}\left(3\cos^2\vartheta - 1\right) + i^{aniso}\left(35\cos^4\vartheta - 30\cos^2\vartheta + 3\right)\right]$	MHz	It is relevant only for nuclei with I > 1/2. Due to the asymmetric distribution of the electronic charge.

$\hat{I}_z$ and $\hat{S}_z$ are the angular quantum momentum operators representing the *z*-component of the magnetisation for the respective spins.

1.4.1 Chemical shift anisotropy (CSA)

The chemical shift anisotropy (CSA) results from the fact that the local electronic distribution surrounding the nuclei may have different orientations with respect B_0.[62,64] As the charge distribution around the nuclei is not being spherical, this causes the electronic cloud of each single nucleus of the sample to interact with B_0 in a different way than the others. As a result, the broad powder patter that is observed in spectrum is made of multiple lines at slightly different in chemical shifts, each corresponding to the single chemical shift of each nucleus.

However, three limit orientations that can be observed arise from the nucleus to be in the xz-plane, the yz-plane or the xy-plane, giving peaks in the NMR spectrum labelled δ_{11}, δ_{22}, and δ_{33} respectively (δ_{11} and δ_{33} are known as the principal components) (**Figure 1.7(a)**)

Considering a carbonyl group as model, when the electron cloud of CO is oriented along the B_0 axis, it resonances at the largest chemical shift, δ_{11} (due to deshielding effect). On the contrary, the smallest shift, δ_{33}, corresponds to the orientation in which the widest electronic density surrounding the CO is oriented along B_0 (shielding effect). Finally, the δ_{22} arises from the perpendicular molecular orientation to the axes of δ_{11} and δ_{33} (**Figure 1.7(b)**).

The whole anisotropic distribution is centred on the centre of gravity of the CSA powder pattern, the isotropic chemical shift, δ_{iso}, that is given by the **Equations 1.19.**

If any of these principal components are equal to each other the lines shape is uniaxial. The deviation from this line shape is given by the asymmetry parameter η, as reported in **Equation 1.10**.

$$\delta_{iso} = \frac{1}{3}(\delta_{11} + \delta_{22} + \delta_{33}) \qquad \textbf{Eq. 1.9}$$

$$\eta = \frac{\delta_{22} - \delta_{11}}{\delta_{33} - \delta_{iso}} \qquad \textbf{Eq. 1.10}$$

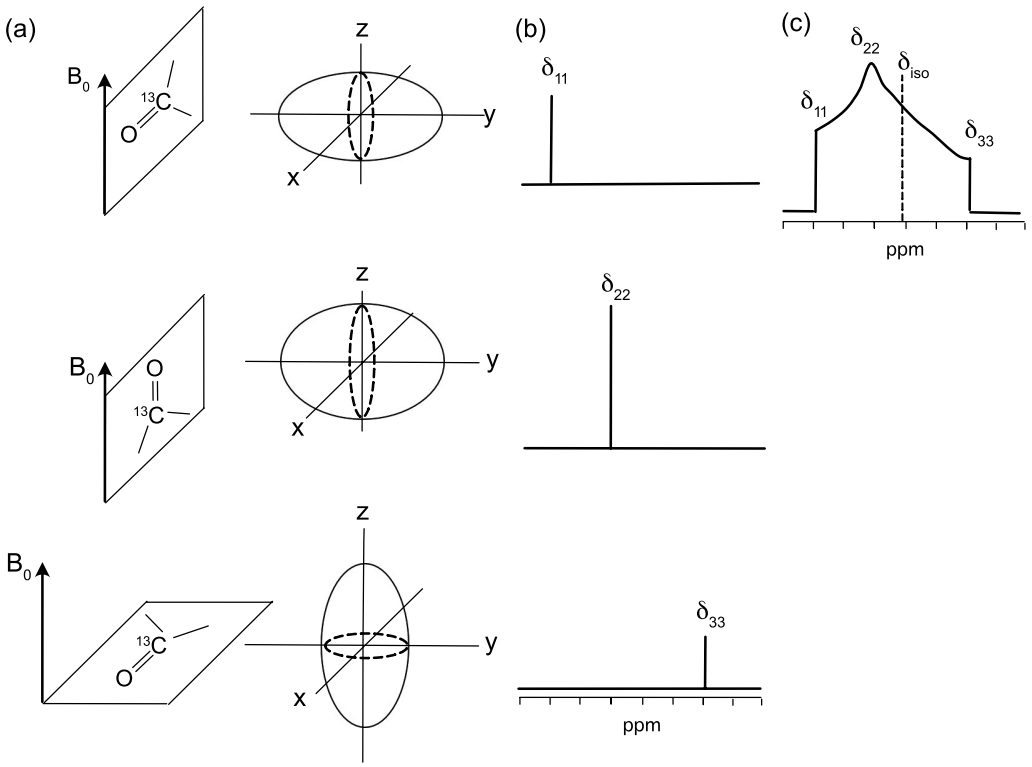

Figure 1.7. (a) Using as model the $^{13}C{=}O$ group, a schematic representation is given for the respective anisotropic chemical shifts of three "limit" possible orientation of a nucleus along B_0. (b) The three limit possible orientations give the respective three signals labelled as δ_{11}, δ_{22}, and δ_{33}. (c) Typical powder pattern created from the infinite number of lines due to every orientation of the nuclei with respect B_0. The position of the δ_{iso} is given by **Eq. 1.9**. Figure adapted from[64]

1.4.2 Dipolar coupling

The dipolar coupling interactions are due to nuclear magnetic moments of two identical or different nuclear spins, i and j, interacting through the space and it depends on the orientation of the internuclear vector between the spins and B_0.[62,64,65] When the spin i is the same as spin j, the interaction is called homonuclear, while if spin i $\neq$ spin j, the interaction is named heteronuclear.

Since each spin represents a nuclear magnetic moment that produces a small magnetic field. Hence, the i spin will experience the magnetic field produced by the j spin and vice-versa when the two spins are within reasonable proximity in the space.

The degree to which spin affects the magnetic field felt by the other spin is characterised by the strength of the dipolar coupling d_{ij}:

$$d_{ij} = \hbar \left(\frac{\mu_0}{4\pi}\right) \frac{\gamma_i \gamma_j}{r_{ij}^3}$$

Where μ_0 is the vaccum permittivity, $\hbar$ is the reduced Planck's constant, γ_i and γ_j are the gyromagnetic ratios of the spin i and j, respectively, and r_{ij} is the distance between the two nuclei.

1.4.3 Magic-angle spinning

All the interactions that have been described (CSA homo and heteronuclear dipolar coupling), which strongly contribute to the broad lines observed in solid spectra, are orientation dependent (anisotropic), and their corresponding Hamiltonians have a spin part as well as a geometric part in their equations. This geometric term is $(3\cos^2 \theta - 1)$ as reported in **Table 1.1**, and it can be averaged to zero when θ = 54º 7 (known as the "magic angle")

If a sample is spinning at the magic angle θ = 54.7° with respect B_0, (**Figure 1.7(a)**), the effects of CSA, dipolar coupling interactions, (and 1st order quadrupolar interactions) can be dramatically averaged out, leading to solid-state NMR spectra with high resolution.

This kind of experimental set-up is called magic angle spinning (MAS) technique, a universally used method in solid-state NMR, and its effect it reported in **Figure 1.8(b)**.[62,64,65]

However, the effect of the MAS in sharpening a powder pattern into a single line is achieved when the spinning frequency is higher, or at least equal, to the magnitude of anisotropic interactions. In addition, if MAS rate is not enough to average CSA, a set of spinning side bands, resonances spaced at intervals of the spin rate at either side of the δ_{iso} are seen in the spectrum.

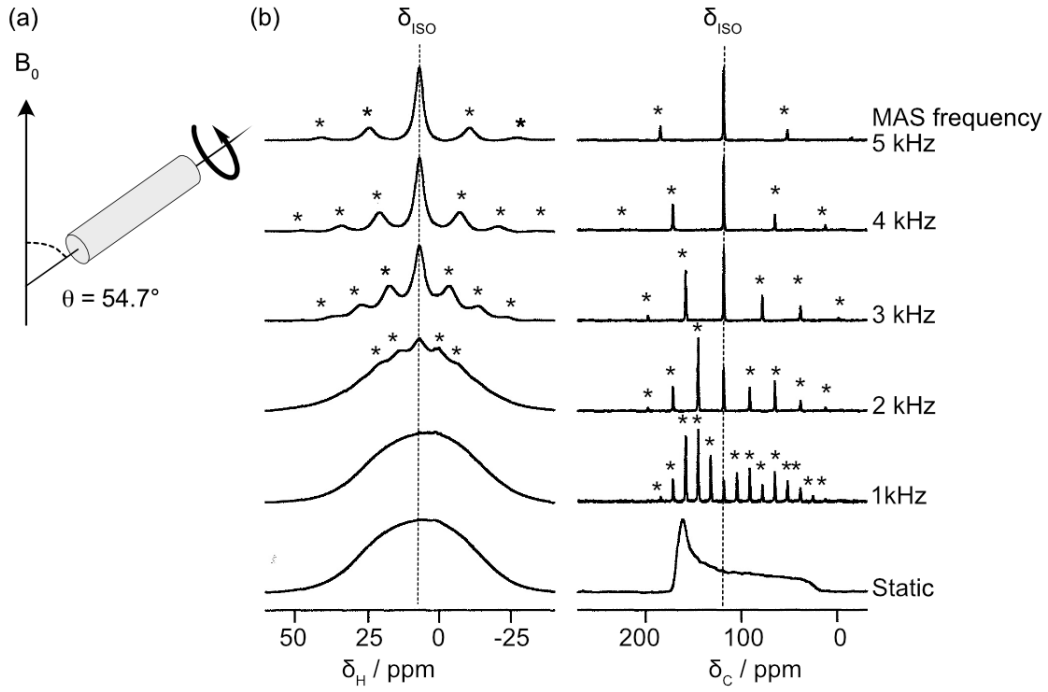

Figure 1.8. (a) In MAS technique, the sample spins at 54.7° to the applied magnetic field. (b) The effect on the MAS frequency on the NMR spectra. The symbol (*) indicates spinning side bands. Figure in panel b is adapted from[65]

1.5 NMR experiments

Solid-state NMR spectroscopy provides an invaluable source of both structural and dynamics information at the atomic scale. In the field of pharmaceutical sciences, NMR allows the determination of the structure of API and polymers, and it is robust technique to study API-polymer miscibility, and to identity site-specific API–polymer intermolecular interactions in ASDs.

The NMR experiments used throughout this thesis are listed and described in the following paragraphs.

1.5.1 Pulse-and-acquire experiment

The simplest NMR experiment is known as pulse-and-acquire (or one pulse) experiments. How this methodology works has been briefly explained using the vector model in paragraph 1.3.1.

Figure 1.9 schematically depicts the pulse-and-acquire pulse sequence. Practically, a π/2 (90º) rf pulse is applied to tilt the bulk magnetisation away from the z axis to the transverse xy-plane. The magnetisation vector then processes along the direction of the magnetic field to restore the initial equilibrium condition, inducing a current in the coil aligned in the transverse plane. This current is then recorded as FID, that is consequently converted into a frequency domain NMR spectrum by applying the Fourier transform.

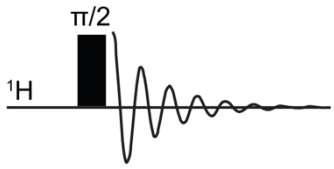

Figure 1.9. Schematic representation of pulse-and-acquire (one pulse) experiment.

1.5.2 Spin lattice relaxation and saturation recovery experiment

The spin-lattice relaxation time T_1 characterises the rate at which the longitudinal component of the magnetisation vector recovers exponentially towards its thermodynamic equilibrium after a rf pulse, losing energy to the nuclei's surroundings (lattice).

The way by which they lose that energy defines the relaxation pathway, and it is known as spin-lattice relaxation. It results in a grown of the z-component of magnetisation to restore the initial equilibrium condition. In contrast, the loss of the spins coherence of the magnetisation observed in the xy-plane, is known as spin-spin relaxation time, T_2.

Relaxation rate strongly depends on CSA and dipolar mechanism, and it can be also affected by quadrupolar and paramagnetic mechanism.[62]

The standard method for measuring T_1 is known as inversion-recovery experiment. **Figure 1.10(a)** shown the pulse sequence of this experiment. The program starts with a π pulse, which inverts the magnetisation along the -z axis. Then a delay period, τ, is applied, during which the magnetisation is allowed to recovery along the z-axis. Finally, a π/2 pulse is applied, and the FID is recorded. The experiment is repeated with different τ delays, allowing determination of of the T_1 value. (**Figure 1.10 (b)**).

An alternative methodology to the inversion recovery experiment widely used in solid-state NMR is the saturation recovery experiment.[66] As shown in **Figure 1.10 (c)**, the experiment consists of a saturation train of a n-series of π/2 pulses separated by time delay, t_{sd}, which causes saturation of the M_0 to zero. After this step, a variable time delay list (τ) (its length increases over a series of experiments) which allow relaxation on the z-axis, is applied followed by a π/2. Then the FID is

recorded. As per the inversion recovery experiment, this method brings to a build-up curve of the magnetisation in which the signal intensities obtained as function of τ can be fitted as an exponential curve to obtain T_1 value.

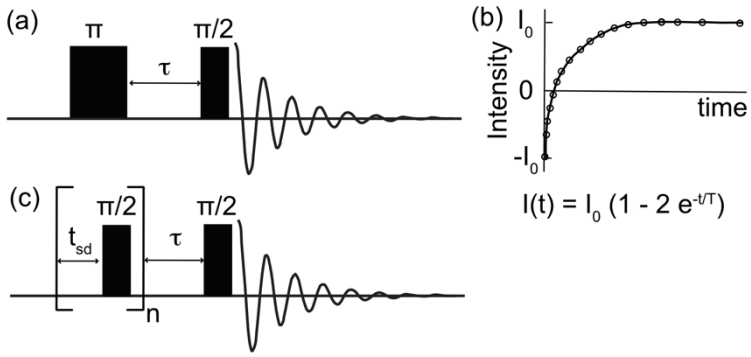

Figure 1.1. (a) The inversion recovery pulse sequence. (b) The signal intensity *vs*. time dataset obtained (o) is fitted with the equation reported to find the T_1 value (c) Pulse sequence for saturation recovery experiment. The full saturation of the magnetisation is ensured from the n-time loop saturation. τ is a variable time delay in which the polarisation is building up.

From a practical point of view, the spin-lattice relaxation time determines what recycle delay between pulses should be used in an NMR experiment. The nuclear spin system must be allowed to relax back to equilibrium before the next pulse is applied and this time period is determined by T_1.

1.5.3 Cross-polarisation experiment

Cross-polarisation (CP) is one of the most widely applied techniques in solid-state NMR.[62] CP methodology is used to assist in observing, to enhance signal-to-noise ratios and, to reduce the acquisition time required to record the NMR signal of dilute spins (low sensitivity nuclei), such as ^{13}C.[67]

Due to its low natural abundance (1.07 %) and low gyromagnetic ratio (6.72 x 10^7 rad T^{-1} s^{-1}) the sensitivity of ^{13}C NMR is hindered, meaning that the acquisition time to record a one pulse direct excitation spectrum would be extremely longer with respect to ^{1}H.

The CP experiment involves the transfer of polarisation from an abundant nucleus of one element (generally ^{1}H or, occasionally ^{19}F) to the dilute nuclei, X (e.g., ^{13}C, ^{15}N), greatly improving the experiment sensitivity up to a value equal to γ_H/γ_X (this ratio is 4 for a CP experiment involving ^{1}H and ^{13}C). Besides this, as usually $T_1(^{1}H) < T_1(X)$ the pulse sequence can be repeated much more rapidly than in a direct-excitation experiment, significantly increase the signal-to-noise ratio in the spectrum.

The pulse sequence of the ^{1}H-^{13}C CP experiment is reported in **Figure 1.11.** After the application of a rf pulse on the ^{1}H channel, a simultaneous pulse applies a spin lock to both ^{1}H and ^{13}C channels. Under this condition, when the spins are in close contact for an adequate period of time (contact time), the magnetisation transfer occurs through from the highly polarised to the less polarised spin.

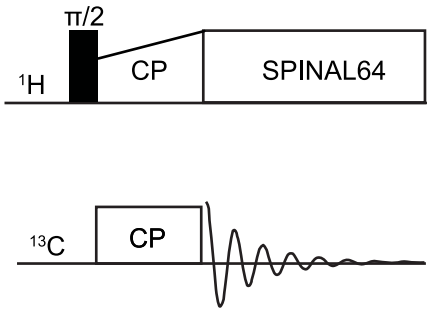

Figure 1.11. The standard CP pulse sequence involving ^{1}H and ^{13}C as dilute nucleus (^{1}H-^{13}C CP)**.** The contact pulse is ramped on the ^{1}H channel. During the signal acquisition on the ^{13}C channel, ^{1}H decoupling signal is obtained using the SPINAL64 heteronuclear decoupling scheme.

In order to maximise the polarisation transfer efficiency, the right experimental conditions are achieved when the ^{1}H and X rf fields fulfil the Hartmann-Hahn match condition[68] as for **Equation 1.11**, where ν_{1_H} and ν_{13_C} are the nutation frequencies of ^{1}H and ^{13}C, respectively.

$$\nu_{1_H} - \nu_{13_C} = n \cdot \nu_{rot} \qquad \textbf{Eq. 1.11}$$

By matching the nutation frequency (or matching them to a spinning sideband if n ≥ 1) the two nuclei are in contact, and magnetisation can effectively be transferred between the two nuclei via dipolar coupling.

After that the magnetisation is then transferred from ^{1}H to ^{13}C, tilting the ^{13}C nuclei into the transverse plan, a FID is recorded in the ^{13}C channel while decoupling occurs on the ^{1}H channel.

Together with CP, another common technique used in solid-state NMR is heteronuclear decoupling. Heteronuclear dipolar coupling, which significantly

contributes to the broadening signals in the solid-state NMR spectra, can be successfully averaged out by the MAS methodology and by applying heteronuclear decoupling, leading to sharper signals, hence simplify the spectrum.

The armoury of the solid-state NMR scientist includes different pulse program usable as effective heteronuclear decoupling. The continuous wave is the simplest, and it consist in a continuous irradiation the sample with rf of a single frequency during the acquisition time. A modern and sophisticated scheme, based on the applying of short rf pulse irradiation, are TPPM[69], SPINAL64[70], and XiX.[71]

SPINAL64 is the heteronuclear decoupling of choice throughout the experiments used in this thesis for its easy optimisation with respect the TPPM program and its high performance at the MAS frequency used.

1.5.4 Cross polarisation phase inversion experiment

Spectral assignment is a key step to assigning/confirm structures. Whilst this is often carried out using CP methodology, more challenging structures require additional information.

A simple ^{1}H-^{13}C CP pulse sequence modification, known as CP phase inversion (CPPI)[72], relying on to distinguish directly CH, CH_2, CH_3 and quaternary carbons in the spectra, making the complete assignment of some complex spectrum very practical.

In this experiment, the standard CP scheme is combined with polarisation inversion step, consisting in a delay time (PI) as in shown in **Figure 1.12**. During this delay, the ^{13}C signals can either decay fast or slowly, as function of the magnitude of the dipolar coupling with the ^{1}H surrounding the ^{13}C. Carbons strongly coupled will decay quickly while, on the contrary, carbons weakly coupled will decay slowly. In the middle of PI, a 180° pulse is applying on the of ^{13}C channel, to enable proper phasing as function of the different carbons behaviour and dipolar coupling. Then the signal is ^{13}C is recorded while SPINAL64 is applied on the ^{1}H channel.

The spectrum then produced permits the direct identification of different types of carbons, which results in quaternary carbon and CH_3 signals being positive phase, CH_2 phase negative, and CH signals are largely suppressed.

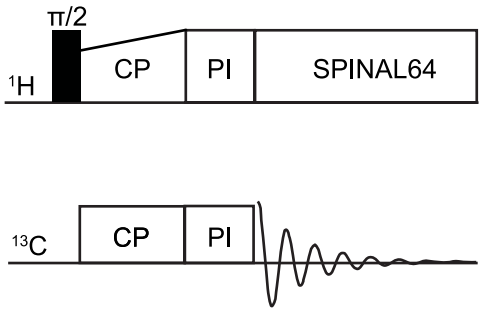

Figure 1.12. The ^{1}H-^{13}C CPPI pulse sequence. It consists in a modification of the CP standard pulse sequence in which a phase inversion step is added.

1.5.5 Measurement of spin-lattice relaxation in the rotating frame experiment

The spin-lattice relaxation in the rotating frame, $T_{1\rho,}$ describes the relaxation time in the rotation frame at the presence of an external rf pulse in the transverse plane (spin lock).[73]

$T_{1\rho}$ is sensitive to slow molecular motions (motions occur on a KHz timescale, from ms to μs), if compared to T_1, hence it leads a sensitive probe of local mobility, highlighting molecular level changes within the system.

The ^{1}H spin-lattice relaxation in the rotating frame (^{1}H $T_{1\rho}$) can be indirectly detected via CP ^{13}C signal detection using the pulse sequence shown in **Figure 1.13** (this experiment is the sequence "cpht1rho" of the Bruker library).

The experiment is based on a modified CP sequence with an additional spin-locking pulse. Before the CP stage, the proton magnetisation is locked along the y-axis for a variable time (vplist) using a spin-locking pulse. During this delay, the ^{1}H magnetisation evolves under the effect of the homonuclear dipolar magnetisation. This results in a difference in the peak intensity dependent on the proton relaxation efficiency in the rotating frame.

The signal intensities obtained as function of delay can be fitted as an exponential decay curve to obtain ^{1}H $T_{1\rho}$ value.

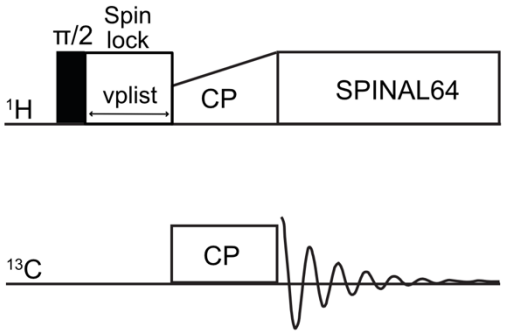

Figure1.13. The “cpht1rho” experiment of the Bruker catalogue allows the indirect ^{1}H $T_{1\rho}$ measurement. The pulse sequence is a modification of the standard CP experiments with an additional spin-lock pulse.

1.5.6 Measurement of ^{13}C spin-lattice relaxation times.

The^{13}C low sensitivity and the inherently long ^{13}C T_1 relaxation time make the detection of ^{13}C relaxation measurements via direct methods (e.g., inversion recovery experiment) extremely time consuming.

To reduce this long acquisition time, ^{13}C relaxation measurement are carried out taking advantage from the CP signal enhancement and short ^{1}H T_1 to achieve maximum signals intensity.

The pulse sequence used for this purpose is depicted in **Figure 1.14.** At the end the contact pulse, the ^{13}C magnetisation is on the xy-transversal plane. According to the pulse scheme, a π/2 pulse around the y- (or -y) axis is applied tilting the magnetisation to the z- (or -z) axis. Then the magnetisation is free to relax over a period τ. Finally, a new π/2 pulse is applied before the signal detection.

The signal intensities obtained as function of the time can be fitted to obtain ^{13}C T_1 values.

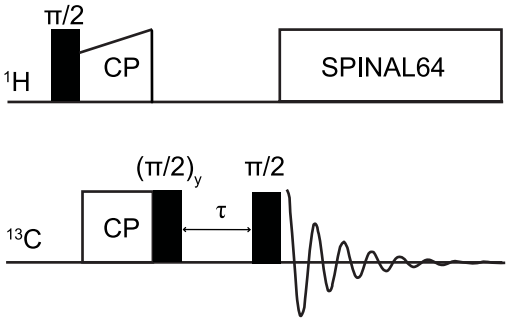

Figure 1.14. The pulse sequence employed to measure ^{13}C T_1 relaxation time. The methodology take advantage from the CP technique.

1.5.7 Two-dimensional NMR spectroscopy

Two-dimensional (2D) NMR spectroscopy represents a useful methodology often used to elucidate chemical structures and to probe selective NMR interactions.

A typical 2D pulse sequence consists of four main acts:

1. preparation period,
2. evolution period, t_1,
3. mixing period,
4. detection period, t_2.

Practically, a 2D spectra is recorded using the basic pulse sequence reported in **Figure 1.15**.

First the evolution period, t_1, is set to zero and a FID is recorded. Then the t_1 is set to Δ_1 (sampling interval in t_1), and a new FID is stored. After that, Δ_1 is increased incrementally over each acquisition in order to build up ta time domain dataset. At the end, the NMR signals recorded as a function of two-time variables, are Fourier transformed to provide a 2D spectrum plotted as intensity against two different frequencies.

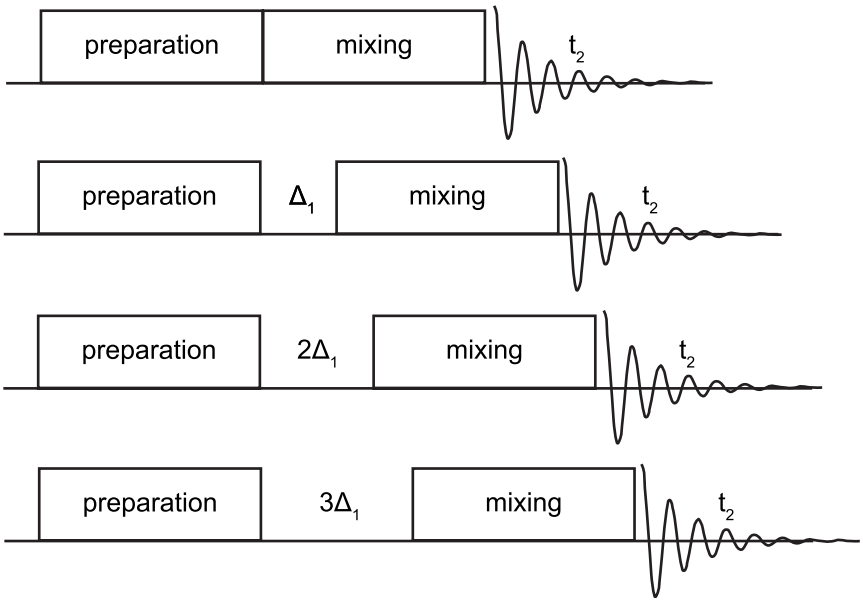

Figure 1.15. Generic 2D pulse sequence scheme. It consists of four different periods named preparation, evolution, mixing and detection.

1.5.7.1 Heteronuclear correlation experiments

The ^{1}H-^{13}C CP heteronuclear correlation (HETCOR) experiment is a well-established NMR method widely used in solid-state NMR.

The HETCOR pulse sequence is shown in **Figure 1.16**.[74] First the ^{1}H magnetisation is tilted on the transversal plane, then during the evolution period experiences frequency switched Lee-Goldburg (FSLG) homonuclear decoupling[75] where it is forced to precess about a field oriented at the magic angle by series of 2π pulses. The effect of the FSLG decoupling is to average the homonuclear dipolar coupling to zero.

After that, the ^{1}H magnetisation is then returned to the transverse axis and CP is used to transfer the frequency encoded proton magnetisation to ^{13}C. Finally, the ^{13}C FID is recorded while ^{1}H SPINAL64 heteronuclear decoupling is applied.

For CP contact times in the range of 2 ms, the resulting 2D spectrum shows dipolar correlations present between carbon resonances and the protons strongly dipolar coupled.

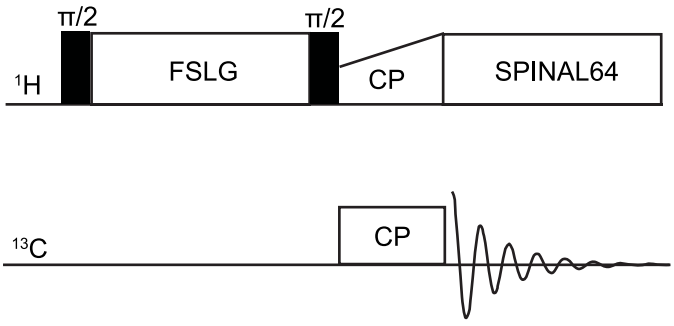

Figure 1.16. The ^{1}H-^{13}C CP HETCOR experiment pulse sequence. The FSLG decoupling during the evolution period leads to average the homonuclear dipolar coupling. The CP is used to enhance the signal of ^{13}C and finally, the signal is recorded applying the SPINAL64 heteronuclear decoupling.

1.5.7.2 Heteronuclear multiple quantum coherence experiment

The identification of hydrogen bonds between HN-X and N-HX species are of fundamental importance to understand the way of self-assembly of complex chemical structures and the study of the chemical-physical stability of certain materials.

Methods based on ^{15}N NMR are generally time consuming and suffer from low sensitivity due to its low natural abundance (0.36%) and low gyromagnetic constant (-2.71 x 10^7 rad T^{-1} s^{-1}), respectively.

Despite the detection of the ^{14}N signal in the solid-state NMR is considered a challenge due to its quadrupolar nature (I =1) and low gyromagnetic constant (1.93 × 107 rad T^{-1} s^{-1}), the development of indirectly detected ^{14}N signal via ^{1}H as for example via 2D ^{14}N-^{1}H heteronuclear multiple quantum correlation (HMQC)[76] permits to overcome this challenge opened up to a route for the identification of intra/intermolecular hydrogen-bonding in complex chemical structures detected through dipolar heteronuclear coupling.[45,46,77,78]

The pulse sequence of the ^{14}N-^{1}H HMQC used throughout this thesis is shown in **Figure 1.17**. This experiment takes advantage of the high natural abundance of ^{14}N (99.6 %), from high MAS frequency (> 60 kHz) and the use of high magnetic field. The pulse scheme ensures that the ^{14}N channel evolution in t_1 is correlate with the ^{1}H evolution in t_2 if there is a coupling between the nuclei. The full rich informative heteronuclear dipolar coupling averaged out by MAS technology are reintroduced during the experiment as they give precious information regarding the nuclear specie close into the space. This is achieved employing the rotary-resonance recoupling R^3 at the n = 2 condition (ν_1 = 2 ν_{MAS}) in which the

heteronuclear dipolar coupling and the CSA are reintroduced, but not the homonuclear dipolar coupling. [79]

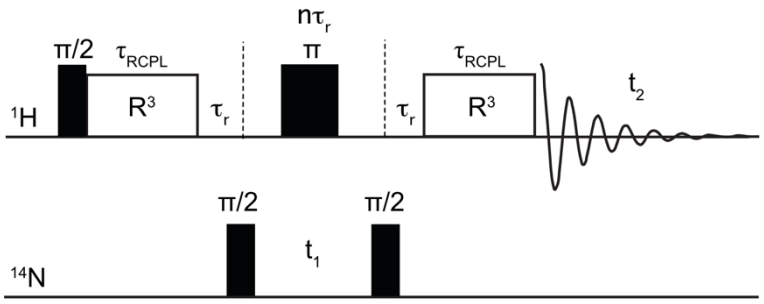

Figure 1.17. The ^{14}N-^{1}H HMQC pulse sequence using the R^3 rotary resonance sequence to recouple heteronuclear dipolar couplings.

1.6 Conclusions

The first part of this introductory chapter describes the ASD technology. This promising technique allows to obtain stable bioavailable amorphous APIs thanks to the presence of a polymer in the dispersion. Indeed, the polymer guarantees the stability of the metastable amorphous API as described by the CNT.

In the second part, after a general introduction on NMR and on the main factors that influence NMR in the solid state, MAS and CP techniques are presented as concrete and routine methods to overcome them.

Finally, the NMR experiments used throughout this thesis for the structural characterization of the components and the stability of ASD are described.

1.7 References

[1] Yang, W. Z.; Gadgil, P.; Krishnamurthy, V. R.; Landis, M.; Mallick, P.; Patel, D.; Patel, P. J.; Reid, D. L.; Sanchez-Felix, M *AAPS J.* **2020**, *22*, 14.

[2] Lipinski, C. A. *Drug Discov. Today: Technol.* **2004**, 1, 337.

[3] O'Donnell, K. P.; Woodward, W. H. *Drug Dev. Ind. Pharm.* **2015**, *41*, 959.

[4.] Chavda, H. V.; Patel, C. N.; Anand, I. S. *Syst. Rev. Pharm.* **2010**, *1*, 62.

[5] Tsume, Y.; Mudie, D. M.; Langguth, P.; Amidon, G. E.; Amidon, G. L. *Eur. J. Pharm. Sci.* **2014**, *57*, 152.

[6] Papich, M. G.; Martinez, M. N. *AAPS J.* **2015**, *17*, 948.

[7] Bauer, J.; Spanton, S.; Henry, R.; Quick, J.; Dziki, W.; Porter, W.; Morris, J. *Pharm. Re.* **2001**, *18*, 859.

[8] Chemburkar, S. R.; Bauer, J.; Deming, K.; Spiwek, H.; Patel, K.; Morris, J.; Henry, R.; Spanton, S.; Dziki, W.; Porter, W.; Quick, J.; Bauer, P.; Donaubauer, J.; Narayanan, B. A.; Soldani, M.; Riley, D.; McFarland, K. *Org. Process Res. Dev*. **2000**, *4*, 413.

[9] Carpentier, L.; Decressain, R.; De Gusseme, A.; Neves, C.; Descamps, M. *Pharm. Res.* **2006**, *23*, 798.

[10] Newman, A., *Pharmaceutical Amorphous Solid Dispersions*. Wiley, Hobken, New Jersey, USA: **2015**.

[11] Rams-Baron, M. J., R.; Boldyreva, E.; Zhou D.; Jamroz, W.; Paluch, M., *Amorphous Drugs*. Springer, Cham, Switzerland: **2018**.

[12] Zhang, M.; Li, H.; Lang, B.; O'Donnell, K.; Zhang, H.; Wang, Z.; Dong, Y.; Wu, C.; Williams, R. O. *Eur. J. Pharm. Biopharm.* **2012**, *82*, 534.

[13] Baghel, S.; Cathcart, H.; O'Reilly, N. J. *J .Pharm. Sci.* **2016**, *105*, 2527.

[14] Fukuoka, E.; Makita, M.; Yamamura, S. *Chem Pharm Bull* **1986**, *34*, 4314.

[15] Yoshioka, M.; Hancock, B. C.; Zografi, G. *J. Pharm. Sci.* **1994**, *83*, 1700.

[16] Hancock, B. C.; Shamblin, S. L.; Zografi, G. *Pharm. Res.* **1995**, *12*, 799.

[17] Masuda, K.; Tabata, S.; Sakata, Y.; Hayase, T.; Yonemochi, E.; Terada, K. *Pharm. Res.* **2005**, *22*, 797.

[18] Crowley, K. J.; Zografi, G. *J. Pharm. Sci.* **2002**, *91*, 492.

[19] Cangialosi, D. *J. Phys.: Condens. Matter* **2014**, *26*, 153101.

[20] Ruckenstein, E.; Djikaev, Y. S. *Adv. Colloid Interface Sci.* **2005**, *118*, 51.

[21] Adrjanowicz, K.; Koperwas, K.; Szklarz, G.; Tarnacka, M.; Paluch, M. *Crystal Growth & Design* **2016**, *16*, 7000.

[22] Jungblut, S.; Dellago, C. *Eur. Phys. J. E. Soft Matter* **2016**, *39*, 1.

[23] Sosso, G. C.; Chen, J.; Cox, S. J.; Fitzner, M.; Pedevilla, P.; Zen, A. *Chem. Rev.* **2016**, *116*, 7078.

[24] Nascimento, M. L. F.; Zanotto, E. D. *J. Chem. Phys.* **2010**, *133*, 174701.

[25] Trasi, N. S.; Baird, J. A.; Kestur, U. S.; Taylor, L. S. *J. Phys. Chem. B* **2014**, *118*, 9974.

[26] Kaminska, E.; Adrjanowicz, K.; Zakowiecki, D.; Milanowski, B.; Tarnacka, M.; Hawelek, L.; Dulski, M.; Pilch, J.; Smolka, W.; Kaczmarczyk-Sedlak, I.; Kaminski, K. *Pharm. Res.* **2014**, *31*, 2887.

[27] Romanini, M.; Lorente, M.; Schammé, B.; Delbreilh, L.; Dupray, V.; Coquerel, G.; Tamarit, J. L.; Macovez, R. *Macromolecules* **2018**, *51*, 9382.

[28] Van den Mooter, G.; Van den Brande, J.; Augustijns, P.; Kinget, R. *J. Therm. Anal. Calorim.* **1999**, *57*, 493.

[29] Newman, A.; Nagapudi, K.; Wenslow, R. *Ther. Deliv.* **2015**, *6*, 247.

[30] Van den Mooter, G. *Drug Discov. Today Technol*. **2012**, *9*, 79.

[31] Craig, D. Q. M. *Int. J. Pharm.* **2002**, *231*, 131.

[32] Kanaujia, P.; Poovizhi, P.; Ng, W. K.; Tan, R. B. H. *Powder Technology* **2015**, *285*, 2.

[33] Van Duong, T.; Van den Mooter, G. *Expert. Opin. Drug. Deliv.* **2016**, *13*, 1681.

[34] Kawabata, Y.; Wada, K.; Nakatani, M.; Yamada, S.; Onoue, S. *Int. J. Pharm.* **2011**, *420*, 1.

[35] Van den Mooter, G.; Craig, D. Q. M.; Royall, P. G. *J. Pharm. Sci*. **2001**, *90*, 996.

[36] Ivanisevic, I. *J Pharm Sci* **2010**, *99*, 4005.

[37] Singh, A.; Van den Mooter, G. *Adv. Drug. Deliv. Rev*. **2016**, *100*, 27.

[38] Janssens, S.; Van den Mooter, G. *J. Pharm. Pharmacol*. **2009**, *61*, 1571.

[39] Tran, T. T. D.; Tran, P. H. L. *Pharmaceutics* **2020**, *12*, 745.

[40] Paudel, A.; Geppi, M.; Van den Mooter, G. *J. Pharm. Sci*. **2014**, *103*, 2635.

[41] Yuan, X.; Xiang, T. X.; Anderson, B. D.; Munson, E. *J. Mol. Pharmaceutics* **2015**, *12*, 4518.

[42] Nie, H.; Su, Y.; Zhang, M.; Song, Y.; Leone, A.; Taylor, L. S.; Marsac, P. J.; Li, T.; Byrn, S. R. *Mol. Pharmaceutics* **2016**, *13*, 3964.

[43] Lubach, J. W.; Hau, J. *Pharm. Res*. **2018**, *35*, 65.

[44] Lu, X.; Huang, C.; Lowinger, M. B.; Yang, F.; Xu, W.; Brown, C. D.; Hesk, D.; Koynov, A.; Schenck, L.; Su, Y. *Mol. Pharmaceutics* **2019**, *16*, 2579.

[45] Grune, M.; Luxenhofer, R.; Iuga, D.; Brown, S. P.; Poppler, A. C. *J. Mater. Chem. B* **2020**, *8*, 6827.

[46] Pugliese, A.; Toresco, M.; McNamara, D.; Iuga, D.; Abraham, A.; Tobyn, M.; Hawarden, L. E.; Blanc, F. *Mol. Pharmaceutics* **2021**, *18*, 3519.

[47] Berendt, R. T.; Sperger, D. M.; Munson, E. J.; Isbester, P. K. *TrAC Trends in Anal. Chem*. **2006**, *25*, 977.

[48] Geppi, M.; Mollica, G.; Borsacchi, S.; Veracini, C. A. *Appl. Spectrosc. Rev*. **2008**, *43*, 202.

[49] Everett, J. R.; Harris, R. K.; Lindon, J. C., *NMR in Pharmaceutical Sciences*. John Wiley & Sons: Chichester, UK, **2015**.

[50] Li, M.; Xu, W.; Su, Y. Solid-state NMR spectroscopy in pharmaceutical sciences. *TrAC Trends Anal. Chem.* **2021**, *135*, 116152

[51] Nair, A. R.; Lakshman, Y. D.; Anand, V. S. K.; Sree, K. S. N.; Bhat, K.; Dengale, S. J. *AAPS PharmSciTech* **2020**, *21*, 309.

[52] Ruff, A.; Fiolka, T.; Kostewicz, E. S. *Eur J Pharm Sci* **2017**, *100*, 42.

[53] Friesen, D. T.; Shanker, R.; Crew, M.; Smithey, D. T.; Curatolo, W. J.; Nightingale, J. A. S. *Mol. Pharmaceutics* **2008**, *5*, 1003.

[54] Ueda, K.; Higashi, K.; Yamamoto, K.; Moribe, K. *Int. J. Pharm.* **2014**, *464*, 205.

[55] Fujii, Y.; Kanamaru, T.; Kikuchi, H.; Yamashita, S.; Sakuma, S. European *J. of Pharm. Sci.* **2011**, *42*, 392.

[56] Lehmkemper, K.; Kyerematen, S. O.; Heinzerling, O.; Degenhardt, M.; Sadowski, G. *Mol. Pharm.* **2017**, *14*, 157-171.

[57] Baird, J. A.; Taylor, L. S. *Adv. Drug Deliv. Rev.* **2012**, *64*, 396.

[58] Pokharkar, V. B.; Mandpe, L. P.; Padamwar, M. N.; Ambike, A. A.; Mahadik, K. R. *Powder Technol*. **2006**, *167*, 20.

[59] Gurunath, S.; Pradeep Kumar, S.; Basavaraj, N. K.; Patil, P. A. *J. Pharm. Res.* **2013**, *6*, 476.

[60] Hore, P. J., *Nuclear Magnetic Resonance*. 2nd ed.; Oxford press, Oxford, England: **2015**.

[61] Keeler, J., *Understanding NMR Spectroscopy*. 2nd ed.; Wiley, West Sussex, England: **2010**.

[62] Duer, M., *Introduction to Solid-State NMR Spectroscopy*. Blackwell Publishing, Oxford, England: **2005**.

[63] Levitt, M. H., *Spin Dynamics.* 2nd ed.; Wiley, West Sussex, England: **2008**.

[64] Laws, D. D.; Bitter, H. L.; Jerschow, A. *Angew. Chem. Int. Ed*. **2002**, *41*, 3096.

[65] Apperley, D. C.; Harris, R. K.; Hodgkinson, P., *Solid-State NMR: Basic Principle & Practice*. Momentum Press, New York, USA: **2012**.

[66] Anderson, J. E.; Ullman, R. *J. Phys. Chem.* **1967**, *71*, 4133.

[67] Pines, A.; Gibby, M. G.; Waugh, J. S. *J. Chem. Phys*. **1973**, *59*, 569.

[68] Hartmann, S. R.; Hahn, E. L. *Phys. Rev.* **1962**, *128*, 2042.

[69] Königsberger, E.; Sterk, H. *J. Chem. Phys*. **1985**, 83, 2723.

[70] Fung, B. M.; Khitrin, A. K.; Ermolaev, K. *J. Magn. Reson.* **2000**, *142*, 97.

[71] Detken, A.; Hardy, E. H.; Ernst, M.; Meier, B. H. *Chem. Phys. Lett.* **2002**, *356*, 298.

[72] Wu, X.; Burns, S. T.; Zilm, K. W. *J. Magn. Reson., Ser. A* **1994**, *111*, 29.

[73] Redfield, A. G. *Phys. Rev*. **1955**, *98*, 1787.

[74] van Rossum, B. J.; Förster, H.; de Groot, H. J. M. *J. Magn. Reson.* **1997**, *124*, 516.

[75] Goldburg, W. I.; Lee, M. *Phys. Rev. Lett*. **1963**, *11*, 255.

[76] Tatton, A. S.; Bradley, J. P.; Iuga, D.; Brown, S. P. *Z. Phys. Chem.* **2012**, *226*, 1187

[77] Tatton, A. S.; Pham, T. N.; Vogt, F. G.; Iuga, D.; Edwards, A. J.; Brown, S. P. *CrystEngComm* **2012**, *14*, 2654.

[78] Tatton, A. S.; Pham, T. N.; Vogt, F. G.; Iuga, D.; Edwards, A. J.; Brown, S. P. *Mol. Pharmaceutics* **2013**, *10*, 999.

[79] Gan, Z.; Amoureux, J. P.; Trébosc, J. *Chem. Phys. Lett.* **2007**, *435*, 163.

Chapter 2: New Development in Understanding Drug-Polymer Interactions in Pharmaceutical Amorphous Solid Dispersions from Solid-State Nuclear Magnetic Resonance

2.1 Overview

Chapter 2 is a review entitle “New Development in Understanding Drug-Polymer Interactions in Pharmaceutical Amorphous Solid Dispersions from Solid-State Nuclear Magnetic Resonance” by Andrea Pugliese, Michael Tobyn, Lucy E. Hawarden, Anuji Abraham and Frédéric Blanc which was submitted at *Molecular Pharmaceutics*.

The author contributions are as follows: A.P. and F.B. wrote the manuscript with consultation from all other authors.

2.2 Abstract

Pharmaceutical amorphous solid dispersions (ASDs) represent a widely used technology to increase the bioavailability of active pharmaceutical ingredients (APIs). ASDs are based on an amorphous API dispersed in a polymer, and their stability is driven by the presence of strong intermolecular interactions between these two species (e.g., hydrogen bond, electrostatic interactions, etc.). The understanding of these interactions at the atomic level is therefore crucial, and solid-state nuclear magnetic resonance (NMR) has demonstrated itself as a very powerful technique for probing API-polymer interactions. The latest review of the field was published in 2014 and highlighted exciting approaches to study the structures and dynamic properties of ASDs largely focusing on changes of chemical shift of "spy atoms" (^{1}H, ^{13}C, and ^{15}N) in one-dimensional (1D) and two-dimensional (2D) homo and heteronuclear correlations experiments to identify API-polymer interactions. The current updated review highlights recent strategies published that enable the identification of API-polymer contacts reporting exciting recent examples using 1D and 2D experiments by exploiting the following emerging approaches of very-high magnetic field and ultra-fast magic angle spinning (MAS). A range of different ASDs spanning APIs and polymers with varied structural motifs is targeted to illustrate new ways to understand the mechanism of stability of ASDs enabling the design of new dispersions.

2.3 Amorphous Solid Dispersions

The formulation of low solubility crystalline active pharmaceutical ingredients (APIs) or drugs in the amorphous form is a recognised robust methodology exploited to improve their dissolution rates and bioavailability.[1,2] ASD's can be used for other purposes, such as the enhancement of stability when salt forms of an API are unstable. Several approaches have been developed to stabilise amorphous solid dispersions (ASDs) among which hot-melt extrusion (HME) and spray-drying (SD) technologies are the most widely used, and the only ones used commercially by the pharmaceutical industry.[3-5] ASDs are formulations of one (or more) active ingredient in the amorphous state stabilised by inert and hydrophilic carrier(s) or matrix in the solid state (usually a polymer and/or additive) aimed at obtaining fully miscible, amorphous and physically stable dispersion.[6-7] HME is utilised extensively for commercial-scale ASDs manufacturing because of several factors: it is mature, well understood process and can be therefore scalable and low cost; it is solvent free and thus environmentally friendly and it operates as a continuous process well suited for large scale production.[2,8] This technology contains several steps as illustrated in **Figure 2.1(a)** in which the drug and the polymer are mixed, melted, dispersed and extruded under specific conditions offering flexibility to be tailored to a range of API, matrix and other excipients while also being suitable to oxygen sensitive and hydrolysable drugs.[3] Two of the most important drawbacks of this technology are the high energy consumption of the process and heating processes preclude the formulation of thermolabile API's.[5] Another widely used technology for commercially manufacturing ASDs in the pharmaceutical industry is spray-drying (SD) methodology that also offers and scalable process, albeit that scaling up is more complex than with HME.[4] The SD

process (**Figure 2.1(b)**) requires an initial API-polymer solution/suspension in a system which might contain water as the feed solution which is then spray dried through a spray-nozzle (component 1 in **Figure 2.1(b)**) for which various design exists (components 2 – 4 in **Figure 2.1(b)**) to accommodate more than one feed or high-pressure.[5] Upon contact of the feed solution droplets with the hot gas/air carrier, the solvent system evaporates quickly leading to dried ASD particles that are separated by the gas stream in the cyclone and then collected. It is likely that the particles, once gathered, are subjected to a secondary drying process to remove solvents and reduce any residual moisture to an appropriate level. The spray dried systems can then be formulated into a conventional tablet system.

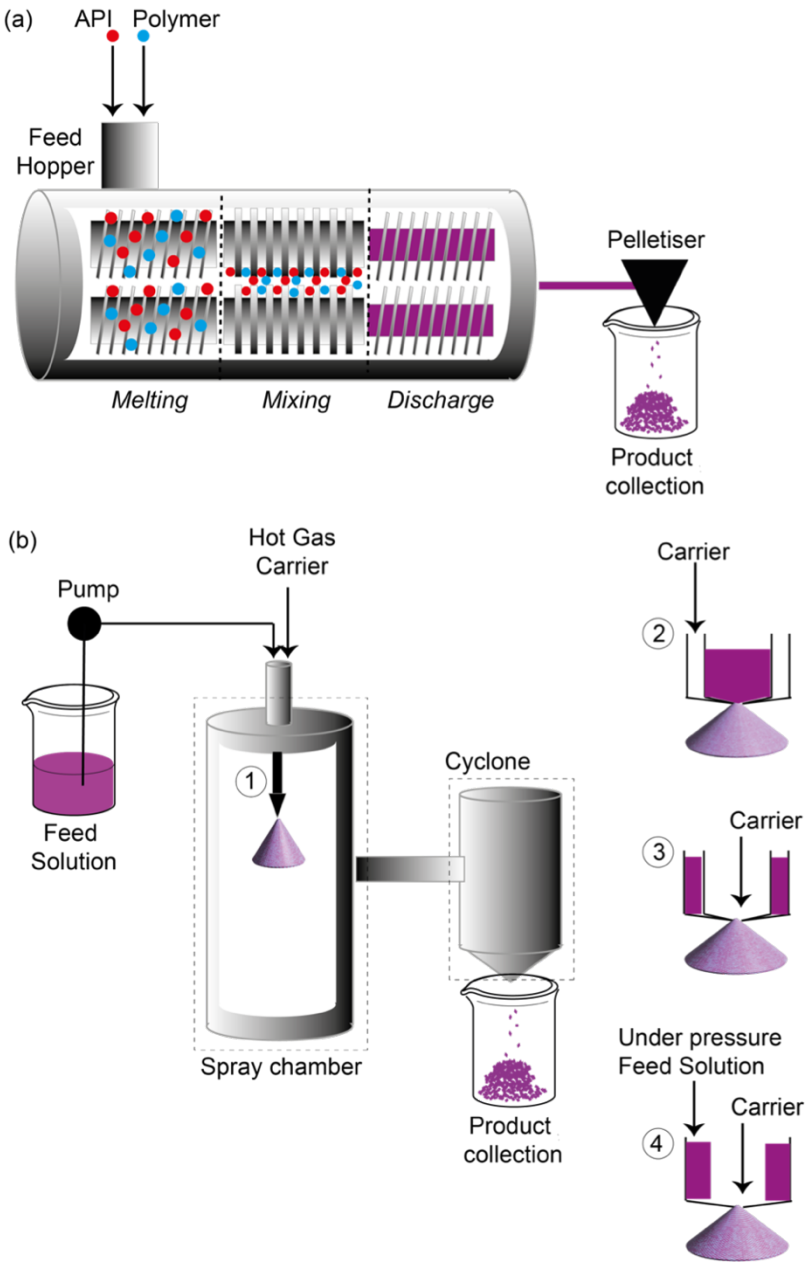

Figure 2.1. Schematics of (a) HME and (b) SD technologies for the preparation of ASDs. In (a), the three main steps are melting, mixing, and discharge where the material cools down and leaves the apparatus. Physical-chemical properties of the final product can be tuneable using different screws design and speed and controlling the temperature. In (b), the spray nozzle (component 1) of the chamber is available in several designs (components 2 – 4) based on the required specific applications. The figure is largely inspired by reference[5].

Polymers in ASDs play a key role in stabilising the thermodynamically metastable nature of the amorphous API. Polymers raise the inherent glass transition temperature (Tg) of the system, which effectively reduces the amorphous molecule's mobility, making it less likely that it will encounter other molecules to kick off the crystallisation process. Further amorphous stability enhancement can be achieved by the existence of specific chemical interaction between the drug and API species to further reduce molecular mobility of the amorphous drug, and increase the Tg of the formulation.[9] The formation of drug-polymer intermolecular interactions, such as hydrogen bonding (H-bond), ionic forces, π−π, or electrostatic interactions, are well established as the most significant interactions capable of stabilising dispersed systems[8] by inhibiting recrystallisation phenomena in the amorphous matrix and preventing competitive API−API or polymer−polymer intramolecular interactions. The identification and the understanding of the physical stability of ASDs remain a significant challenge and opens exciting future prospective designing ASDs stabilised by suitable and tuneable API-polymer interactions.[10]

Historically, thermal analysis methods, such as differential scanning calorimetry (DSC) and temperature-modulated DSC, have often been employed to elucidate API-polymer interactions in ASDs, allow Tg measurements from which miscibility of the various ASD components can be inferred from.[11,12] One such approach is the Gordon−Taylor model [13] hat estimates the Tg of an ideal binary mixture (Tg_{mix}), where significant deviations between the predicted Tg_{mix} and experimentally determined Tg provide useful information about interactions between the various constituents of the mixture, and potentially repulsive interactions which destabilise the system.[14,15]

A range of analytical methods including vibrational, Raman, and Fourier-transform infrared (FT-IR) spectroscopies have been used to provide atomic scale

information about solid dispersions. Raman applications specifically include the measurements of crystallisation rate,[16] while confocal Raman microscopy and Raman imaging have been employed in mapping solid dispersions to identify and discriminate crystalline/amorphous domains[17] thereby providing indirect information about the existence of API-polymer interactions. Evidence of recrystallisation phenomena can be observed from changes in band wavelength and comparison of bands intensity ratio or from the study of spatially time-resolved Raman generated using multivariate curve resolution that leads to monitor the evolution of an amorphous drug in ASD. FT-IR methods probe H-bond in specific functional groups such as hydroxyl, amino, and carbonyl groups and permit identification of this specific interaction in the API and/or the polymer.[18] It has been shown that when those functional groups are involved in H-bond interactions, a simultaneous decrease in the stretching frequency and a widening of their absorption bands are observed due to smaller intermolecular distances between the donor−acceptor groups.[19]

Solid-state Nuclear Magnetic Resonance (NMR) has emerged as a significantly powerful tool for accessing structural and dynamics information across the biological, chemical, material and physical sciences.[20,21] In particular, NMR plays an important role in pharmaceutical sciences[22,23] to enable structural understanding of API [24] and polymer[25,26] identify crystalline polymorphs[27], monitor drug recrystallisation phenomena from amorphous systems, and understand API-polymer interactions in ASDs.[28,29] The latter direction has been reviewed in 2014[39] and the purpose of this review is to discuss the recent exciting literature in the field while the interested readers are referred to several excellent monographs for the basics of NMR[40-43] and in the solid-state.[20,44,45] This review specifically reports on experimental NMR approaches to identify the presence of inter and intramolecular API-polymer interactions in ASDs prepared

by HME or SD technologies with examples based on a range of structurally different drugs and polymers.

One-dimensional (1D) experiments can be employed to highlight the presence of API-polymer interactions based on changes in chemical shifts for certain signal(s) in the spectra of the ASD compared with those of the amorphous API or polymer. 1D experiments are also useful to identity API recrystallisation processes from line shape analysis and relaxation measurements. We then show that the nature of the API-polymer interactions can be revealed by two-dimensional (2D) homo- and hetero-nuclear NMR correlations. In particular, we exemplify ^{1}H-^{13}C/^{19}F heteronuclear correlation (HETCOR) and ^{1}H-^{1}H dipolar double quantum (DQ) correlation as experiments identifying site-specific intermolecular contacts between API and polymer. Finally, we reveal how 2D experiment carried out at ultra-fast magic angle spinning (MAS) frequency (> 60 kHz) and very-high magnetic field (> 600 MHz, 14.1 T) and involving quadrupolar and/or low gyromagnetic nuclei (*i.e.* ^{14}N) can be used to probe API- polymer interactions.

2.4 Chemical shift as a unique observable of API-polymer interaction

The most straightforward experimental approaches currently used to characterise novel ASDs often include 1D NMR spectra data collection involving most, if not all, NMR active isotopes. This is accomplished from typically recording ^{1}H, ^{19}F, ^{13}C and ^{15}N NMR nuclei (as applicable) in which the chemical shielding interactions have been demonstrated to be very sensitive to subtle changes in local electronic environment, indicating the presence of API-polymer interactions in ASDs.

Solid-state NMR spectroscopy deals with powder samples consisting of many crystallites randomly oriented, hence the nuclear spin interactions such as chemical shielding, dipole- dipole coupling, and in cases involving nuclear spin larger than 1/2 (e.g., ^{14}N), quadrupolar coupling, are all orientation dependent (or anisotropic). This results in a range of resonance frequencies leading to NMR signal broadening.[20,44] These anisotropic interactions can be successfully average out by magic angle spinning (MAS), in which the sample is spun at an angle of 54.7° (magic angle) with respect the direction of static magnetic field. Under conditions where the MAS frequency is in the same order of magnitude (or greater) than the NMR interactions, the broadened resonances observed in static (non spinning) solid-state NMR spectra largely vanish to yield narrower lines.

The direct observation of ^{1}H and ^{19}F NMR signals have been used to detect polymorphs in crystalline samples, to distinguish multiple APIs in ASDs, and have allowed the identification of molecular interactions between various components of the dispersion from chemical shift changes.[8,39] In addition, in 1D experiments, comparison of linewidths can be used to discriminate crystalline API from amorphous API as the latter experiences severe inhomogeneous line broadening

arising from a large distribution of chemical environments randomly distributed[39,46], an effect that is not averaged out by MAS. The low receptivity of ^{13}C and ^{15}N arising from both low natural abundance (1.1 and 0.4%, respectively) and poor intrinsic sensitivity can significantly be overcome by the transfer of polarisation from highly receptive nuclei (usually ^{1}H or ^{19}F). In the solid state, this now routine approach is called cross polarisation (CP) in which the polarisation transfer is radio frequency driven by heteronuclear dipolar coupling.[45] This allows for spectra with higher signal-to-noise ratios to be obtained in a reasonable amount of experimental time (hours) for most ASDs even at relatively high API loading.

Figure 2.2 shows 1D ^{13}C and ^{15}N CP spectra that were successfully exploited to highlight H- bond interactions in ASDs between ketoconazole (KTZ) and a range of different polymers (such as poly(acrylic acid) (PAA), poly(2-hydroxyethylmethacrylate) (PHEMA) and poly(vinyl pyrrolidone) (PVP)) with API concentration ranging between 4 and 12 wt %.[28] The ^{13}C CP MAS spectrum (**Figure 2.2(a)**) of the KTZ-PAA ASD reveals that the *C*OOH signal of PAA experiences a change of shift to lower frequency relative to the physical mixture and PAA itself, that can be attributed to the disruption of the dimeric H-bond of PAA, hence indicating that the *C*OOH is involved in stabilising the amorphous API. The ^{15}N CP MAS spectra of KTZ- PAA ASDs at different PAA loading (**Figure 2.2(b)**) show the existence of two N3 imidazole nitrogen signals at around 260 and 240 ppm that can be attributed to "free" KTZ and to a N3 engaged in an H-bond, respectively, as this 20 ppm change in shift is typical of H-bond interactions and supports that the most basic imidazole N3 nitrogen is engaged in stabilising the KTZ.[47] No changes in ^{15}N chemical shift is observed for the other imidazole nitrogen N1 signal or the piperazine nitrogens highlighting that the KTZ-PAA H-

bond interactions occur exclusively between the most basic imidazole N3 nitrogen and the COOH PAA.

While no changes in ^{13}C chemical shift are observed between KTZ, KTZ-PHEMA ASD and physical mixture (**Figure 2.2(c)**), the ^{15}N chemical shift of the N3 nitrogen KTZ in KTZ-PHEMA ASD is observed at a lower frequency than in KTZ itself and indicates that this site is involved in the formation of API-polymer interaction likely with the -OH group of PHEMA.

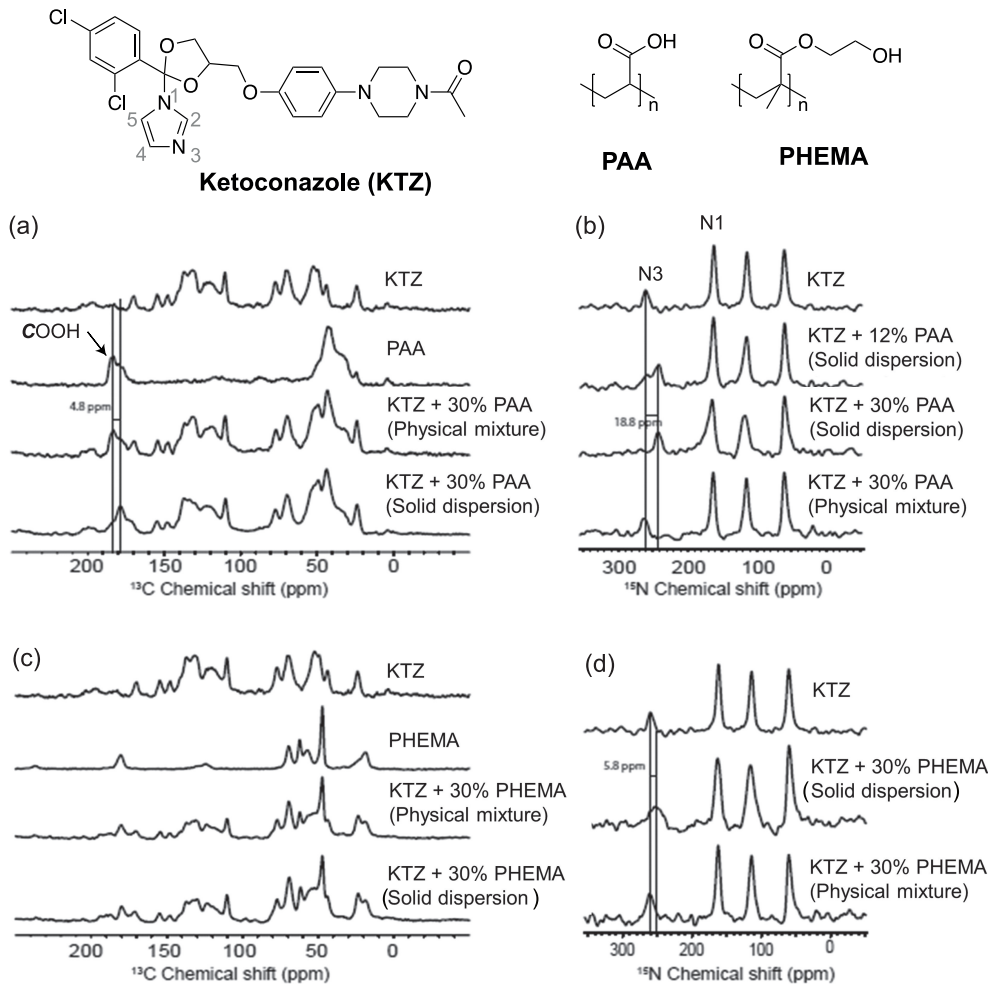

Figure 2.2. Comparison of the (a,c) ^{13}C and (b,d) ^{15}N CP MAS NMR spectra of amorphous KTZ, PAA and PHEMA polymers, their physical mixtures and ASDs. The vertical black lines highlight differences in chemical shifts in the ASDs with respect the individual components, indicating the presence of API-polymer interactions. The chemical structures of KTZ and polymers are shown on the top of the figure. Reprinted with permission from[28]. Copyright 2015 American Chemical Society.

Recently, a new class of ASDs has emerged, where a second polymer is added to the formulation. The capability of NMR to characterise this complex ternary ASD has been demonstrated using KTZ-HPMC-PAA ASD.[48] While no changes in

chemical shift were highlighted in the ^{13}C spectra for the binary system KTZ-HPMC ASDs (**Figure 2.3(a))** and excluded the possibility of interaction between the compounds, ^{13}C spectroscopic data for both KTZ-PAA and KTZ-HPMC-PAA dispersions (**Figure 2.3(b)** and **(c)**) showed some interesting similar spectral features. In both systems, the intensity of the peak corresponding to the PAA dimer form (at 182 ppm) decreases with respect to the free form (at 177 ppm), changes intensity across the drug loading and, interestingly, a new peak at 172 ppm emerges corresponding to hydrogen bonded KET. Changes in chemical shift have been also highlighted in the ^{15}N spectra for both the binary KTZ-PAA and the ternary KTZ-HPMC-PAA ASDs (**Figure 2.3(d)**), suggesting of a proton transfer or salt formation.[32] These results probe the presence of ionic and H-bond interactions both in binary KTZ-PAA and ternary KTZ-PAA-HPMC ASDs, supported respectively, by the loss of PAA dimers resulting from the KTZ-PAA interaction and by the presence of the signal at 172 ppm that indicate the presence of hydrogen bonded KTZ.

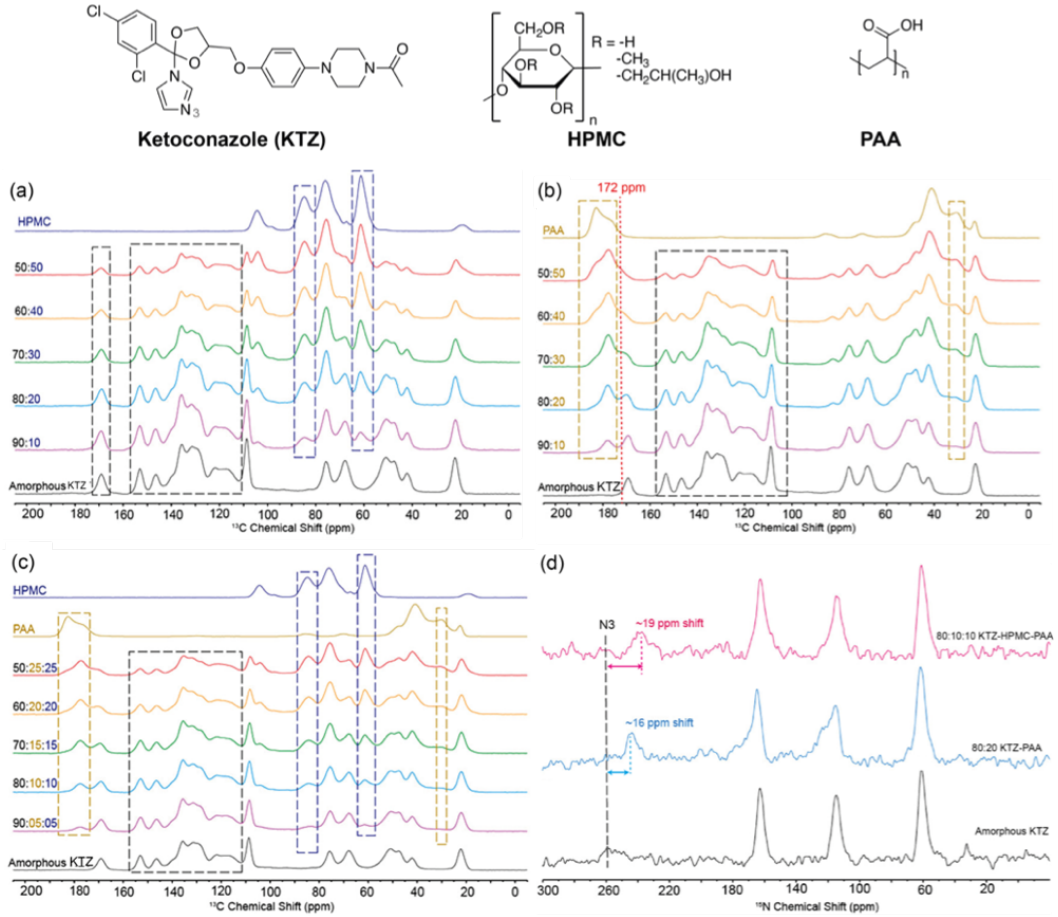

Figure 2.3. ^{13}C CP MAS spectra of (a) KTZ-HPMC, (b) KTZ-PAA, and (c) KTZ-HPMC-PAA ASDs at different drug loadings. (d) ^{15}N CP MAS spectra of amorphous KZT, KTZ-PAA, and the ternary KTZ-HPMC-PAA ASDs. Chemical structure of KTZ, HPMC, and PAA are given on the top of the figure. Reprinted with permission from[48]. Copyright 2020 American Chemical Society.

Acid-base interactions are also known to contribute significantly to API stabilisation in ASDs and are often much stronger than H-bonds, therefore offering exciting opportunities and attracting significant interests. However, only few acidic polymers in the pharmaceutical armoury are known and include PAA, hydroxypropylmethylcellulose (HPMC), hydroxypropylmethylcellulose acetate

succinate (HPMC-AS) and poly(methacrylic acid-co-ethyl acrylate). These are, however, weakly acidic and not prone to protonate weakly basic moieties in APIs. Polystyrene sulfonic acid (PSSA) polymer, which is currently not a pharmaceutically approved polymer, turned out as a promising inhibiter of re-crystallisation for several APIs in ASDs by forming strong acid-base interactions.[49] Given that both lapatinib (LB) and Gefitinib (GB) contain a range of basic nitrogen containing moieties such as anilinoquinazoline and amino groups, ^{15}N NMR spectroscopy has revealed itself to enable identification of their acid-base interactions with HPMC-phthalate (HPMC-P) and PSSA acidic polymers (**Figure 2.4**)[29,30] by taking advantages of the sensitivity of ^{15}N chemical shifts to strong H-bond and protonation.[50] Comparison of the ^{15}N CP MAS NMR spectra of crystalline LB freebase, crystalline LB phthalate salt with their amorphous LB and LB-HPMC-P ASDs (**Figure 2.4(a)**) clearly show two peaks at around -350 and -335 ppm in the ASD that are attributed to the free amino N4 and protonated N4 signals, respectively. This therefore indicates the presence of acid base interaction between the protonated N4 in LB with HPMC-P, presumably via the -COO^- group and reveals for the amino (N4) signal (see grey shadow area) a significant change of chemical shift of around 17 ppm as expected between the LB phthalate salt (in which the N4 site is protonated) and freebase. While the N4 amine peak in the ^{15}N spectrum of amorphous LB appears at around -348 ppm as a single broad peak, the corresponding spectrum of the LB-HPMC-P ASDs shows the presence of two clear peak at around -350 and -355 ppm attributable respectively to the free amorphous amino N4 signal and protonated N4, as per comparison with the spectra of amorphous LB and LB phthalate salt reference sample. The existence of the protonated amine in the ASDs almost certainly means that a solid solution of the protonated LB at N4 unit in the negatively charged polymer exists. Interestingly, for the HPMC-P dispersion, the position of the N1 aniline peak does

not experience any significative change. This suggest that N1 sites are not involved in any interaction and confirming that this nitrogen is not protonated in the dispersions.

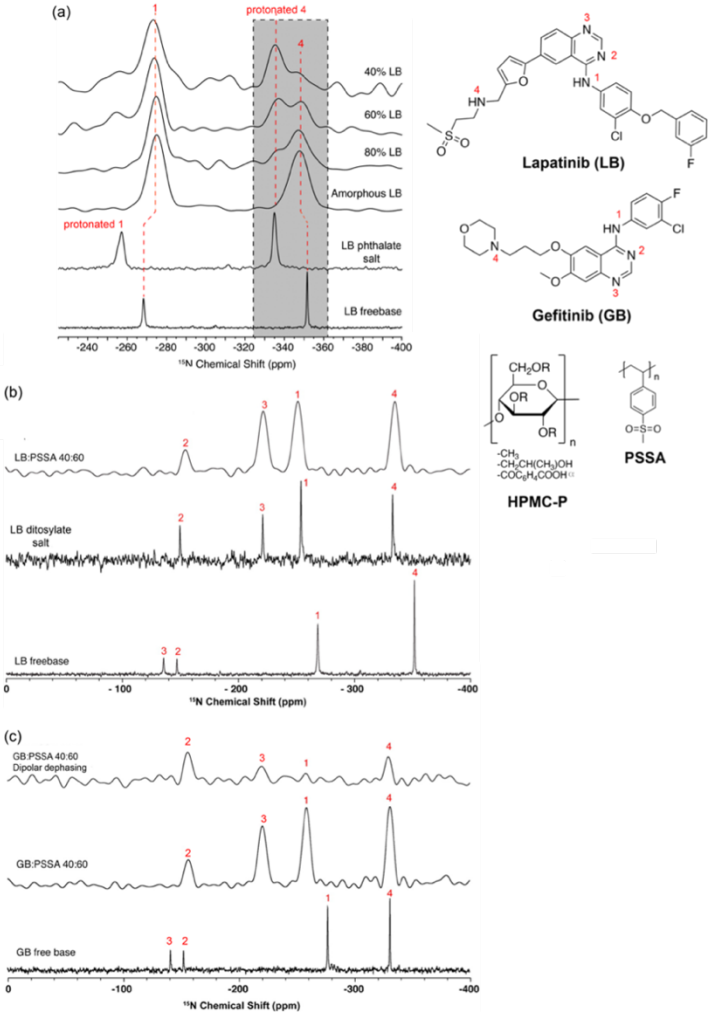

Figure 2.4. (a) ^{15}N CP spectra of 40, 60, 80 wt % LB-HPMC-P ASDs, amorphous LB, LB phthalate salt and freebase drug. The peak at -335 ppm in the ASD's spectrum indicates the presence of protonated amino group, hence highlighting the presence of API-polymer ionic interaction. Reprinted with permission from[29]. Copyright 2015 American Chemical Society. (b) ^{15}N CP spectra of LB freebase, LB ditosylate salt and 40 wt % LB-PSSA ASD. The large change in chemical shifts observed for N2 and N3 between the LB freebase and ASDs indicates protonation. (c) ^{15}N CP spectra of gefitinib (GB) freebase, 40 wt % LB-PSSA ASD and ^{15}N dipolar dephased spectrum of LB-PSSA ASD. Spectral assignments and chemical structures of LB, GB, HPMC-P, and PSSA are given in the figure. Reprinted with permission from[30]. Copyright 2016 American Chemical Society.

A similar approach was used to probe acid-base interactions in LB-PSSA and GB-PSSA ASDs and the corresponding ^{15}N CP MAS NMR[29,30] spectra of LB, GB, and ASDs with PSSA (**Figures 2.4(b)** and **(c)**) reveal important contribution to API-polymer interactions.[50] In both LB- and GB-PSSA ASD, the ^{15}N NMR signals of the quinazoline N sites (N3 both in LB and in GB) undergo a large shift of ~ 80 ppm to higher frequency with respect crystalline LB/GB, indicating preferential protonation of this more basic quinazoline N site. Moreover, protonation of both amine N1 and N4 signals in LB-PSSA ASD is evidenced by their similar ^{15}N shifts vs. LB salt confirming double protonation of the API by PSSA and strong acid-base interactions.

The presence of API-polymer interactions in the GB-PSSA ASD established above involving the quinazoline N site is not linked to a change in ^{15}N chemical shift of the ternary amine N4 (**Figure 2.4(c)**). Nevertheless, evidence of N4 being involved in the API-polymer interaction is supported by dipolar dephasing (interrupted decoupling) experiments[51] that selectively select nuclear spins strongly coupled to ^{1}H. The corresponding ^{15}N spectrum of the 40 wt % GB- PSSA ASD highlights lower signal intensity of the N1, N3, and N4 signals vs. N2, confirming their protonation.

Acid-base interactions have been also identified in indomethacin (IMC)-methacrylate copolymer Eudragit® E (EE) ASDs solely from ^{15}N NMR spectra[32] while overlapping ^{13}C signals between API and polymer prevented changes in chemical shifts to be observed. The ^{15}N CP MAS NMR spectra of the 20 – 60 wt % IMC-EE ASDs exhibit two peaks at around - 360 ppm, attributable to the EE amino signal, and at around -344 ppm, which intensity increases with drug loading. This is further supported by some ^{15}N ^{1}H dipolar dephasing experiment carried out on the 40 % wt IMC-EE ASD that clearly shows this latter signal at - 344 ppm with

reduced signal intensity, indicating strong coupling to a proton, hence suggesting a protonated EE amino signal involved in the acid-base interaction with the IMC.

Hydroxypropylmethylcellulose acetyl succinate polymer (HPMC-AS) has recently been widely used to stabilise API in ASDs.[34,35,38,52,53] This is due to its unique physical-chemical properties such as high glass transition temperature (around 120 °C) and the presence of both acetyl (A) and succinoyl (S) moieties (Figure 5) which allow for effective inhibition of drug crystallisation from amorphous dispersion forming hydrophobic interactions with the drug.[54,55] There is also evidence that HPMC-AS can stabilise drug in solution in *in vitro* systems and, potentially, the gastric milieu, further enhancing bioavailability of the drug by maintaining it at (or even above, at least temporarily) the saturation solubility of the drug.[56-58]

HPMC-AS was initially developed as a polymer for enteric coating of tablets, to prevent dissolution of tablets, and therefore the drug, in the stomach, or upper regions of the small intestine. Different ratios of the succinic acid (which confer pH dependent solubility) and acetic acid groups (which hinder solubility) render the different grades of the polymer soluble at different pH ranges, with three grades available. The different ratios of these groups may be important in forming bonds and interactions with API's.

The formation of specific API-polymer interactions as it has been explored in a study in which carbamazepine (CBZ) was formulated with HPMC, HPMC-A, and HPMC-S.[33] In this work, CBZ-HPMC, CBZ-HPMC-A, and CBZ-HPMC-S were prepared by SD methodology and the API-polymer contacts were determined from multinuclear 1D NMR spectra (**Figure 2.5**).

In crystalline CBZ, the amide C1 signal resonates at 159 ppm in the spectrum and is shifted upon CBZ dispersion in HPMC, HPMC-A, and HPMC-S polymers (**Figure 2.5(a)**). These changes could confirm the amorphous behaviour of the dispersions

as such changes in chemical shift between are consistent with the retention of intermolecular interactions between crystalline and amorphous specie[46], and can be used as rough indications of API-polymer interactions, that have to be confirmed by further investigations.

More interestingly, evidence of the presence of CBZ-polymer interactions in ASDs can be found by considering both the ^{1}H and ^{13}C NMR spectra shown in **Figure 2.5(b)** and **(c)**, respectively. In contrast with the spectra of HPMC and HPMC-A polymers, the evidence of a signal at 14 ppm in the ^{1}H ultra-fast MAS (70 kHz) spectrum of 33 wt % CBZ-HPMC-S ASDs, together with the shift of the carboxyl succinoyl group C4 signal, support the presence of H- bond between CBZ and HPMC-S.[25] In a similar way, the carbonyl of the acetyl substituent C2 signal slightly shifts to lower frequencies as drug load increases, indicating the presence of H-bond between CBZ and HPMC-A.

Figure 2.5(d) shows the ^{1}H-^{15}N CP-based HSQC filter experiment carried out on 33 wt % ^{15}N-labeled CBZ–HPMC/HPMC-A/HPMC-S ASDs. All ^{1}H spectra are dominated by the polymer signal at around 5.5 ppm, however an extra signal in the form of a shoulder at around 7.5 ppm is also observed for both the CBZ-HPMC-A and CBZ-HPMC-S. The presence of this signal at higher chemical shift corroborates the H-bond between the acetyl carbonyl and the CBZ's NH_2 and between both the succinoyl's carbonyls and the CBZ's NH_2 in CBZ-HPMC-A and CBZ- HPMC-S ADSs, respectively. Taking together, these results point out to the critical role that the subsistent groups A and S have in forming specific interactions with CBZ.

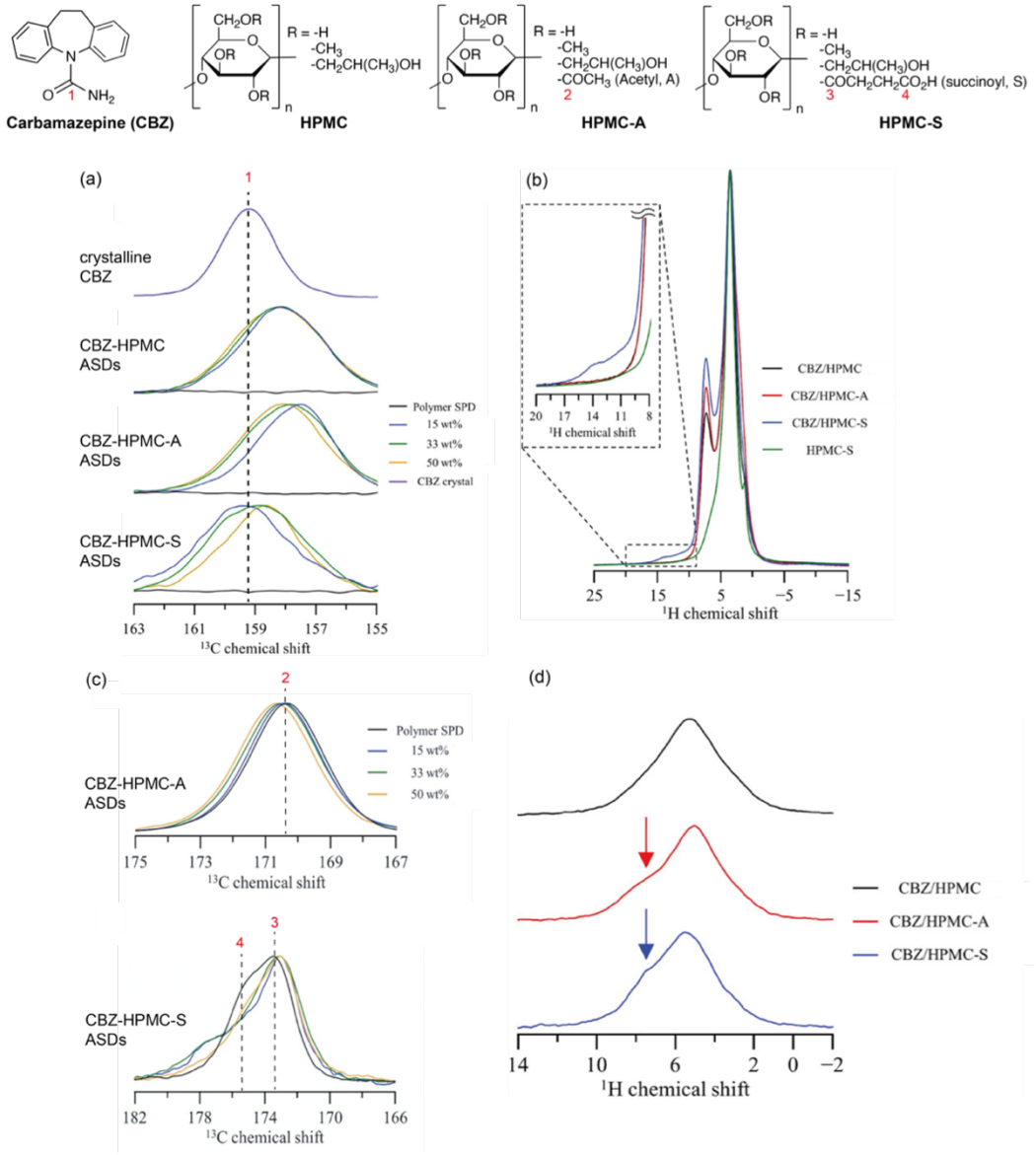

Figure 2.5. Magnified view of ^{13}C CP MAS NMR spectra of the (a) amide region of CBZ, (b) ^{1}H ultra-fast MAS spectra of 33 wt % CBZ-HPMC, HPMC-A, HPMC-S ASDs, and HPMC-S polymer, and (c) the carbonyls region of the polymers. (d) ^{15}N CP based HSQC filter ^{1}H MAS spectra of 33 wt % CBZ-HPMC, HPMC-A, and HPMC-S ASDs. The structure of CBZ, HPMC, HPMC-A and HPMC-S are given on the top of the figure. Reprinted with permission from[33]. Copyright 2019 American Chemical Society.

As previously reported, HPMC itself does not exhibit excellent ability of promoting the formation of H-bond with CBZ, while the use of α-Glycosyl rutin (Rutin-G), a non-polymeric additive, brings to the formation of CBZ-Rutin-G H-bond and hence leads to significantly stabilised amorphous CBZ. This outcome is supported by both 1D NMR experiments and 2D heteronuclear correlation NMR experiment and quantum mechanical calculations.[59]

Finally, the extraordinary versatility of NMR as an invaluable toolkit in the determination of the strength and extent of H-bond has been demonstrated in an exciting work in which felodipine (FEL) API-different PVP-substituted polymers ASDs were thoroughly studied.[60] Supported by changes in ^{13}C chemical shifts and spectral intensities the degree of FEL-polymer H-bond was rank in the following ordered as PVP > (poly(vinylpyrrolidone-co-vinylacetate)) PVP-VA > (poly(vinyl acetate)) PVAc. This result clearly indicates how the nature, strength and type of different H-bond acceptors influence the formation of effective and strong API-polymer interactions.

2.5 2D correlation NMR experiments as a toolkit to probe API-polymer contacts at molecular level.

At the molecular level, the chemical species directly involved in the API-polymer interactions, as well as the observation of structural effects can be obtained from 2D NMR approaches. 2D correlation experiments often allow the direct detection of API–polymer contacts by correlating different nuclei, restoring spectral resolution and/or reintroducing through-space dipolar coupling interactions averaged by MAS. The HETCOR experiment has proven itself a useful technique in that respect and enables correlation spectra between heteronuclei commonly present in API (e.g., usually ^{13}C but also recently ^{19}F) with the ^{1}H nucleus. The use of the ^{1}H nucleus in one of the spectral dimensions enhances the sensitivity of the experiment while the use of a heteronucleus in the other spectral dimension enhances the specificity.

An empiric estimation of the range of spin diffusion effects occurring in an HETCOR experiment can be obtained according to **Equation 2.1**, in which L, D and t are the maximum diffusion path length, spin diffusion coefficient and the time, respectively, while the brackets denote an ensemble average:

$$\langle L^2 \rangle = 6\ D\ t \qquad \textbf{Eq. 2.1}$$

For a 500 μs contact time, **Eq. 2.1** yields an average L of about 5 Å as a maximum range over which ^{1}H-^{1}H spin diffusion can occur within the ^{1}H spin-lock during the contact time of a CP-HETCOR experiment. Regarding the direct dipolar ^{1}H-X interaction, that magnitude of this interaction that is transferred by the CP-HETCOR experiment is limited in range to 3-5 Å.[12] Experimentally, it has been

demonstrated that ^{19}F-^{13}C HETCOR experiments carried out at contact times of 6 ms and 8 ms can directly probe API-polymer contacts for spatially close species of 5.5 Å and 8 Å, respectively.[61]

In addition to the HETCOR experiment, methods based on the detection of homonuclear dipolar coupling, such as ^{1}H-^{1}H double quantum (DQ) correlation (for example, using the back to back (BABA) recoupling scheme[62]) have been exploited to detect API-polymer proximities in ASDs.

More recently molecular associations have been also identified via ^{14}N-^{1}H 2D experiments methodology. Despite the high natural abundance of ^{14}N (99.6 %), its low gyromagnetic ratio and large quadrupolar interaction make its direct detection in the solid state a challenge and the development of indirectly detected ^{14}N via ^{1}H, for example via 2D ^{14}N-^{1}H HMQC (heteronuclear multiple quantum coherence)[63,64] at high magnetic field (> 16.4 T) and ultra-fast MAS frequency (> 50 kHz), has enabled to solve this challenge and opened up new adventures, in particular in pharmaceutical sciences.[38,65-68]

Recent technological advancements have allowed for the development of both magnets that can handle very-high magnetic field and probes that can operate under ultra-fast MAS condition. In particular, this latter progress has benefitted the significantly increase in resolution of ^{1}H solid-state NMR spectra by averaging out of the ^{1}H-^{1}H mononuclear dipolar interactions and opening the way to access further detailed on the structure and dynamics information in pharmaceutical formulations.[69]

Clofazimine (CLF) API - HPMC-P polymer molecular interaction has been elucidated from 1D and 2D experiments.[31] **Figure 2.6(a)** shows the ^{13}C CP MAS NMR spectra of CLF-HPMC-P dispersions as a function of different API loadings. The carboxyl acid in HPMC-P (red in **Figures 2.6(a)** and **(b)**) and CHN in CLF (green) signals were used as spy signals to detect the presence of API-polymer

interactions, and interestingly, variations in chemical shifts for both signals are observed. The changes in ^{13}C chemical shifts observed for the carboxyl acid (from around 170 ppm HPMC-P to 174.2 ppm in the dispersions) coupled to the one of the CNH in the ASD (by 2.5 ppm against the amorphous CLF) are attributed to carboxylate group bonding to CLF.

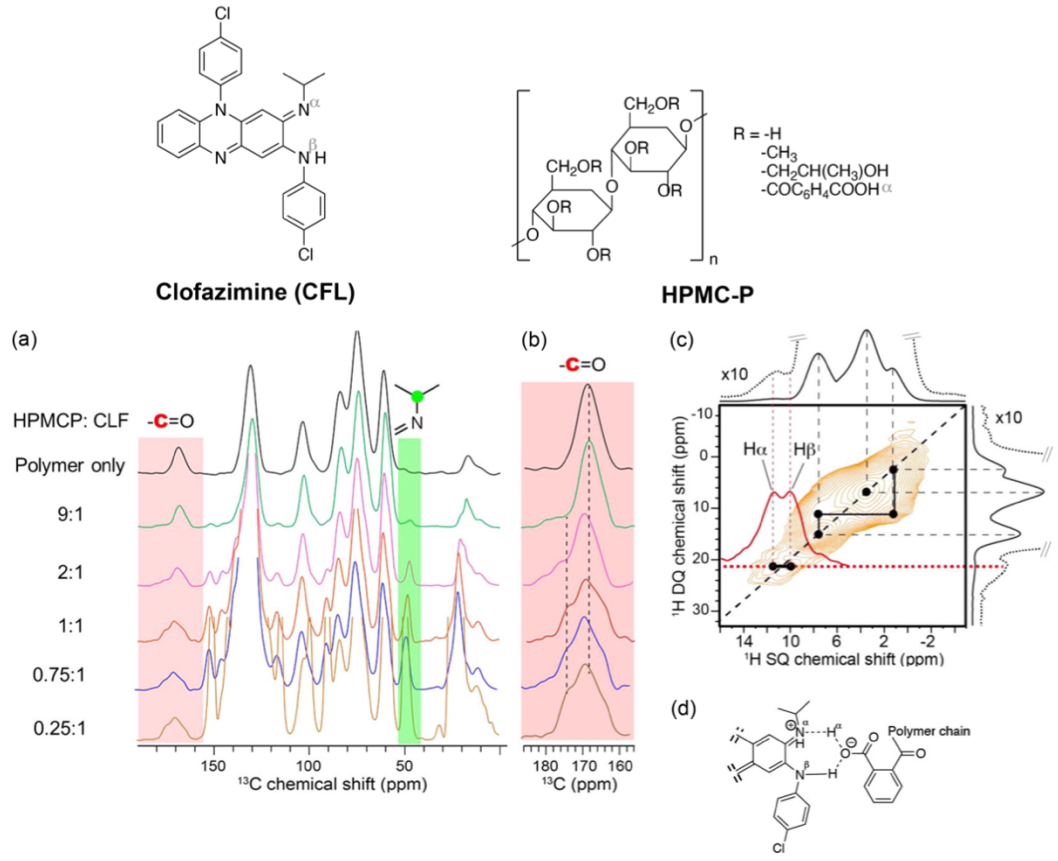

Figure 2.6. (a) ^{13}C CP MAS NMR spectra of CLF−HPMC-P dispersions as a function of API content. (b) Magnified view of the 157−183 ppm region. (c) ^{1}H-^{1}H DQ BABA correlation spectrum of 50 wt % CLF-HPMC-PASD exhibits a correlation between Hα and Hβ indicating the presence of carboxylate - CNH molecular interaction. The ^{1}H spectra of the CLF-HPMC-P dispersion is given on the top. (d) Schematic representation of the API-polymer interaction via proton transfer. The chemical structures of CFL and HPMC-P are given on top. Reprinted with permission from[31]. Copyright 2016 American Chemical Society.

In order to further refine the nature of the molecular interaction occurring in this dispersion, useful and detailed information were obtained from 2D ^{1}H-^{1}H DQ BABA experiment on the 50 wt % CFL-HPMC-P ASD. The 1D ^{1}H NMR spectrum obtained under ultra-fast MAS condition of 60 kHz (top spectrum in **Figure 2.6(c)**) shows

two signals at 11.5 and 10 ppm which are correlated as revealed from the 2D ^{1}H-^{1}H DQ BABA spectrum (**Figure 2.6(c)**). Interestingly, these signals have equal peak intensity (see red slice in **Figure 2.6(c)**) and their high chemical shits indicate strong H-bonding of a proton adjacent to a nitrogen atom. Considering the chemical structures of both API and polymer, these two new resonances can be assigned to the existing Nβ -Nα and the newly formed Nα-Hα contacts (see **Figure 2.6(d)**). These molecular interactions indicate a transfer proton mechanism from Hα to Nα with a concerted formation of the interaction between COO^- moieties with Nβ.

The capability of HPMC derivatives such as HPMC-P and HPMC-AS polymers in stabilising amorphous APIs in ASDs by forming API-polymer interactions has been also demonstrated with posaconazole (POSA, **Figure 2.7**).[34] ^{1}H-^{13}C HETCOR spectrum of 30 wt % POSA–HPMC-AS ASD (**Figure 2.7(a)**) and reveal correlated ^{13}C and ^{1}H signals at around 154 and 2 ppm, respectively, demonstrating an intermolecular H-bond interaction between the carbonyl C41 carbon of the POSA triazole ring and the HPMC-AS hydroxyl group. Another electrostatic intermolecular interaction is revealed in the HETCOR spectrum of the 30 wt % isotopically labelled ^{13}C-C44, ^{15}N-N42 and ^{15}N-N43 sites POSA in HPMC-AS ASD (**Figure 2.7(b)**) from the correlation involving ^{13}C at 136 ppm with ^{1}H at 4 ppm that indicates spatial contact of the POSA triazole ring with the -CH_2 adjacent to the carboxylic moiety in the S group. In a similar fashion, the HETCOR spectrum of 30 wt % POSA–HPMC-P ASD (**Figure 2.7(c)**) highlights two spatial proximities: an electrostatic interaction between the HPMC-S carboxylic group with the POSA triazole ring at 168 ppm/4 ppm; and a π-π aromatic stacking interaction between the HPMC-P aromatic carbons and the POSA proton attached to C46/47. These data clearly indicate the role played by the substituent groups of the HPMC

backbone, as the presence of hydroxyl and carbonyl groups, triazole moieties and difluorophenyl rings favour the potential formation of strong interactions with the A and S substituents of HPMC-AS.

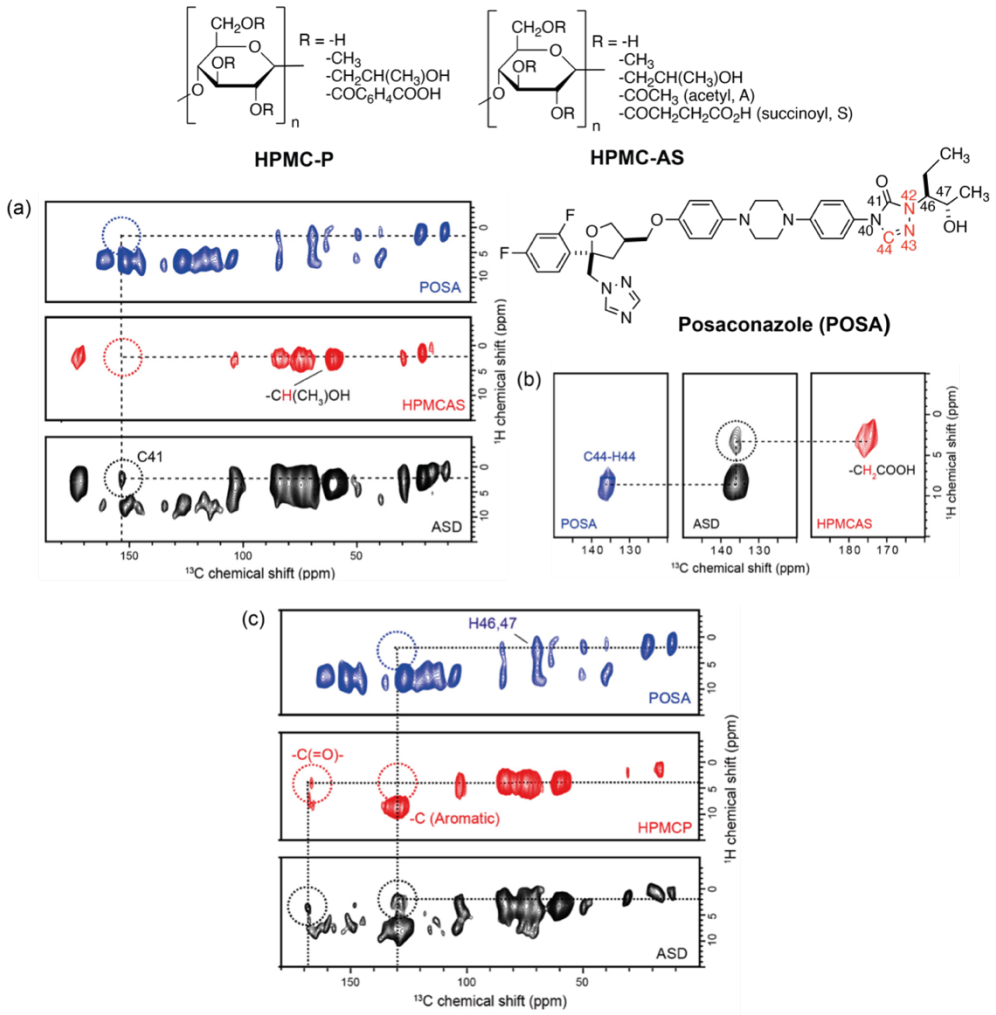

Figure 2.7. (a) ^{13}C CP HETCOR spectra of POSA, HPMC-AS and 30 wt % POSA–HPMC-AS ASD. (b) ^{13}C CP HETCOR spectra of isotopically labelled ^{13}C-C44, ^{15}N-N42 and ^{15}N-N43 sites POSA, as an ASD in HPMC-AS, and HPMC-AS. (c) ^{13}C CP HETCOR spectra of POSA, HPMC-P and 30 wt % POSA–HPMC-AS ASD. The correlations highlighted in the black circle in all ASDs HETCOR spectra indicate the carbon signals involved in API-polymer interactions. All the spectra were carried out at a MAS frequency of 12 kHz, with a contact time of 2 ms. Chemical structures of POSA, HPMC-P and HPMC-AS are given on the bottom of the figure. Isotopically labelled C44, N42 and N43 atoms are highlighted in red. Reprinted with permission from[34]. Copyright 2019 American Chemical Society.

The presence of F atoms in the chemical structure of POSA also allows further investigation on the presence of API-polymer interactions involving these fluorinated moieties and exciting outcomes have been reported from the characterisation of a 30 wt % POSA-HPMC-AS ASD using 2D ^{1}H-^{19}F HETCOR.[35] The corresponding spectra for crystalline and amorphous POSA (blue and red, respectively in **Figure 2. 8(a)**) show similar correlations between the aromatic fluorines of the difluorophenyl group with both aromatic protons (7.5 ppm) and aliphatic protons (1.5 ppm), due to intermolecular “head-to-tail” packing. The extra correlation at around 4 ppm that appears in the HETCOR spectrum of the ASD (**Figures 2.8(a)** and **(b)**) additionally suggests the presence of an H-bond POSA-HPMC-AS interaction, likely between the hydroxyl group of HPMC-AS and the difluorophenyl group of POSA, as schematically illustrated in **Figure 2.8(c).**

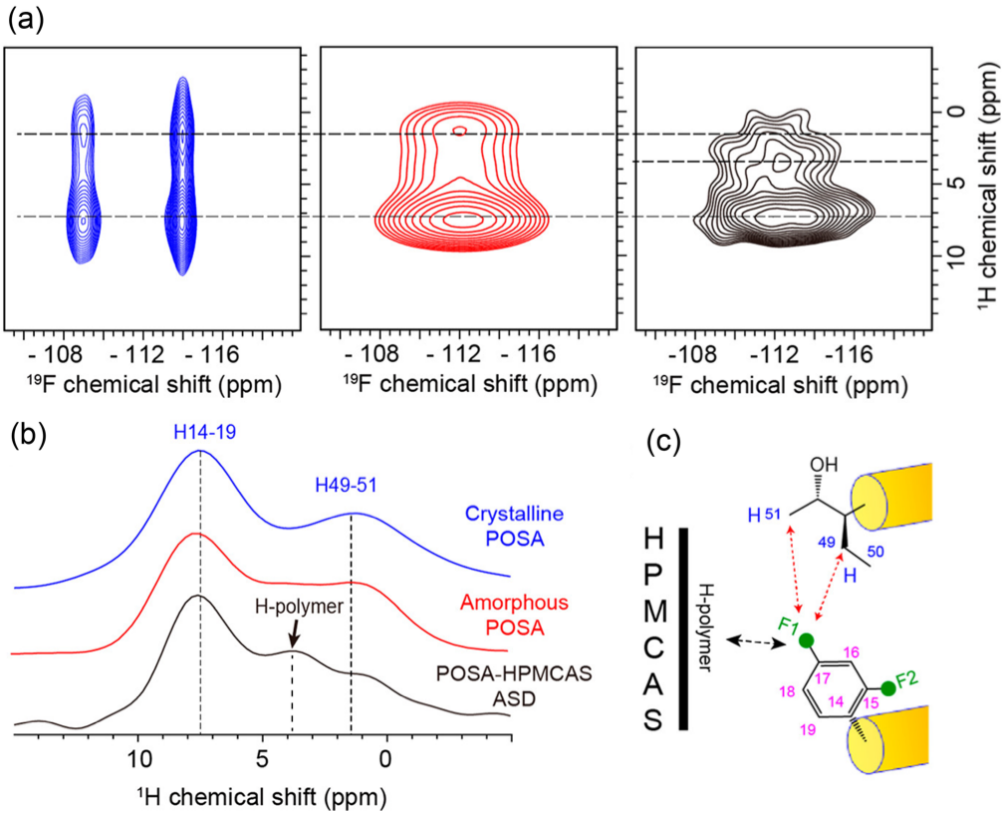

Figure 2.8. (a) ^{1}H-^{19}F HETCOR spectra of crystalline (blue), amorphous POSA (red), and 30 wt. % POSA–HPMC-AS ASD (black). (b) ^{1}H spectrum extracted from the HETCOR spectra at ^{19}F chemical shifts of around -114 (for crystalline POSA), -112 (for amorphous POSA), and -112 ppm (for the ASD), respectively. (c) Schematic representation of intermolecular interactions in amorphous POSA (red dashed arrows) and between POSA and HPMC-AS (black dashed arrow). Reprinted with permission from[35]. Copyright 2020 American Chemical Society.

The versatility of HPMC-AS in forming drug polymer interactions, hence stabilising ASDs has also been probed in the acetaminophen-HPMC-AS dispersions (**Figure 2.9**).[38] For the ASDs with drug loading > 20 wt %, ^{1}H-^{13}C HETCOR correlation experiments identify spatial proximities between aromatic protons of the acetaminophen with the cellulose backbone protons of the HPMC-AS polymer while the presence of H-bonds between API and polymer was established from

^{14}N-^{1}H HMQC experiments. The ^{14}N-^{1}H HMQC spectra of a 10 and 20 wt % acetaminophen-HPMC-AS ASDs (**Figure 2.9**) indicate the presence of interactions between the acetaminophen ^{14}N signal with the -OCH_3 signal (H8) of the polymer, hence highlighting a closer contact between API and polymer that can be reasonable attributed to the presence of H-bond between this amide donor and oxygen acceptor. In contrast, the ^{14}N-^{1}H HMQC spectrum of the 40 wt % ASD exhibits correlations between the acetaminophen ^{14}N signal with all acetaminophen protons in the crystalline form, suggesting the absence of API-polymer interaction, instability, and API recrystallisation with loading > 40 wt %.

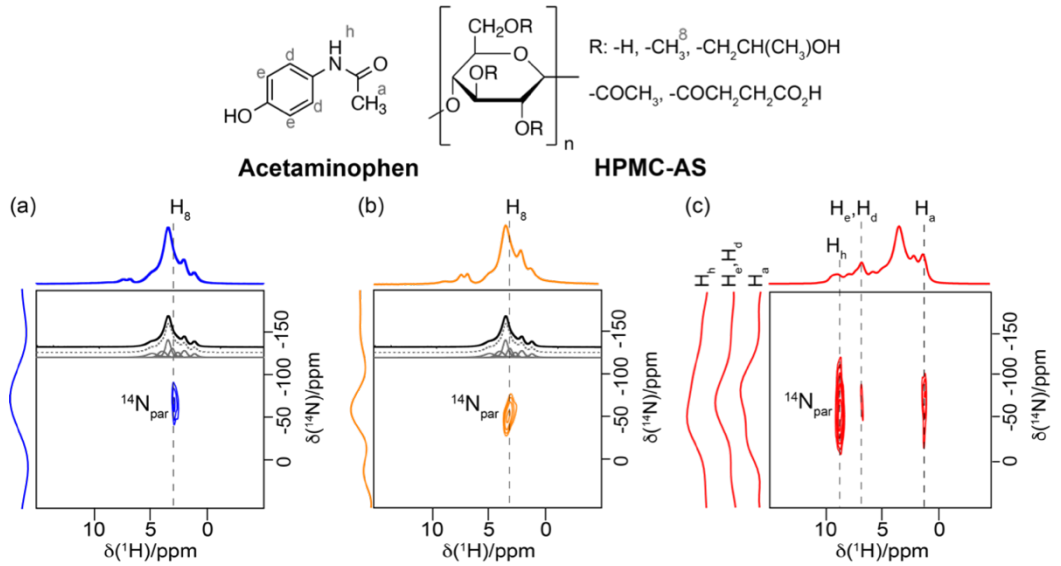

Figure 2.9. ^{14}N-^{1}H HMQC spectra of 10 wt % (blue), 20 wt % (orange), and 40 wt % (red) acetaminophen–HPMC-AS ASDs. The deconvoluted ^{1}H spectra of the HPMC-AS are given in black. Spectra on the left of the 2D HMQC are the ^{14}N slices extracted at the indicated ^{1}H chemical shift in dashed black lines. Chemical structures of acetaminophen and HPMC-AS are given on top. Reprinted with permission from[38]. Copyright 2021 American Chemical Society.

The evaluation and the evidence of API-polymer interactions in rafoxanide (RAF)-PVP ASDs at drug loading of 25, 33, and 50 wt % (**Figure 2.10**), prepared via SD using two different feed solutions aqueous (a 70%:30% mixture of 0.1 M NaOH solution and acetone) and organic (80%:20% acetone/ethanol mixture), have been probed using 1D ^{13}C and ^{15}N CP experiments and further investigated carrying out 2D ^{1}H-^{1}H RFDR (radio frequency driven recoupling)[37] experiments at MAS = 110 kHz, at 18.8T (**Figure 2.10**), that leads to determine ^{1}H-^{1}H proximities by recoupling homonuclear dipolar interactions. For the 50 wt % RAF-PVP ASD made from aqueous condition, the spectrum recorded at short mixing time τ_{RFDR} of 7.2 ms (**Figure 2.10(a)**) shown correlation between the PVP aliphatic protons (2-3.5 ppm) with the RAF aromatic protons (ca. 7.5 ppm), and more importantly, exhibits long range intermolecular correlations between RAF aromatic protons and PVP aliphatic protons (peaks circled in red). Moreover, thanks to the enhanced ^{1}H resolution likely due to the benefit of very-high magnetic field together with the ultra-fast MAS condition, the enlarged RFDR spectrum (**Figure 2.10 (c)**) illustrates the presence of cross peaks between the amide ^{1}H of RAF with the aliphatic ^{1}H of PVP and highlights the expected amide – aromatic protons intramolecular correlation, indicating the presence of API-polymer intermolecular H-bond interaction involving RAF and PVP. Reasonably, the formation of this interaction is due to the aqueous feed solution used during the SD process. In the aqueous condition, the presence of the NaOH can ionise the RAF phenolic hydroxyl group promotion the formation of H-bond between the RAF amide, as a donor, and PVP carbonyl, as an acceptor.

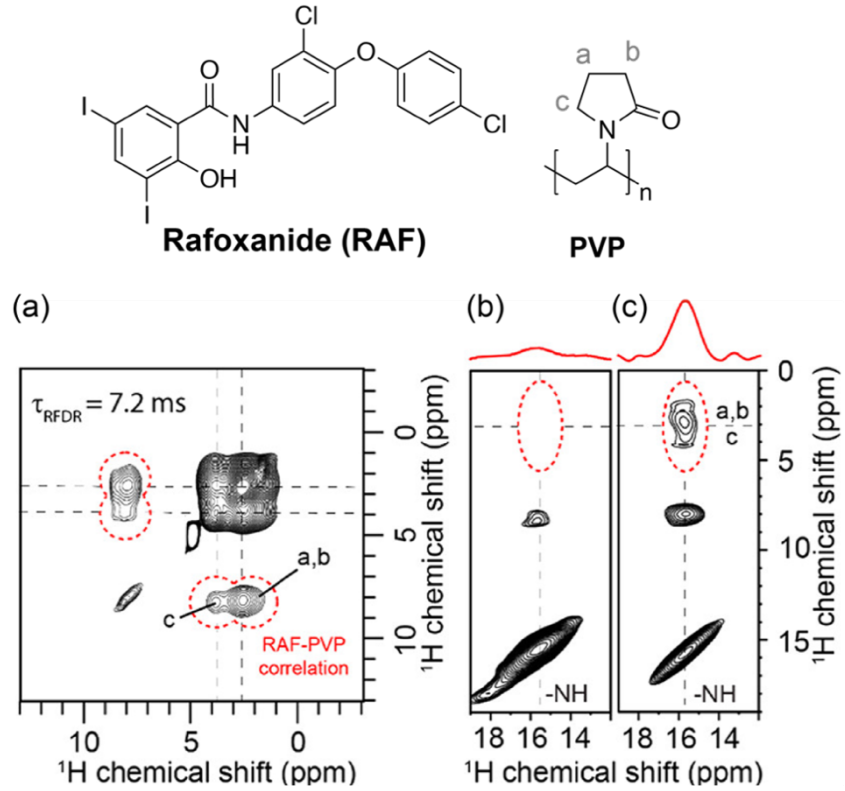

Figure 2.10. (a) ^{1}H-^{1}H RFDR spectra of 50 wt % RAF-PVP ASD SD from under aqueous condition carried out at mixing time τ_{RFDR} of 7.2 ms. Enlarged region of ^{1}H-^{1}H RFDR spectra carried out at (b) low and (c) very-high magnetic field, showing the evidence of the presence of RAF-PVP H-bond. Correlation peaks are highlighted with a red dot line. Chemical structure of RAF and PVP are given on top. Reprinted with permission from[37]. Copyright 2020 American Chemical Society.

2.6 Conclusions

In this review, we have described the latest applications of solid-state NMR spectroscopy approaches employing 1D and 2D data acquisition strategies approaches to identify and provide understanding of API-polymer interactions in pharmaceutical formulations. These studies revealed that changes of ^{1}H, ^{13}C, and ^{15}N chemical shifts in ASDs when compared with their individual components allowed the identification of API-polymer interactions such as H-bond or ionic one, while correlation spectroscopy from 2D NMR spectra has proved itself to be an excellent tool kit for molecular level identification of chemical species involved in the API-polymer contacts, providing essential information to understanding the nature of the stabilising interactions.

Moreover, NMR methodologies can play an important role as an orthogonal approach to the various more commonly used methods such as ultraviolet spectroscopy (UV), IR and X-ray powder diffraction (XRD), in order to strengthen understanding of stability mechanism of ASDs.[28,30,31,33] Furthermore, NMR spectroscopy can be an effective and a powerful technique to aid the pharmaceutical scientist to design new potential ASDs.

Continuous development in NMR is leading to the design of increasingly sophisticated and sensitive methods and this will certainly open up opportunities to understand ASD systems, and therefore allow the rational design of appropriate systems, rather than the current empirical approach. The dynamic nuclear polarisation (DNP) technique, thanks to its enhanced sensitivity compared to traditional NMR, has been successfully applied to field of pharmaceutical sciences. Pioneering work exploring the dependence of DNP enhancement on sample composition, radical concentration, relaxation properties of the API, excipients and

formulations, types of polarizing agents and proton density have been published and offer exciting perspectives.[70,71]

2.7 References

[1] Edueng, K.; Mahlin, D.; Bergstrom, C. A. S. *Pharm. Res.* **2017**, *34,* 1754.

[2] Rams-Baron, M. J., R.; Boldyreva, E.; Zhou D.; Jamroz, W.; Paluch, M., *Amorphous Drugs*. Springer, Cham, Switzerland: 2018.

[3] Vasconcelos, T.; Marques, S.; das Neves, J. *Adv. Drug. Deliv. Rev.* **2016**, *100,* 85.

[4] Davis, M.; Walker, G. *J. Control Release* **2018**, *269,* 110.

[5] Bhujbal, S. V.; Mitra, B.; Jain, U.; Gong, Y.; Agrawal, A.; Karki, S.; Taylor, L. S.; Kumar, S.; Tony Zhou, Q. *Acta. Pharm. Sin. B* **2021**, *11,* 2505.

[6] Baghel, S.; Cathcart, H.; O'Reilly, N. J. *J .Pharm. Sci.* **2016**, *105,* 2527.

[7] Singh, A.; Van den Mooter, G. *Adv. Drug. Deliv. Rev.* **2016**, *100,* 27.

[8] Newman, A., *Pharmaceutical Amorphous Solid Dispersions*. Wiley, Hobken, New Jersey, USA: **2015**.

[9] Van Duong, T.; Van den Mooter, G. *Expert. Opin. Drug. Deliv.* **2016**, *13,* 168.

[10] Wang, Y.; Wang, Y.; Cheng, J.; Chen, H.; Xu, J.; Liu, Z.; Shi, Q.; Zhang, C. *Crystals* **2021**, *11,* 1440.

[11] Van den Mooter, G.; Van den Brande, J.; Augustijns, P.; Kinget, R. *J. Therm. Anal. Calorim.* 1999, *57,* 493.

[12] Pham, T. N.; Watson, S. A.; Edwards, A. J.; Chavda, M.; Clawson, J. S.; Strohmeir, M.; Vogt, F. G. *Mol. Pharmaceutics* **2010**, *7,* 1667.

[13] Gordon, M.; Taylor, J. S. *Rubber Chem. Technol.* **1953**, *26,* 323.

[14] Tobyn, M.; Brown, J.; Dennis, A. B.; Fakes, M.; Gao, Q.; Gamble, J.; Khimyak, Y. Z.; McGeorge, G.; Patel, C.; Sinclair, W.; Timmins, P.; Yin, S. *J. Pharm. Sci.* **2009**, *98,* 3456.

[15] McNamara, D.; Yin, S.; Pan, D.; Crull, G.; Timmins, P.; Vig, B. *Mol. Pharmaceutics* **2017**, *14,* 377.

[16] Furuyama, N.; Hasegawa, S.; Hamaura, T.; Yada, S.; Nakagami, H.; Yonemochi, E.; Terada, K. *Int. J. Pharm.* **2008**, *361,* 12.

[17] Breitenbach, J.; Schrof, W.; Neumann, J. *Mol. Pharm.* **1999**, *16,* 1109.

[18] Taylor, L. S.; Zografi, G. *Pharm. Res.* **1997**, *14,* 1691

[19] Tran, T. T. D.; Tran, P. H. L. *Pharmaceutics* **2020**, *12,* 745.

[20] Laws, D. D.; Bitter, H. L.; Jerschow, A. *Angew. Chem. Int. Ed.* **2002**, *41,* 3096.

[21] Reif, B.; Ashbrook, S. E.; Emsley, L.; Hong, M. *Nat. Rev. Methods Primers* **2021**, *1,* 1.

[22] Everett, J. R.; Harris, R. K.; Lindon, J. C., *NMR in Pharmaceutical Sciences*. John Wiley & Sons: Chichester, UK, **2015**.

[23] Holzgrabe, U.; Wawer, I.; Diehl, B., *NMR spectroscopy in Pharmaceutical Analysis*. Elsevier Science: Oxford, **2008**.

[24] Pellecchia, M.; Bertini, I.; Cowburn, D.; Dalvit, C.; Giralt, E.; Jahnke, W.; James, T. L.; Homans, S. W.; Luchinat, C.; Meyer, B.; Oschkinat, H.; Peng, J.; Schwalbe, H.; Siegal, G. *Nat. Rev. Drug Discov.* **2008**, *7,* 738.

[25] Pugliese, A.; Hawarden, L. E.; Abraham, A.; Tobyn, M.; Blanc, F. *Magn. Reson. Chem.* **2020**, *58,* 1036.

[26] Pisklak, D. M.; Zielinska-Pisklak, M.; Szeleszczuk, L.; Wawer, I. *J. Pharm. Biomed. Anal.* **2016**, *122,* 29.

[27] Harris, R. K. *J Pharm Pharmacol* **2007**, *59,* 225.

[28] Mistry, P.; Mohapatra, S.; Gopinath, T.; Vogt, F. G.; Suryanarayanan, R. *Mol. Pharmaceutics* **2015**, *12,* 3339.

[29] Song, Y.; Yang, X.; Chen, X.; Nie, H.; Byrn, S.; Lubach, J. W. *Mol. Pharmaceutics* **2015**, *12,* 857.

[30] Song, Y.; Zemlyanov, D.; Chen, X.; Nie, H.; Su, Z.; Fang, K.; Yang, X.; Smith, D.; Byrn, S.; Lubach, J. W. *Mol. Pharmaceutics* **2016**, *13,* 483.

[31] Nie, H.; Su, Y.; Zhang, M.; Song, Y.; Leone, A.; Taylor, L. S.; Marsac, P. J.; Li, T.; Byrn, S. R. *Mol. Pharmaceutics* **2016**, *13,* 3964

[32] Lubach, J. W.; Hau, J. *Pharm. Res.* **2018**, *35,* 65.

[33] Ishizuka, Y.; Ueda, K.; Okada, H.; Takeda, J.; Karashima, M.; Yazawa, K.; Higashi, K.; Kawakami, K.; Ikeda, Y.; Moribe, K. *Mol. Pharmaceutics* **2019**, *16,* 2785.

[34] Lu, X.; Huang, C.; Lowinger, M. B.; Yang, F.; Xu, W.; Brown, C. D.; Hesk, D.; Koynov, A.; Schenck, L.; Su, Y. *Mol. Pharmaceutics* **2019**, *16,* 2579.

[35] Lu, X.; Li, M.; Huang, C.; Lowinger, M. B.; Xu, W.; Yu, L.; Byrn, S. R.; Templeton, A. C.; Su, Y. *Mol. Pharmaceutics* **2020**, *17,* 2585.

[36] Lu, X.; Huang, C.; Li, M.; Skomski, D.; Xu, W.; Yu, L.; Byrn, S. R.; Templeton, A. C.; Su, Y. *J. Phys. Chem. B* **2020**, *124,* 5271.

[37] Li, M.; Meng, F.; Tsutsumi, Y.; Amoureux, J. P.; Xu, W.; Lu, X.; Zhang, F.; Su, Y. *Mol. Pharmaceutics* **2020**, *17,* 2196.

[38] Pugliese, A.; Toresco, M.; McNamara, D.; Iuga, D.; Abraham, A.; Tobyn, M.; Hawarden, L. E.; Blanc, F. *Mol. Pharmaceutics* **2021**, *18,* 3519.

[39] Paudel, A.; Geppi, M.; Van den Mooter, G. *J. Pharm. Sci.* **2014**, *103,* 2635.

[40] Levitt, M. H., *Spin Dynamics*. 2nd ed.; Wiley, West Sussex, England: **2008**.

[41] Keeler, J., *Understanding NMR Spectroscopy*. 2nd ed.; Wiley, West Sussex, England: **2010**.

[42] Gunther, H., *NMR Spectroscopy: Basic Principles, Concepts, and Applications in Chemistry*. 3rd ed.; Wiley, Weinheim, Germany: **2013**.

[43] Hore, P. J., *Nuclear Magnetic Resonance*. 2nd ed.; Oxford press, Oxford, England: **2015**.

[44] Duer, M., *Introduction to Solid-State NMR Spectroscopy*. Blackwell Publishing, Oxford, England: **2005**.

[45] Apperley, D. C.; Harris, R. K.; Hodgkinson, P., *Solid-State NMR: Basic Principle & Practice*. Momentum Press, New York, USA: **2012**.

[46] Lu, X.; Xu, W.; Hanada, M.; Jermain, S. V.; Williams, R. O., 3rd; Su, Y. *J. Pharm. Biomed. Anal.* **2019**, *165,* 47.

[47] Schuster, I. I.; Roberts, J. D. *J. Org. Chem.* **1979**, *44,* 3864.

[48] Sarpal, K.; Tower, C. W.; Munson, E. J. *Mol. Pharmaceutics* **2020**, *17,* 787.

[49] Van Eerdenbrugh, B.; Taylor, L. S. *CrystEngComm* **2011**, *13,* 6171.

[50] Li, Z. J.; Abramov, Y.; Bordner, J.; Jason Leonard; Medek, A.; Trask, A. V. *J. Am. Chem. Soc.* **2006**, *128,* 8199.

[51] Smernik, R. J.; O'ades, J. M., K. *Eur. J. Soil Sci.* **2001**, *52,* 103.

[52] Demuth, B.; Galata, D. L.; Balogh, A.; Szabo, E.; Nagy, B.; Farkas, A.; Hirsch, E.; Pataki, H.; Vigh, T.; Mensch, J.; Verreck, G.; Nagy, Z. K.; Marosi, G. *Eur. J. Pharm. Sci.* **2018**, *121,* 301.

[53] Monschke, M.; Wagner, K. G. *Pharmaceutics* **2020**, *12,* 541.

[54] Friesen, D. T.; Shanker, R.; Crew, M.; Smithey, D. T.; Curatolo, W. J.; Nightingale, J. A. S. *Mol. Pharmaceutics* **2008**, *5,* 1003.

[55] Sarabu, S.; Kallakunta, V. R.; Bandari, S.; Batra, A.; Bi, V.; Durig, T.; Zhang, F.; Repka, M. A. *Carbohydr. Polym.* **2020**, *233,* 115828.

[56] Indulkar, A. S.; Box, K. J.; Taylor, R.; Ruiz, R.; Taylor, L. S. *Mol. Pharmaceutics* **2015**, *12,* 2365.

[57] Taylor, L. S.; Zhang, G. G. Z. *Adv. Drug Deliv. Rev.* **2016**, *101,* 122.

[58] Newman, A.; Hastedt, J. E.; Yazdanian, M. *AAPS Open* **2017**, *3*, 7.

[59] Aoki, C.; Ma, X.; Higashi, K.; Ishizuka, Y.; Ueda, K.; Kadota, K.; Fukuzawa, K.; Tozuka, Y.; Kawakami, K.; Yonemochi, E.; Moribe, K. *Int. J. Pharm.* **2021**, *600,* 120491.

[60] Sarpal, K.; Delaney, S.; Zhang, G. G. Z.; Munson, E. J. *Mol. Pharmaceutics* **2019**, *16,* 4836.

[61] Abraham, A.; Crull, G. *Mol. Pharmaceutics* **2014**, *11,* 3754.

[62] Feike, M.; Demco, D. E.; Graf, R.; Gottwald, J.; Hafner, S.; Spiess, H. W. *J. Magn. Reson., Ser. A* **1996**, *122,* 214.

[63] Gan, Z.; Amoureux, J. P.; Trébosc, J. *Chem. Phys. Lett.* **2007**, *435,* 163.

[64] Tatton, A. S.; Bradley, J. P.; Iuga, D.; Brown, S. P. *Z. Phys. Chem.* **2012**, *226,* 1187.

[65] Tatton, A. S.; Pham, T. N.; Vogt, F. G.; Iuga, D.; Edwards, A. J.; Brown, S. P. *CrystEngComm* **2012**, *14,* 2654.

[66] Maruyoshi, K.; Iuga, D.; Antzutkin, O. N.; Alhalaweh, A.; Velaga, S. P.; Brown, S. P. *ChemCommun* **2012**, *48,* 10844.

[67] Tatton, A. S.; Pham, T. N.; Vogt, F. G.; Iuga, D.; Edwards, A. J.; Brown, S. P. *Mol. Pharmaceutics* **2013**, *10,* 999.

[68] Grune, M.; Luxenhofer, R.; Iuga, D.; Brown, S. P.; Poppler, A. C. *J. Mater. Chem. B* **2020**, *8,* 6827.

[69] Quinn, C. M.; Wang, M.; Polenova, T. *Methods Mol. Biol.* **2018**, *1688,* 1.

[70] Ni, Q. Z.; Yang, F.; Can, T. V.; Sergeyev, I. V.; D'Addio, S. M.; Jawla, S. K.; Li, Y.; Lipert, M. P.; Xu, W.; Williamson, R. T.; Leone, A.; Griffin, R. G.; Su, Y. *J. Phys. Chem. B* **2017**, *121,* 8132.

[71] Zhao, L.; Pinon, A. C.; Emsley, L.; Rossini, A. J. *Magn. Reson. Chem.* **2018**, *56,* 583.

Chapter 3: Solid-state nuclear magnetic resonance studies of hydroxypropylmethylcellulose acetyl succinate polymer, a useful carrier in pharmaceutical solid dispersions

3.1 Overview

Chapter 3 is a paper entitled “Solid-state nuclear magnetic resonance studies of hydroxypropylmethylcellulose acetyl succinate polymer, a useful carrier in pharmaceutical solid dispersions” by Andrea Pugliese, Lucy E. Hawarden, Anuji Abraham, Michael Tobyn, and Frédéric Blanc which was published in *Magnetic Resonance in Chemistry* **2020**, 58, 1036.

The author contributions are as follows: L.E.H., M.T., and F.B. devised the project. A.P. conducted all the NMR experiments. Full data analysis and interpretation were undertaken by A.P. assisted in a couple of instances by A.A.. A.P. wrote the manuscript with feedback from F.B., and consultation from all other authors.

3.2 Abstract

Hydroxypropylmethylcellulose (HPMC) acetyl succinate (HPMC-AS) is a key polymer used for the enablement of amorphous solid dispersions (ASDs) in oral solid dosage forms. Choice of the appropriate grade within the material is often made empirically by the manufacturer of small-scale formulations, followed by extensive real time stability. A key factor in understanding and predicting the performance of an ASD is related to the presence of hydrogen (or other) bonds between the polymer and active pharmaceutical ingredient (API), which will increase stability over the parameters captured by miscibility and predicted by the Gordon–Taylor equation. Solid-state nuclear magnetic resonance (NMR) is particularly well equipped to probe spatial proximities, for example, between polymer and API; however, in the case of HPMC-AS, these interactions have been sometimes difficult to identity as the carbon-13 NMR spectra assignment is yet to be firmly established. Using feedstock, selectively substituted HPMC polymers, and NMR editing experiments, we propose here a comprehensive understanding of the chemical structure of HPMC-AS and a definitive spectral assignment of the ^{13}C NMR spectra of this polymer. The NMR data also capture the molar ratios of the acetate and succinate moieties present in HPMC-AS of various grades without the need for post treatment required by chromatography methods commonly use in pharmacopoeia. This knowledge will allow the prediction and measurement of interactions between polymers and APIs and therefore a rational choice of polymer grade to enhance the solid state stability of ASDs.

3.3 Introduction

Active pharmaceutical ingredients (APIs) are often available in the thermodynamically stable crystalline form and exhibit poor water solubility[1], hence poor bioavailability.[2] Amorphous drugs are therefore attractive due to their increased rate of dissolution enhancing the bioavailability of the active ingredient. However, their development is often hampered by their tendency to recrystallise to the most thermodynamically stable polymorph.

To address this challenge, several strategies based on formulation in polymers have been used to make amorphous solid dispersions (ASDs).[3] An ASD is a formulation of one or more API into a solid biocompatible polymer matrix that aims to stabilise the API in its amorphous form and increase bioavailability.[4] The most common methods to prepare ASDs include solvent evaporation[5], spray drying[6], cryo-milling[7], hot melt extrusion[8], nano-solid suspension formation using controlled precipitation[9], and solvent-free supercritical fluid processing.[10] It is widely recognised that the polymer plays a crucial role in stabilising the ASD and that the formulation of the API and polymer into a solid dispersion prevents API crystallisation and consequently improves physical stability.[11–13] This is mostly due to a synergetic effect that includes increase of the glass transition temperature (Tg) of the final mixture high Tg polymers (anti-plasticising effect), reducing molecular mobility of the amorphous API and the formation of specific API–polymer interactions.[14]

A number of polymers have been considered as excipients in ASDs and can be classified as polyglycols (e.g., poly(ethylene glycol)[PEG][15] and poly(ethylene oxide)[PEO][16]), polyvinyl (e.g., poly(vinyl pyrrolidone) [PVP][17] and poly(vinyl pyrrolidone)-co-vinyl acetate [PVP-PA][18]) and cellulose (e.g.,

hydroxypropylmethylcellulose [HPMC][19] and HPMC acetyl succinate [HPMC-AS],[20] **Figure 3.1**).

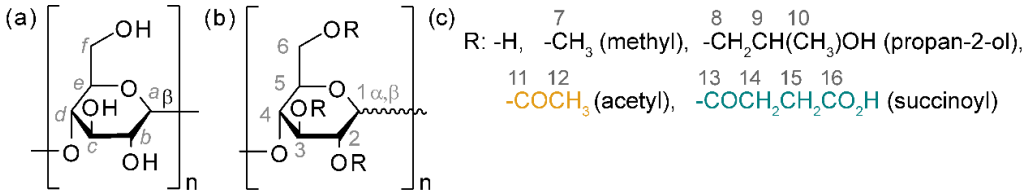

Figure 3.1 The pulp (a) is the chemical precursor of hydroxypropylmethylcellulose (HPMC). The HPMC structure consists of the (b) 6-carbon ring unit of glucose bonded to hydrogen, methyl, and propan-2-ol R groups given in (c). Esterification of HPMC yields HPMC-acetyl succinate that is made from the glucose unit and all the substituent R groups in (c). HPMC-acetyl and HPMC-succinoyl are made from the glucose unit and only the acetyl and succinoyl R groups, respectively. The wavy line in panel (b) represents the chemical bond of the anomeric carbon: The glucose ring exists in two different cyclic hemiacetal α- and β- glucopyranose in which the anomeric carbon is a stereogenic centre and has two different configurations.

The choice of a suitable polymer to make a specific ASD is dictated by the chemical physical properties required such as Tg, thermal stability, the dissolution profiles in organic solvent, its performance in dissolve API, and the API under consideration.

It has been described that HPMC-AS is a promising solid matrix for developing homogeneous amorphous dispersions[21] of low-solubility drugs due to its high glass temperature value (Tg is in order of 120 °C)[22] and its amphiphilic nature arising from the existence of hydrophobic (e.g., succinoyl, **Figure 3.1(b)**) and hydrophilic (e.g., acetyl) groups in its chemical structure.[21]

Due to the presence of acetyl (A) and succinoyl (S) groups, HPMC-AS allows the formation of stable ASD and inhibition of the API crystallisation by the formation of intermolecular interactions.[23,24] A and S can establish specific interactions with the drug, which could be tuned by different levels of acetyl and succinoyl substitution in the polymers. Materials with different contents of A and S are commercially available and labelled as L, M, and H grades depending on the A/S ratio according to the specifications given by different vendors.[25–27]

Solid-state nuclear magnetic resonance (NMR) has been demonstrated as one of the most informative analytic technique used in the field of pharmaceutical sciences.[28,29] NMR allows the structural characterisation of drugs[30] and excipients[31], identification of drug polymorphs[32], understanding of molecular mobility and physical stability of solid dispersions[33], and the study and identification of specific intramolecular interactions in the solid dispersion.[34] The knowledge of the accurate assignments of the NMR signals in the HPMCAS polymer used for ASDs plays a crucial role in understanding HPMC-AS–API interactions and is required to study the overall stability and dynamics of the ASD. Many reports provide evidence of intermolecular interactions between API and polymer using computational, thermal, and spectroscopic methods, offering a partial NMR polymer assignments. The presence of hydrogen bonds in API–PVP solid dispersions has been probed by Fourier-transform infrared spectroscopy, Raman, and NMR spectroscopy, confirming ideal mixing behaviour of the two components.[35] Drug–polymer interactions between polystyrene sulfonic acid and lapatinib and gefitinib have been shown via the presence of acid-base interactions using a combination of analytic techniques, including solid-state NMR, ultraviolet spectroscopy, and Fourier-transform infrared spectroscopy.[36] Recently, a study by Ishizuka *et al*.[23] has probed intermolecular interactions between carbamazepine (CBZ) and HPMC-AS collating data obtained by studying CBZ in

HPMC-A and CBZ in HPMC-S in individual solid dispersions. Without a complete assignment of the ^{13}C spectrum and only attributing the signal at ~170 ppm to the carbonyl of the acetyl group in HPMC-AS spectrum, the authors were able to identify the presence of intermolecular bonds between the drug and HPMC-AS. In particular, they have demonstrated the presence of a hydrogen bond between the acetate substituent of the polymer and the CBZ's amine group and between both the carbonyl and the amine groups of CBZ, proving the crucial role played by the acetate and succinoyl group in stabilisation of the final solid dispersion. X. Lu *et al*.[24] detected specific intra-molecular interactions in amorphous dispersions made by posaconazole (POSA), as API, and HPMC-AS and hypromellose phthalate at different API loading. They were able to identify interactions by combining one-dimensional, two-dimensional, and advanced NMR techniques with isotopic labelling. The authors identified hydrogen bonding like interaction between the POSA's triazole ring and the –CH moiety of the propan-2-ol substituent group of HPMC-AS as well as an electrostatic like interaction between the triazole and the deprotonated succinoyl carboxylic group. π-π aromatic packing and electrostatic interactions were also detected between POSA and the hypromellose phthalate polymer. In that paper, the authors also reported a preliminary assignment of the ^{13}C CP magic angle spinning (MAS) NMR spectrum of HPMC-AS; however, little details were given.

Here, we report a comprehensive NMR structural elucidation study of HMPC-AS, which provides an enhanced and more accurate assignment than those previously reported in the literature in which the ^{13}C NMR spectra of a range of common pharmaceutical excipients used in solid dispersion are described.[37] This is achieved by exploiting a stepwise approach relying on consecutive substitution of the HPMC polymer with acetate, succinate, and a mixture of acetate and succinate

moieties, combined with acquisition of well-resolved and ^{1}H-edited ^{13}C NMR spectra and their thorough deconvolution. Additionally, it is demonstrated that it is possible to estimate the various contents of A and S directly from the experimentally obtained ^{13}C NMR spectra to capture the different grades of HPMCAS. These results could enable more effective identification of the presence of specific-site intermolecular interactions, pinpointing which organic functionalities are involved in specific interactions. In the specific case of HPMC-AS, this allows the possibility of tuning the A/S ratio in the sample to maximise the stabilisation effect of the polymer on the final ASD.

3.4 Materials and method

3.4.1 Materials

3.4.1.1 General considerations

Pulp polymer and HPMC were obtained from Shin-Etsu Chemical Co., Ltd. HPMC-AS polymers branded AQOAT®, AFFINSOL™, and AQUASOLVE™ with different acetate/succinate ratios were provided by Shin-Etsu Chemical Co, Ltd., DuPont Nutrition & Biosciences, and Ashland, respectively. Acetic anhydride and succinic anhydride (both 99% grade) used in the synthesis of HPMC-A and HPMC-S were obtained from Sigma-Aldrich. Acetic acid (99.8% grade), sodium acetate anhydrous

(A.C.S. grade), and sodium chloride (reagent grade) were provided by Acros organics, Spectrum, and Fisher, respectively. All other materials were used as received. ^{13}C liquid state NMR spectra were obtained on a Bruker Avance 500-MHz spectrometer with the solvent peak as the internal reference. Melting points (m.p.) were measured using the Edu-Lab melting point apparatus SRL MLTP 08019-200.

Table 3.1 gives the weight percentage contents of A and S in the HPMC-AS used in this work, which are obtained from liquid chromatography methods as described in the United States/National Formulary and Japanese pharmacopoeia and given in the certificate of analysis provided by the vendors. The percentage contents in weight of A and S are then converted to degree of substitution (DS).[38]

Table 3.1. Degree of substitution (DS) of acetate (A) and succinate (S) moieties in the various Hydroxypropylmethylcellulose-AS polymers studied here as a function of manufacturers and grade. A% and S% values are given by the vendor in the certificate of analysis, and they represent wt%. DS (A) and DS (S) represent the degree of substitution of A and S in all polymers

Polymer series:	AQOAT®			AFFINISOLTM			AQUASOLVE TM		
Grade:	L	M	H	L	M	H	L	M	H
A %:	7.9	9.1	11.5	8.1	9.6	11.6	8.1	10.8	13.6
S %:	14.8	11.0	7.4	15.1	11.3	6.9	16.3	11.4	6.0
DS (A):	0.18	0.21	0.27	0.19	0.22	0.27	0.19	0.25	0.32
DS (S):	0.14	0.11	0.07	0.15	0.11	0.07	0.16	0.11	0.06
DS(A)/DS(S):	1.3	1.9	3.6	1.3	2.0	3.9	1.2	2.2	5.3

3.4.1.2 Synthesis of HPMC-A

In a 500-ml 2-neck round bottom flasks equipped with a reflux condenser, HPMC (2910; 30.0 g, 94 mmol) was added to glacial acetic acid (300 ml) at 80–90 °C under mechanical vigorous stirring using a Teflon stir blade over 1–2 min. Upon HPMC dissolution, anhydrous sodium acetate (30.0 g, 365 mmol) was added and stirred until completely dissolved, which was followed by addition of acetic anhydride (66.34 g, 650 mmol) over 5 min. The resulting mixture was then stirred at a moderate speed (200–250 rpm) for 6 hr at 80–90 °C and was quenched by pouring it into 10% NaCl solution in water (1.4 L). The resulting precipitate was collected by filtration and then suspended in fresh 10% NaCl (0.7 L) in a laboratory blender and mixed until well dispersed (1–2 min). The precipitate was again collected by filtration, resuspended a second time in 10 % NaCl solution, dispersed then recollected by filtration. After drying, the wet-cake was purified by three washes in hot distilled water (0.7 L each) at 70–80 °C. Finally, the precipitate was placed in an 80 °C oven to dry, leading a white granular solid (25.5 g). ^{13}C NMR (125 MHz, DMSO-d_6): 169.4 ppm, 169.2, 168.9, 168.4, 101.3, 99.1, 83.3, 82.6, 81.3, 79.7, 76.5, 75.1, 74.9, 74.8, 74.0, 73.5, 73.0, 71.8, 71.5, 70.3, 69.0, 68.9, 65.1, 64.9, 62.5, 59.3, 58.9, 58.8, 58.7, 58.5, 58.1, 57.6, 57.4, 55.4, 20.4, 20.1, 19.9, 19.8, 16.0. All peaks are broad. m.p.: 184–214 °C. Integration of the acetate carbonyls to the anomeric carbon of the glucose ring gave an acetate DS of 0.60.

3.4.1.3 Synthesis of HPMC-S

In a 500-ml 2-neck round bottom flasks equipped with a reflux condenser, HPMC (2910; 30.0 g, 94 mmol) was dissolved under vigorous mechanical stirring in glacial acetic acid (300 ml) at 80–90 °C. When the mixture appears to be clear, anhydrous sodium acetate (30.0 g, 365 mmol) was added under vigorous stirring followed by succinic anhydride (3.51 g, 33 mmol), and the reaction mixture was left at 80–90 °C for 6 hr. After cooling down to room temperature overnight, the polymer was isolated by pouring the crude into a 20% NaCl solution in water (1.5 L) followed by filtration. The precipitate was suspended twice in fresh 20% NaCl solution (0.7 L) in a laboratory blender mixing at the high speed for 1–2 min and collected by filtration. The wet-cake was dissolved in 1.0 L of distilled water and then heated to 80–90 °C while stirring. The polymer began to phase separate as an offwhite solid precipitate that was collected to lead the final product (18.6 g of yellowish solid) after drying. ^{13}C NMR (125 MHz, DMSO-d_6): 172.5 ppm, 171.2, 171.0, 170.3, 169.5, 169.2, 102.2, 101.6, 101.3, 83.4, 82.6, 79.8, 77.9, 76.5, 75.1, 74.9, 74.1, 73.5, 73.0, 71.9, 70.5, 69.1, 65.1, 64.8, 62.6, 59.3, 58.8, 58.1, 28.8, 28.4, 20.4, 20.0, 19.7, 19.5, 18.9, 16.7, 16.1. All peaks are broad. m.p.: 204–234 °C. Integration of the acetate carbonyls to the anomeric carbon of the glucose ring gave an acetate DS of 0.15.

3.4.1.4 NMR spectra

All solid-state NMR spectra were acquired at 9.4 T using a Bruker Avance III HD NMR spectrometer equipped with a 4-mm HXY triple-resonance MAS probe in double resonance mode. ^{1}H and ^{13}C channels were tuned at ν_0 = 400.13 and 100.67 MHz, respectively. All experiments were performed under MAS at a frequency ν_r = 12.5 kHz and at room temperature (298 K). All ^{1}H pulses and SPINAL-64 heteronuclear decoupling[39] during ^{13}C detection were obtained at a radio frequency (rf) field amplitude of 83 kHz. The ^{1}H-^{13}C cross polarisation (CP) spectra[40] were carried out using a ^{13}C rf field amplitude of around 45 kHz ramped to obtain maximum signal at a ^{1}H rf field of 60 kHz. A 2-ms contact time during CP was applied. Based on the ^{1}H T_1 spin-lattice relaxation times values, evaluated using the saturation recovery pulse sequence, recycle delays of 3 s were used in all the experiments.[41] ^{13}C CP phase inversion (CPPI)[42] experiments were performed using an optimised polarisation inversion period of 60 μs. All ^{13}C spectra were referenced to the tertiary carbon of adamantane at 29.45 ppm.[43] The chemical shifts of all assigned resonances are quoted within an accuracy of ±1 ppm due to the broad line widths observed. Deconvolution of the experimental spectra was carried out in TopSpin 4.0.6 using the solid line shape analysis routine. Deconvolution for signals in the 160 and 190 ppm region were carried out using an optimised fixed ratio for Lorentzian to Gaussian line shape of 1:6. The parameters for the ^{13}C CP kinetics (CP signal intensity *vs*. contact time) build up curves were obtained by fitting the data sets using **Equation 3.1** below,[40] where $S(t_c)$, S_0, t_c, T_{HX}, and $T_{1\rho}$ are the amount of signal at contact time t_c, the maximum obtainable intensity in absence of relaxation, the time constant for CP, and the relaxation time in the rotating frame, respectively:

$$S(t_c)=S_0\left[1-\exp\left(\frac{-t_c}{T_{HX}}\right)\right]\exp\left(\frac{-t_c}{T_{1\rho}}\right) \qquad \textbf{Eq. 3.1}$$

The first term of this equation accounts for the polarisation build up whereas the second exponential term accounts for the relaxation decay.

3.5 Results and discussion

HPMC-A and HPMC-S differ for the presence of only acetate and succinate groups, respectively, bonded to the 6-carbon ring unit of cellulose (**Figure 3.1(a)**). HPMC-AS is prepared by esterification of HPMC with a mixture of acetic acid anhydride and succinic acid anhydride in acetic acid and sodium acetate.[44] The mono-esterified derivatives HPMC-A and HPMC-S (**Figure 3.1**) are also prepared from HPMC using acetic and succinic acid anhydrides, respectively, as summarised in **Scheme 3.1**.

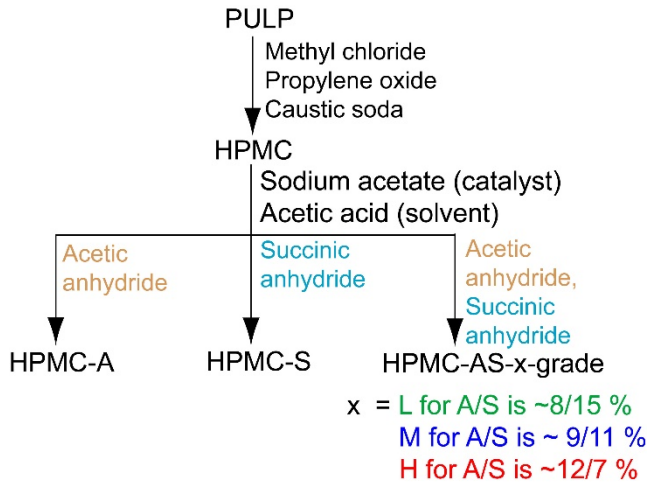

Scheme 3.1. Synthetic pathway in which the pulp, as starting material, was transformed in the samples used in this work. A, acetyl; HPMC, hydroxypropylmethylcellulose; S, succinoyl.

The pulp (also referred as cellulose) consists of a polysaccharide constituted linear chain of β-1,4-linked D-glucose residues, and exhibits complexity at the molecular level.[45] Cellulose is an allomorphic material composed of two native crystalline forms (cellulose I α and β), another allomorphic form (cellulose II) and an amorphous phase[45] and the chemical structure of the polymeric unit is given in

Figure 3.1(a). **Figure 3.2(a)** shows the ^{13}C CP MAS spectrum of the pulp with the assignment proposed based on the previous literature, supported by both experimental data[46] and computational study.[47] The spectrum exhibits clusters of signals for C*a*, C*b,c,e*, C*d* and C*f* at 104 - 108 ppm, 70 – 78 ppm, 82 - 90 ppm and 60 - 68 ppm, respectively, arising from the presence of allomorphic and amorphous forms of cellulose. **Figure 3.2(b)** also gives the ^{13}C CP-based edited experiment we have recorded using the CPPI sequence (in which the phase of the signals depends on the carbon types with quaternary carbon and CH_3 signals being positive, CH_2 negative and CH signals largely suppressed).[48] In the ^{13}C CPPI spectrum, the intensity of C*a*, C*d*, C*b,c,e* peaks is highly reduced as expected for CH moieties and partial inversion is only observed for the C_f cluster (CH_2 group), likely originating from different spin dynamics between the various forms.[45]

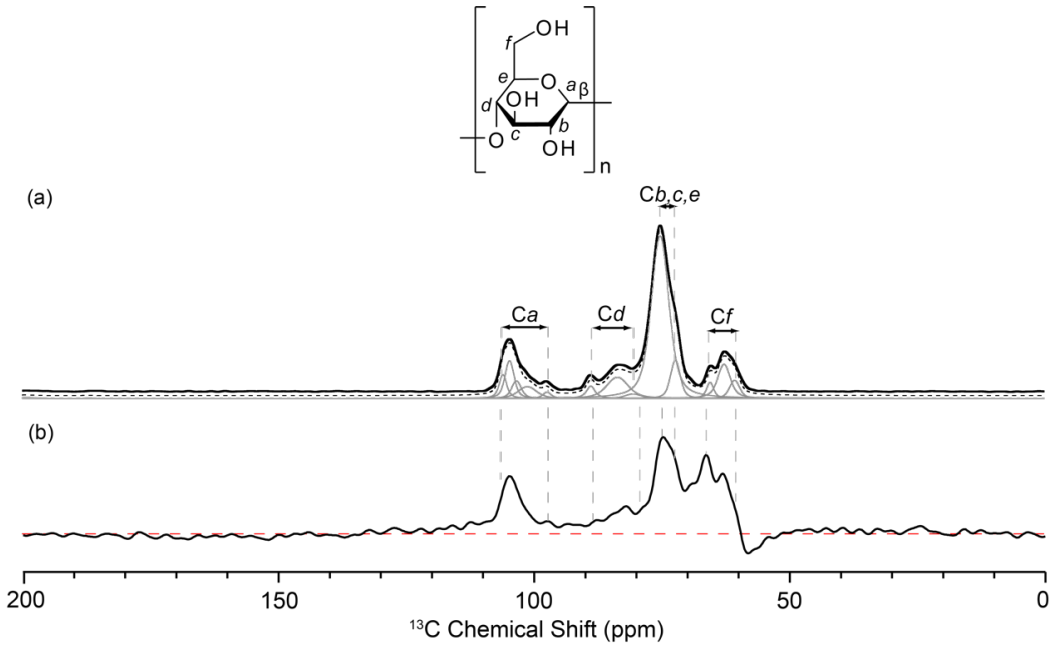

Figure 3.2. (a) ^{13}C CP MAS and (b) ^{13}C CPPI MAS spectra of pulp and its chemical structure. The proposed assignments are based on the previous literature.[46,47] The simulated spectrum (dashed black) and the spectral deconvolution (grey line) is given. The red dashed line in (b) marks the zero intensity signal.

The assignment of the ^{13}C CP MAS spectrum can be used for stepwise assignment of all the samples studied in this work, as the pulp is the chemical precursor of all the polymers used (**Scheme 3.1**).

The assignment of the ^{13}C MAS NMR spectra of HPMC-AS is initially based on the partial spectral assignment of unsubstituted HPMC. The ^{13}C CP spectrum of HPMC is shown in **Figure 3.3(a)** and its assignment is based on comparisons with previous ^{13}C NMR spectra of excipients and carbohydrates[37], well-established understanding of ^{13}C chemical shielding[49] including computed shifts, prior literature[37,50], and a ^{13}C CP-based edited experiment given in **Figure 3.3(b)** using the CPPI sequence. The ^{13}C spectrum of HPMC clearly exhibits two signals at around 104 and 98 ppm, corresponding to the two different anomeric C1α and C1β (**Figure 3.1(a)**) which appear at two chemical shifts due to the different

electronic distribution at the anomeric centres.[51] The peaks at 84 and 76 ppm correspond to C4 and C2,3, respectively. The intense peak at 61 ppm, that is significantly reduced in the ^{13}C CPPI spectrum, can be attributed to the CHs' C5,9. Spectral deconvolution reveals shoulders at about 71 and 59 ppm that appear negative and positive in the ^{13}C CPPI spectrum and are assigned to the CH_2s' C6,8 and methyl C7, respectively. We note that the previous partial ^{13}C spectral assignment indicates the 71 and 61 ppm signals (appearing at 75 and 60 ppm in the literature)[37] to correspond to C2,3,5,9 and C6,7,8, respectively, and this is not in agreement with the negative phase for CH_2s groups and reduced signal intensities for CHs groups observed in the ^{13}C CPPI spectrum (**Figure 3.3(b)**).

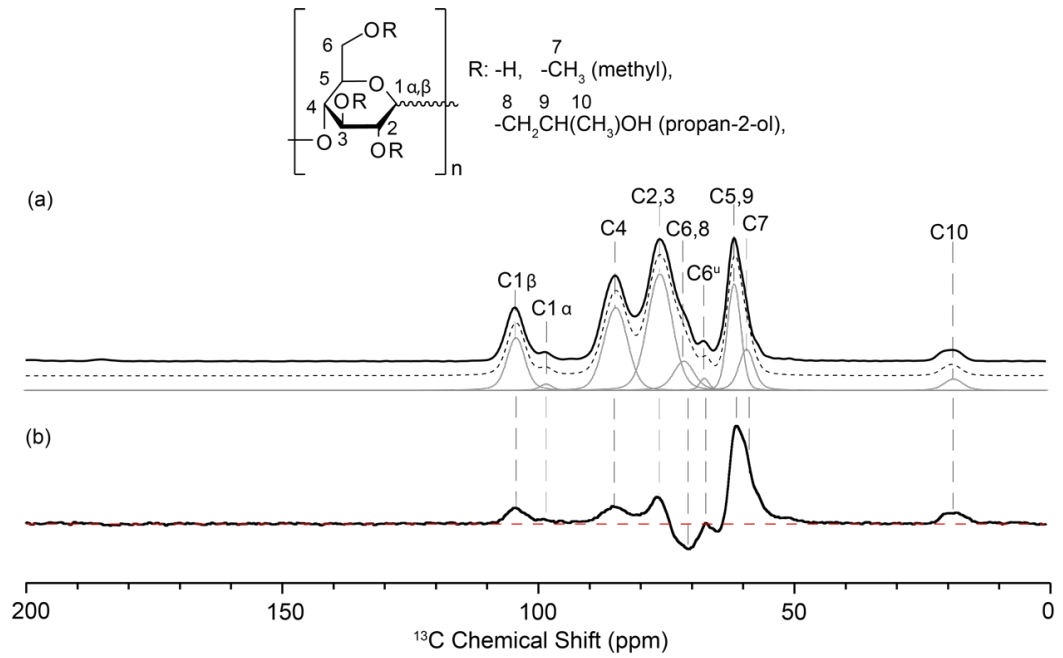

Figure 3.3. (a) ^{13}C CP MAS and (b) ^{13}C CPPI MAS spectra of HPMC and its chemical structure. The simulated spectrum (dashed black) and the spectral deconvolution (grey line) are given for the CP spectrum. The red dashed line in (b) marks the zero intensity signal.

The small signal labelled as $C6^u$ (where 'u' means unsubstituted) in the spectra at about 67 ppm is tentatively attributed to carbon C6 in the glucose unit corresponding to some residual unsubstituted hydroxyl group[52], this assignment is based on the chemical shift observed for the carbon C_f of the pulp (**Figure 3.2(a)** and **(b)**).[44,45] It is estimated that around 20% of hydroxyl groups in HPMC are unsubstituted by methoxy and hydroxypropyl groups.[52] These residual groups are subsequently reacted during the synthesis of HPMC-AS.

In order to unambiguously assign the ^{13}C CP MAS NMR spectra of HMPC-AS, we also recorded the spectra of HMPC-A and HPMC-S polymers prepared by esterification of HPMC (see synthesis section for further details). The respective ^{13}C NMR spectra of these polymers (**Figure 3.4(a)** and **(b)**) differ from the spectrum of HPMC (**Figure 3.3(a)**) by the presence, in HPMC-A, of two extra peaks at 170 and 21 ppm corresponding to the carbonyl (C11) and methyl groups (C12) of the acetyl, respectively, and, in HPMC-S, of resonances at 173 and 30 ppm of the carbonyl (C13,16) and methylene (C14,15) carbons of the succinoyl group. We were unable to resolve the two different carbonyls (ester C13 and carboxylic acid C16) of the succinoyl group, despite the expected 3-4 ppm difference in solution state[49] which is ascribed to signal broadening of the 173 ppm resonance (full width at half maximum ~ 500 Hz *vs.* 250 Hz for C11 in HPMC-A).

The signal assignment for the HPMC-AS AQOAT® series (**Figure 3.4(c)**, **(d1)**, and **(e)**) was carried out using assignments obtained for HPMC, HPMC-A, and HPMC-S and the ^{13}C CPPI spectrum obtained on HPMC-AS M grade given in **Figure 3.4(d2)**. The spectra exhibit resonances for both the acetyl and succinoyl groups in addition to the signals that come from HPMC. The carbonyl carbons of the acetyl (C11) and succinoyl (C13,16) groups are partially resolved, enabling their (semi)quantification (see below). Similarly, in the aliphatic region of the spectra,

resonances for the acetyl (C12 at 21 ppm) and succinoyl (C14,15 at 30 ppm) groups as well as the C10 in HMPC are clearly visible.

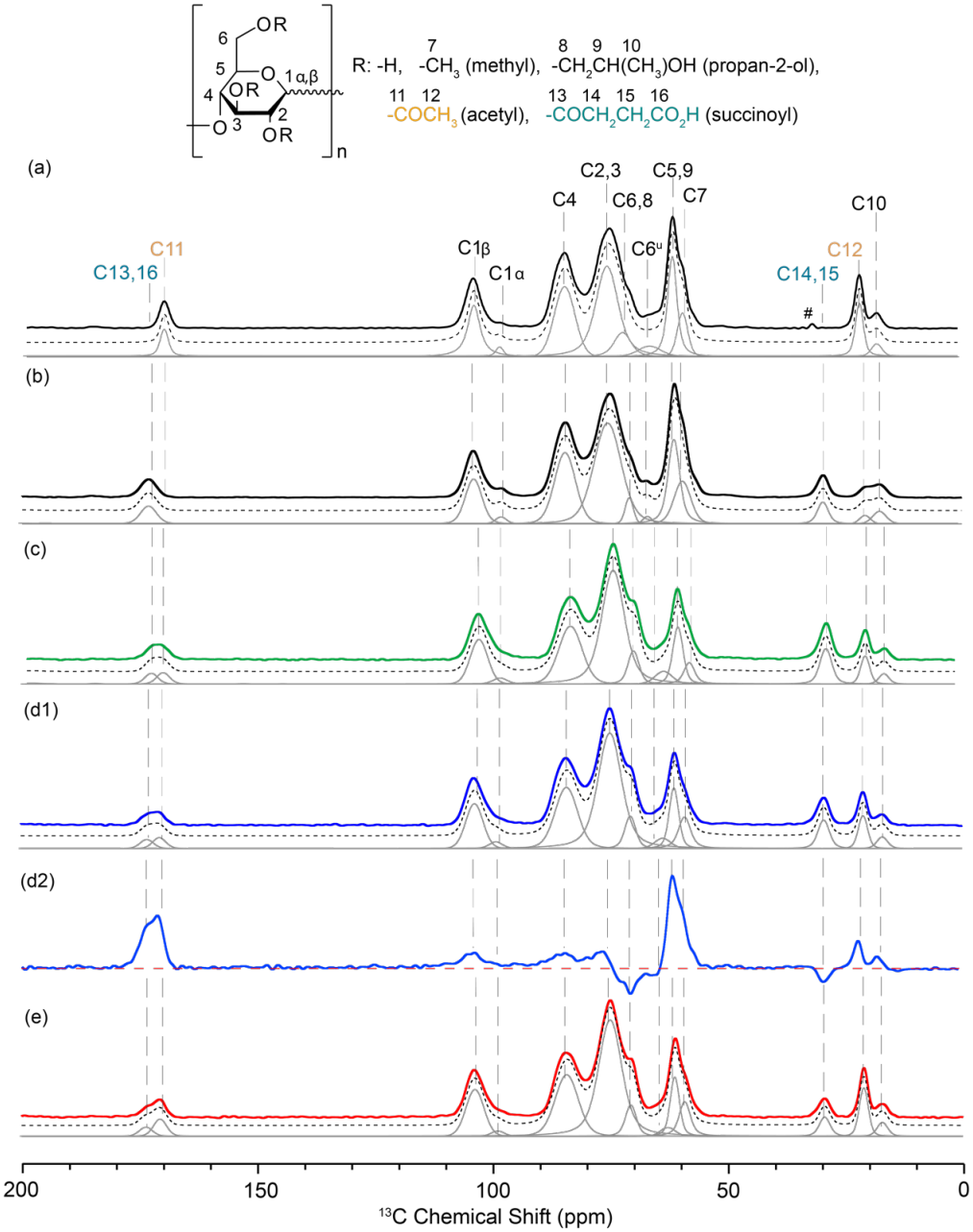

Figure 3.4. ^{13}C CP MAS spectra of (a) HPMC-A, (b) HPMC-S and Shin-Etsu AQOAT® HPMC-AS in (c) L-, (d1) M-, and (e) H-grades. The ^{13}C CPPI spectra of Shin-Etsu HPMC-AS-M polymer is given in (d2). The red dashed line marks the zero intensity signal. The simulate spectrum (dashed black) and the spectral deconvolution (grey line) are given for each spectrum. The signal at 31 ppm (labelled with #) indicates some acetate present in the sample due to transesterification with acetic acid solvent during the synthesis.

Figures 3.5 and **3.6** show the ^{13}C CP MAS NMR spectra obtained for HPMC-AS AFFINISOL™ and AQUASOLVE™ polymers, respectively. The signals are comparable to the AQOAT® series and are assigned in the same way.

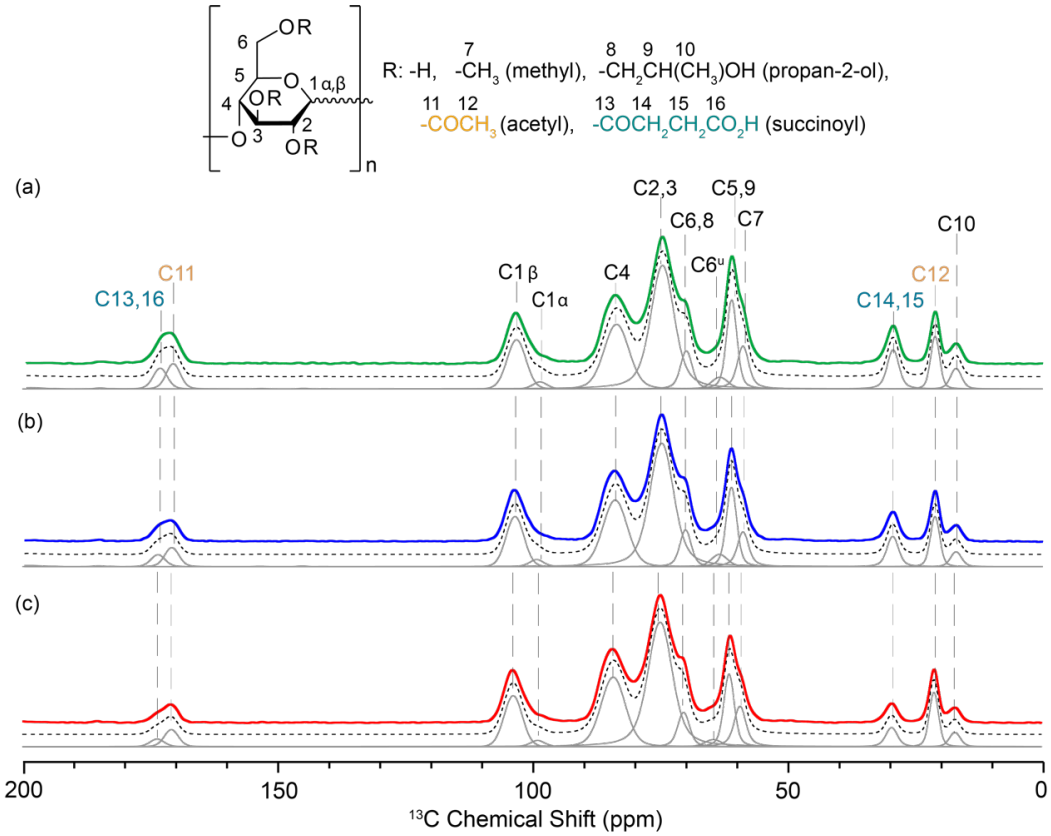

Figure 3.5. ^{13}C CP spectra of the DuPont AFFINISOL™ HPMC-AS series at (a) L grade, (b) M grade, and (c) H grade of acetyl/succinoyl ratio. The simulated spectrum (dashed black) and the spectral deconvolution (grey line) are given for each spectrum. The structure of the HPMC-AS polymer is shown on the top of the figure.

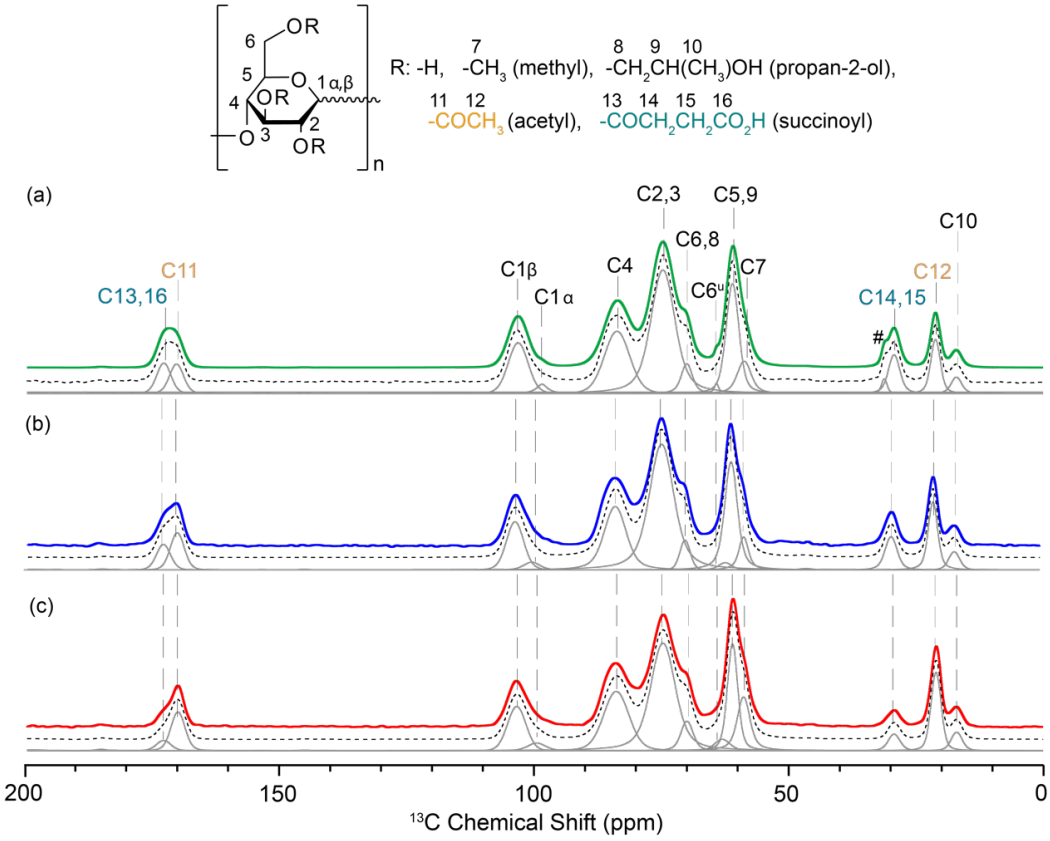

Figure 3.6. ^{13}C CP spectra of the Ashland AQUASOLVE™ at (a) L grade, (b) M grade, and (c) H grade of acetyl/succinoyl ratio are reported. The simulated spectrum (dashed black) and the spectral deconvolution (grey line) are given for each spectrum. The signal labelled with # indicates the presence of some acetate in the sample due to transesterification with acetic acid solvent. The structure of the HPMC-AS polymer is shown on the top of the figure.

Some small changes in chemical shifts were observed (**Table 3.2**) between the samples from different vendors rather than samples of different A/S ratio, further confirming that the carbon chemical shifts are not A/S ratio dependent.

Table 3.2. ^{13}C nuclear magnetic resonance spectral assignments chemical shifts in parts per million for all polymers studied

Polymer	C1α	C1β	C2	C3	C4	C5	C6	C7	C8	C9	C10	C11	C12	C13	C14	C15	C16
HPMC	104(/)	98(/)	76(/)	76(/)	84(/)	61(+)	71(-)	59(+)	71(-)	61(+)	19(+)	n.a.	n.a.	n.a.	n.a.	n.a.	n.a.
HPMC-A	104	98	76	76	84	61	71	59	71	61	17	170	21	n.a.	n.a.	n.a.	n.a.
HPMC-S	104	98	76	76	84	61	71	59	71	61	17	n.a.	n.a.	173	30	30	173
AQOAT®	104(/)	98(/)	76(/)	76(/)	84(/)	61(+)	71(-)	59(+)	71(-)	61(+)	14(+)	171(+)	21(+)	173(+)	30(-)	30(-)	173(+)
AFFINISOLTM	104	98	75	75	84	60	71	59	71	61	17	171	21	173	30	30	173
AQUASOLVETM	104	100	75	75	84	60	71	58	71	60	17	171	21	173	29	29	173

n.a. = not applicable. (+), (-) and (/) refer to the positive phase, negative phase and largely suppressed signal intensities for the ^{13}C CPPI spectra on selected polymers.

Although CP MAS NMR experiments are inherently not quantitative, the similar structure of the HPMC-AS polymers allows some (semi)quantitative consideration of the various groups present. The signals for carbons C11 (in A) and C13,16 (in S) were used as probes to quantify the A/S molar ratio from the experimental NMR spectra as both these carbonyl carbons exhibit similar CP kinetics (**Figure 3.7** and **Table 3.3**), as revealed by recording ^{13}C CP MAS spectra at different CP contact times, and illustrated by fitting the obtained ^{13}C CP polarising build-up curves (signal intensities vs. CP contact times) data (see experimental section for the equation).[40] We note that although C12 (in A) or C14,15 (in S) are well resolved, it is not possible to use them for the (semi)quantification due to the different nature of these carbons (CH_3 *vs*. CH_2 groups, respectively), which show significantly different CP kinetics between themselves and C11 and C13,16.

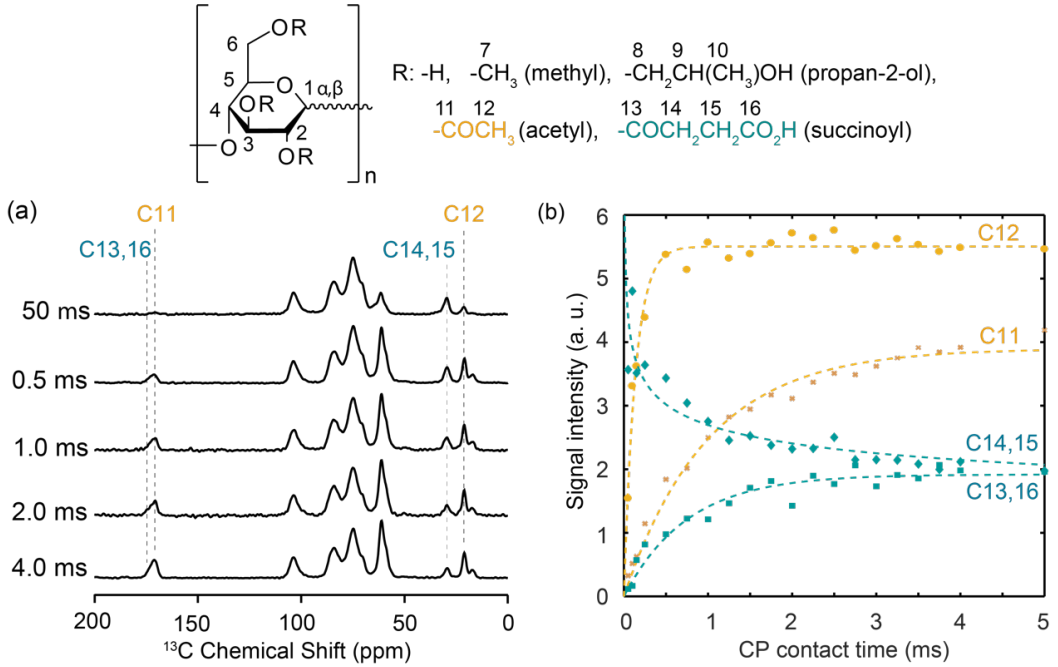

Figure 3.7. (a) ^{13}C cross polarisation (CP) magic angle spinning nuclear magnetic resonance spectra of the Shin-Etsu AQOAT® hydroxypropylmethylcellulose acetyl succinate M-grade polymer recorded at selected CP contact times (and its structure). (b) ^{13}C CP polarising build up curves (CP kinetics) for C11, C12, C13,16, and C14,15 carbons. The dashed lines are fit to the data using **Equation 3.1** (see experimental section)[40]

Table 3.3. ^{13}C CP polarising build up curves fitting parameters for **Equation 3.1** for the ShinEtsu AQOAT® HPMC-AS M-grade polymer. See experimental section for further details.

Carbon	S_0	T_{HX} (ms)	$T_{1\rho}$ (ms)
C11	3.9 ± 0.4	1.0 ± 0.2	n.d.
C12	5.9 ± 0.4	0.2 ± 0.1	n.d.
C13,16	1.9 ± 0.4	0.8 ± 0.2	n.d.
C14,15	-0.2 ± 0.3	n.d.	0.03 ± 0.02

n.d. = not determined

Figure 3.8 shows a magnified view of the signals related to the carbonyl groups of the acetate and succinate (190–160 ppm region of the ^{13}C CP MAS NMR spectra). The spectra show different integrals for the characteristic C11 resonance in the A group and the C13,16 signals in the S group and allow comparison between vendors and grades. The different A/S molar ratios in each polymer can be obtained from the NMR integrals. It is found that for each vendor, the ratio DS(A)/DS(S) increases from the L to M to H nominal grade polymers (**Table 3.1**), which is in agreement with the increase in acetate content. The molar ratios found between these functional groups by NMR closely reflects the DS ratios determined by liquid chromatography and captured in the relevant certificates of analysis (**Table 3.4**).

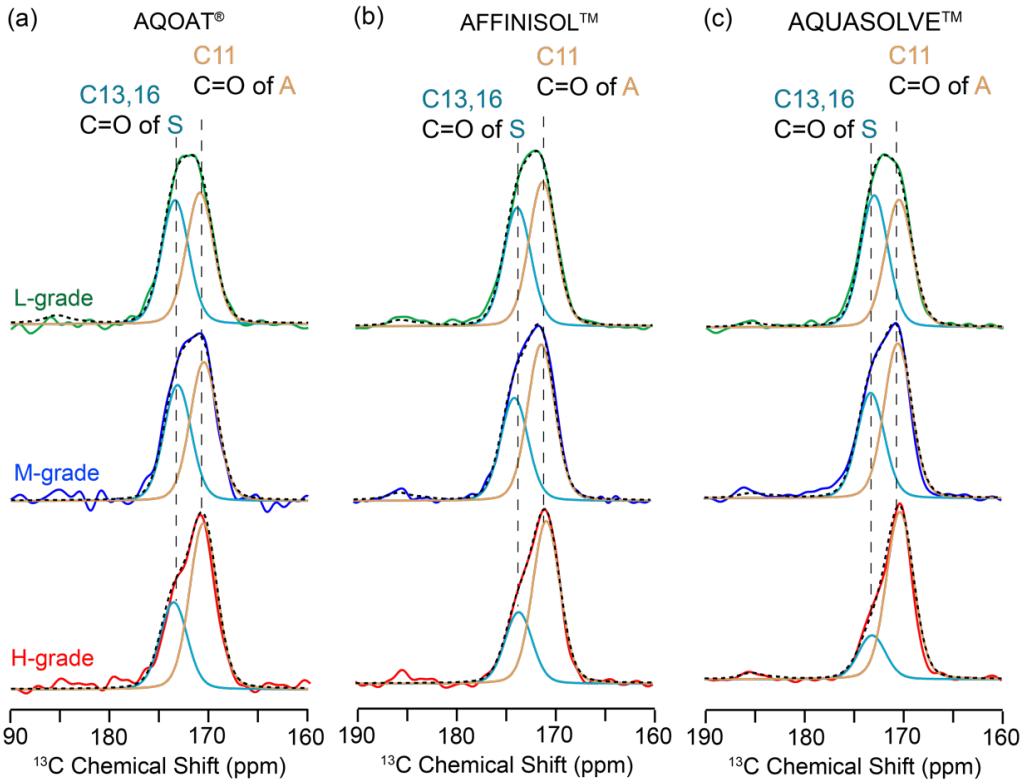

Figure 3.8. Magnified view of the 190–160 ppm region for hydroxypropylmethylcellulose acetyl succinate polymers as function of the grades for the (a) AQOAT®, (b) AFFINISOL™, and (c) AQUASOLVE™ series. Signals arising from the succinoyl and acetyl groups are given in turquoise and gold, respectively

Table 3.4. Estimated mol A/S ratio values obtained experimentally from NMR, using the integrals for C16,13 and C11 as discussed in the text. The nominal DS A/S ratios obtained from liquid chromatography are given in brackets (see **Table 3.1**).

	AQOAT®	AFFINISOL™	AQUASOLVE™
L-grade	2.0 ± 0.1 (1.3)	2.4 ± 0.1 (1.3)	2.1 ± 0.1 (1.2)
M-grade	2.4 ± 0.1 (1.9)	3.2 ± 0.2 (2.0)	3.1 ± 0.1 (2.2)
H-grade	3.6 ± 0.6 (3.6)	4.5 ± 0.1 (3.9)	7.5 ± 0.2 (5.3)

3.6 Conclusion

We have presented a structural elucidation of the different grades of HPMC-AS, containing different acetyl and succinoyl contents and its precursors using ^{13}C CP MAS NMR and ^{13}C-edited spectra, and refined the published spectral assignment. We demonstrated that this approach allows an estimation of the molar ratio of both groups and complements the liquid chromatography method used in the field. The knowledge of the structure and dependency of the ^{13}C chemical shifts on the local chemical environments will allow spatial interactions between this polymer and APIs to be detected and understood in ASDs. The work illustrates that the complexity of the HPMC-AS structure requires access to ^{13}C CP MAS NMR spectra and knowledge of ^{13}C chemical shifts of each specific batch of polymer to ensure that any change in chemical shifts in the ASDs are precisely captured.

3.7 References

[1] L. Carpentier, R. Decressain, A. De Gusseme, C. Neves, M. Descamps, *Pharm. Res.* **2006**, *23*, 798.

[2] R. O. Williams, M. Zhang, H. Li, B. Lang, K. O'Donnell, H. Zhang, Z. Wang, Y. Dong, C. Wu, *Eur. J. Pharm. Biopharm*. **2012**, *82*, 534.

[3] S. Baghel, H. Cathcart, N. J. O'Reilly, *J. Pharm. Sci.* **2016**, *105*, 2527.

[4] G. Van Den Mooter, J. Van Den Brande, P. Augustijns, R. Kinget, *J. Thermal Anal.* **1999**, *57*, 493.

[5] K. J. Crowley, G. Zografi, *Pharm. Res.* **2003**, *20*, 1417.

[6] H. Takeuchi, S. Nagira, H. Yamamoto, Y. Kawashima, *Int. J. Pharm.* **2005**, *293*, 155.

[7] K. J. Crowley, G. Zografi, *J. Pharm. Sci.* **2002**, *91*, 2150.

[8] Z. Dong, A. Chatterji, H. Sandhu, D. S. Choi, H. Chokshi, N. Shah, *Int. J. Pharm.* **2008**, *355*, 141.

[9] A. Rezaei Mokarram, A. Kebriaee Zadeh, M. Keshavarz, A. Ahmadi, B. Mohtat, *DARU J. Pharm. Sci.* **2010**, *18*, 185.

[10] K. Gong, R. Viboonkiat, I. U. Rehman, G. Buckton, J. A. Darr, *J. Pharm. Sci.* **2005**, *94*, 2583.

[11] G. Van Den Mooter, D. Q. M. Craig, P. G. Royall, *J. Pharm. Sci.* **2001**, *90*, 996.

[12] M. Yoshioka, C. Bruno, B. C. Hancock, G. Zografi, *J. Pharm. Sci.* **1995**, *84*, 983.

[13] D. Mcnamara, S. Yin, D. Pan, G. Crull, P. Timmins, B. Vig, *Mol. Pharm.* **2017**, *14*, 377.

[14] Y. Song, X. Yang, X. Chen, H. Nie, S. Byrn, J. W. Lubach, *Mol. Pharm.* **2015**, *12*, 857.

[15] D. Law, E. A. Schmitt, K. C. Marsh, E. A. Everitt, W. Wang, J. J. Fort, S. L. Krill, Y. Qiu, *J. Pharm. Sci.* **2004**, *93*, 563.

[16] D. S. Jones, Y. Tian, S. Li, T. Yu, O. A. Abu-Diak, G. P. Andrews, *J. Pharm. Sci*. **2016**, *105*, 3064.

[17] P. Gupta, V. K. Kakumanu, A. K. Bansal, *Pharm. Res*. **2004**, *21*, 1762.

[18] K. Lehmkemper, S. O. Kyerematen, O. Heinzerling, M. Degenhardt, G. Sadowski, *Mol. Pharm.* **2017**, *14*, 157.

[19] J. C. Dinunzio, J. R. Hughey, C. Brough, D. A. Miller, R. O. Williams, J. W. McGinity, *Drug Dev. Ind. Pharm.* **2010**, *36*, 1064.

[20] F. Tanno, Y. Nishiyama, H. Kokubo, S. Obara, *Drug Dev. Ind. Pharm*. **2004**, *30*, 9.

[21] D. T. Friesen, R. Shanker, M. Crew, D. T. Smithey, W. J. Curatolo, J. A. S. Nightingale, *Mol. Pharm*. **2008**, *5*, 1003.

[22] K. Lehmkemper, S. O. Kyerematen, O. Heinzerling, M. Degenhardt, G. Sadowski, *Mol. Pharm.* **2017**, *14*, 4374.

[23] Y. Ishizuka, K. Ueda, H. Okada, J. Takeda, M. Karashima, K. Yazawa, K. Higashi, K. Kawakami, Y. Ikeda, K. Moribe, *Mol. Pharm.* **2019**, *16*, 2785.

[24] X. Lu, C. Huang, M. B. Lowinger, F. Yang, W. Xu, C. D. Brown, D. Hesk, A. Koynov, L. Schenck, Y. Su, *Mol. Pharm.* **2019**, *16*, 2579.

[25] Dow Chemical Co., AFFINISOLTM HPMCAS for Spray-Dried Dispersion (SDD), **2014**.

[26] Ashland, AQUASOLVETM. Physical and Chemical Properties Handbook, **2016**.

[27] ShinEtsu Co., Hypromellose Acetate Succinate Shin-Etus AQOAT, **2005**.

[28] J. R. Everett, R. K. Harris, J. C. Lindon (Eds), *NMR in Pharmaceutical Sciences,* John Wiley & Sons Ltd, Chichester, UK **2015**.

[29] U. Holzgrabe, I. Wawer, B. Diehl (Eds), *NMR Spectroscopy in Pharmaceutical Analysis*, Elsevier Science, Oxford **2008**.

[30] M. Pellecchia, I. Bertini, D. Cowburn, C. Dalvit, E. Giralt, W. Jahnke, T. L. James, S. W. Homans, H. Kessler, C. Luchinat, B. Meyer, H. Oschkinat, J. Peng, H. Schwalbe, G. Siegal, *Nat. Rev. Drug Discov*. **2008**, *7*, 738.

[31] D. M. Sperger, E. J. Munson, *AAPS PharmSciTech* **2011**, *12*, 821.

[32] R. K. Harris, *J. Pharm. Pharmacol.* **2007**, *59*, 225.

[33] A. Paudel, M. Geppi, G. Van Den Mooter, *J. Pharm. Sci.* **2014**, *103*, 2635.

[34] A. S. Tatton, T. N. Pham, F. G. Vogt, D. Iuga, A. J. Edwards, S. P. Brown, *Mol. Pharm.* **2013**, *10*, 999.

[35] M. Tobyn, J. Brown, A. B. Dennis, M. Fakes, Q. I. Gao, J. Gamble, Y. Z. Khimyak, G. McGeorge, C. Patel, W. Sinclair, P. Timmins, *J. Pharm. Sci.* **2009**, *98*, 3456.

[36] Y. Song, D. Zemlyanov, X. Chen, H. Nie, Z. Su, K. Fang, X. Yang, D. Smith, S. Byrn, J. W. Lubach, *Mol. Pharm.* **2016**, *13*, 483.

[37] D. M. Pisklak, M. A. Zielinska-Pisklak, Ł. Szeleszczuk, I. Wawer, *J. Pharm. Biomed. Anal.* **2016**, 122, 81.

[38] O. Petermann, M. Brackhagen, M. Sprehe, R. B. Appell, Eur. Pat. Off. **2018**, EP2964679B.

[39] B. M. Fung, A. K. Khitrin, K. Ermolaev, *J. Magn. Reson.* **2000**, *142*, 97.

[40] D. C. Apperley, R. K. Harris, P. Hodgkinson, *Solid-State NMR: Basic Principle & Practice*, Momentum Press, LLC, New York **2012**.

[41] R. R. Ernst, G. Bodenhausen, A. Wokaun, Principles of Nuclear Magnetic Resonance in One and Two Dimensions, Oxford Science Publications, Oxford **1990**.

[42] X. Wu, S. T. Burns, K. W. Zilm, *J. Magn. Reson. A* **1994**, *111*, 29.

[43] C. R. Morcombe, K. W. Zilm, *J. Magn. Reson.* **2003**, *162*, 479.

[44] Y. Onda, H. Muto, K. Maruyama, U.S. Pat. **1978**, US4226981A.

[45] A. Idström, S. Schantz, J. Sundberg, B. F. Chmelka, P. Gatenholm, L. Nordstierna, *Carbohydr. Polym.* **2016**, *151*, 480.

[46] H. Kono, S. Yunoki, T. Shikano, M. Fujiwara, T. Erata, M. Takai, *J. Am. Chem. Soc*. **2002**, *124*, 7506.

[47] H. Yang, T. Wang, D. Oehme, L. Petridis, M. Hong, J. D. Kubicki, *Cellul*. **2018**, *25*, 23.

[48] J. Xu, R. Y. Dong, V. Domenici, C. A. Veracini, *J. Phys. Chem. B* **2006**, *110*, 9434.

[49] R. M. Silverstein, F. X. Webster, D. J. Kiemle, D. L. Bryce, *Spectrometric Identification of Organic Compounds*, 8th ed., Wiley, New York **2005**.

[50] P. L. Nasatto, F. Pignon, J. L. M. Silveira, M. E. R. Duarte, M. D. Noseda, M. Rinaudo, *Polymers*. **2015**, *7*, 777.

[51] Y. Y. Chen, S. Y. Luo, S. C. Hung, S. I. Chan, D. L. M. Tzou, *Carbohydr. Res.* **2005**, *340*, 723.

[52] S. Warashina, M. Tobyn, Personal Communication, **2019**.

Chapter 4: Drug−Polymer Interactions in Acetaminophen/ Hydroxypropyl-methylcellulose Acetyl Succinate Amorphous Solid Dispersions Revealed by Multidimensional Multinuclear Solid-State NMR Spectroscopy

4.1 Overview

Chapter 4 is a paper entitled “Drug−Polymer Interactions in Acetaminophen/ Hydroxypropylmethylcellulose Acetyl Succinate Amorphous Solid Dispersions Revealed by Multidimensional Multinuclear Solid-State NMR Spectroscopy” by Andrea Pugliese, Michael Toresco, Daniel McNamara, Dinu Iuga, Anuji Abraham, Michael Tobyn, Lucy E. Hawarden, and Frédéric Blanc which was published in *Molecular Pharmaceutics*, **2021**, 18, 3519.

The author contributions are as follows: M. Tobyn, L.E.H, and F.B. devised the project. M. Toresco and D.M. synthesised the amorphous solid dispersions, A.P. conducted all the NMR experiments, with support from D.I. with the ^{14}N-^{1}H HMQC experiment recorded at the Warwick 850 MHz facility. Data analysis and interpretation were undertaken by A.P., D.I., A.A. and F.B.. A.P. and F.B. wrote the manuscript with consultation from all other authors.

4.2 Abstract

The bioavailability of insoluble crystalline active pharmaceutical ingredients (APIs) can be enhanced by formulation as amorphous solid dispersions (ASDs). One of the key factors of ASD stabilization is the formation of drug−polymer interactions at the molecular level. Here, we used a range of multidimensional and multinuclear nuclear magnetic resonance (NMR) experiments to identify these interactions in amorphous acetaminophen (paracetamol)/ hydroxypropylmethylcellulose acetyl succinate (HPMC-AS) ASDs at various drug loadings. At low drug loading (<20 wt. %), we showed that $^{1}H-^{13}C$ through-space heteronuclear correlation (HETCOR) experiments identify proximity between aromatic protons in acetaminophen with cellulose backbone protons in HPMC-AS. We also show that $^{14}N-^{1}H$ heteronuclear multiple quantum coherence (HMQC) experiments are a powerful approach in probing spatial interactions in amorphous materials and establish the presence of hydrogen bonds (H-bond) between the amide nitrogen of acetaminophen with the cellulose ring methyl protons in these ASDs. In contrast, at higher drug loading (40 wt. %), no acetaminophen/HPMC-AS spatial proximity was identified and domains of recrystallisation of amorphous acetaminophen into its crystalline form I, the most thermodynamically stable polymorph, and form II are identified. These results provide atomic scale understanding of the interactions in the acetaminophen/HPMC-AS ASD occurring via H-bond interactions.

4.3 Introduction

Biopharmaceutical class II active pharmaceutical ingredients (APIs) (or drugs) exhibit poor bioavailability as a result of low aqueous solubility, accompanied by high biological membrane permeability.[1] API can exist either in the crystalline form, characterised by a three-dimensional (3D) structure in which molecules are packed in a regularly ordered repeating pattern, or amorphous form defined as an ensemble of molecules/units arranged randomly. The energy barrier required to break down the long-range structure means that crystalline systems can show low solubility and a low kinetic rate of dissolution. In amorphous systems, the lack of long-range order greatly enhances the apparent solubility and rate of dissolution.[2] From a thermodynamic viewpoint, the crystalline state is low energy and stable in contrast to the amorphous state, which is marked as high energy and unstable. The metastable nature of the amorphous state leads to the likelihood of physical instability and recrystallisation promoted by external factors such as temperature or humidity.[3] Converting crystalline drugs to their amorphous counterpart is one of the most promising approaches in pharmaceutical material sciences to enhance APIs' solubility and bioavailability. This strategy can be adopted only as long as a supersaturated solution of amorphous API can be maintained in the aqueous medium over time.[4]

Amorphous solid dispersions (ASDs) have been extensively used to stabilise supersaturated solution of APIs, resulting in a general increase for oral bioavailability of poorly soluble drugs.[5−7] An ASD can be defined as a dispersion of one or more APIs in a solid state inert carrier, usually an amorphous polymer[8], and can be prepared by a range of manufacturing processes[9], including spray drying[10], spray freeze drying[11], and hot melt extrusion.[12] Polymers such as

poly(ethylene glycol) (PEG)[13], poly(ethylene oxide) (PEO)[14], poly- (vinyl pyrrolidone) (PVP)[15], poly(vinyl pyrrolidone)−co-vinyl acetate (PVP−VA)[16], hydroxypropylmethylcellulose (HMPC)[17], and hydroxypropylmethylcellulose acetyl succinate (HPMC-AS)[18] have been successfully used in ASDs. In particular, HPMC-AS has recently been suggested as a promising solid matrix to formulate ASDs[19] due to its high glass transition temperature, Tg, in the order of 120 °C,[20] its amphiphilic nature arising from the existence of hydrophilic (e.g., acetyl, A) and hydrophobic (e.g., succinoyl, S) functional groups, and the capability to tune the A and S contents.

It has been demonstrated that the polymer in ASDs plays a crucial role in stabilizing the amorphous form of the drug.[21] The choice of a suitable polymer to formulate a specific dispersion largely depends on several chemical−physical properties such as Tg, thermal stability, dissolution profile, performance in dissolving API, and capability to stabilise amorphous drugs.[22] These characteristics contribute to the stabilization of the ASD, which is due to the polymer's antiplasticizing effect, reducing molecular mobility of the amorphous API, and the formation of specific API−polymer interactions.[21] Intermolecular interactions such as hydrogen bonding (H-bond), ionic forces, $\pi-\pi$, or electrostatic interactions are well established as the most significant interactions capable of stabilizing such dispersed systems[4] by inhibiting recrystallisation phenomena in the amorphous matrix and preventing competitive API−API or polymer−polymer intramolecular interactions. Recently, the HPMC-AS polymer[23] has been widely used to prepare ASD due to its remarkable ability in stabilizing amorphous dispersions arising from the formation of strong API−HPMC-AS interactions.[24]

The elucidation of the nature of the interaction between drugs and polymers and detecting recrystallised drugs in ASDs constitute some of the most significant challenges in pharmaceutical material sciences and require the exploitation of a range of characterization approaches, often combining powder X-ray diffraction (PXRD), thermal analysis, vibrational methods, and solid-state nuclear magnetic resonance (NMR) spectroscopy.[25,26] The PXRD patterns of amorphous solids result in broad diffuse scattering signals due to the lack of long range order. Nevertheless, PXRD methods can provide significantly useful information on the residual crystalline content in ASDs, for example, during stability studies.[27] Thermal analysis, including differential scanning calorimetry (DSC) and temperature-modulated DSC (mDSC)[28], have been employed to estimate the residual crystallinity in amorphous systems[29] and are often used to determine Tg values and detect thermal events revealing crystallisation and melting phenomena.[30] DSC therefore allows to detect miscibility of individual components of an ASD, where the observation of a single Tg indicates miscibility between API and the polymer.[31] Gordon−Taylor's (GT) model[32] can be used to estimate the Tg of an ideal binary mixture (Tg_{mix}) with significant deviations between predicted Tg_{mix} and experimentally determined Tg providing useful information about the interactions between the components in the mixture [4,25,26], as the presence of API−API or API−polymer interactions can affect the Tg value of the system, while agreement suggests systems with the absence of specific drug−polymer interactions. Furthermore, access to ASD stability can be also obtained using thermodynamic modelling and short- to medium-term physical stabilities of several API−polymer blend ASDs. These include acetaminophen−HPMC-AS dispersions under controlled temperature and relative humidity (RH) conditions which have been determined for the 20 and 40 wt. % formulation to be up to 6 and 1 month(s), respectively.[33] This work highlights a

reduction of stability of these systems with the increase of the polymer content and an increase of RH.

A range of analytical methods including vibrational, Raman, Fourier-transform infrared (FT-IR) spectroscopy, and solid-state nuclear magnetic resonance (NMR) spectroscopies have been used to provide atomic scale information about solid dispersions. Raman applications include the measurements of crystallisation rate[34] and mapping solid dispersions to identify and discriminate crystalline/amorphous domains.[35] FT-IR methods can be used to probe H-bonds for specific functional groups including hydroxyl, amino, and carbonyl groups when present in the API and/or the polymer molecular structure.[36] It has been demonstrated that when those functional groups are involved in H-bonding interactions, a simultaneous decrease in the stretching frequency and a widening of their absorption bands are observed due to smaller intermolecular distances between the donor−acceptor groups.[37]

NMR spectroscopy has proved itself as a powerful technique by providing an invaluable source of both structural and dynamics information at the atomic scale thereby being demonstrated as one of the most powerful methods of characterization. In particular, in the field of pharmaceutical sciences[38,39], NMR allows the determination of the structure of drugs[40] and polymers.[41] Recently, NMR has emerged as a robust approach in (pharmaceutical) amorphous dispersions to identity site-specific API−polymer intermolecular interactions from changes in chemical shift values.[42−45] For example, using one-dimensional (1D) and two-dimensional (2D) NMR experiments, electrostatic interactions and H-bonding were identified in amorphous posaconazole (POSA) dispersion in HPMC-AS and involved the POSA's triazole and difluorophenyl ring moieties with some of the HPMC-AS's substituent groups.[44]The presence of π−π aromatic packing interaction between POSA and HPMC-phthalate (HPMC-P) amorphous dispersion

has also been highlighted.[44] Drug− polymer interactions in carbamazepine (CBZ) in HPMC, HPMC-A, and HPMC-S dispersions have also been established[42] and identified H-bonding between the CBZ's $-NH_2$ group with the acetyl moiety in HPMC-A and between both CBZ $-NH_2$'s and carbonyl groups of the succinyl group in HPMC-S. This demonstrates the important role that both acetyl and succinyl groups of HPMC-AS could play in the formation of stable API−polymer connections. 2D NMR techniques that include homonuclear and heteronuclear correlation spectroscopy are widely used to detect intramolecular interaction by exploiting the homo- and heteronuclear through-space dipolar coupling between the nuclei. To increase the NMR sensitivity and hence to have access to high resolution spectra and enabling proton detection, the use of ultrafast magic angle spinning (MAS) experiments, with frequency in the 50−110 kHz range, has also recently emerged. They enable fast characterization of pharmaceutical compounds and formulation by probing API−polymer interaction,[45] allowing NMR crystallography approaches[46] and understanding of low drug-loaded formulation.[47] The $^{14}N-^{1}H$ heteronuclear multiple-quantum coherence (HMQC)[48] experiment carried out at the high magnetic field and at ultrafast MAS conditions under direct ^{1}H signal detection has been robustly employed to probe interactions in crystalline systems[49,50] and recently to highlight molecular association and interactions in amorphous dispersions.[51,52] $^{14}N-^{1}H$ HMQC spectra were used to identify hydrogen bonding interaction in a nicotinamide palmitic acid cocrystal and acetaminophen−PVP amorphous dispersion.[50] The versatility of this experiment was demonstrated by providing information on the symmetry of the nitrogen environment and through-space proximities in paclitaxel-loaded polymer micelles amorphous formulations.[52] The $^{14}N-^{1}H$ HMQC experiment has however, to the best of our knowledge, not been used so far to investigate API−polymer interactions in HPMC-AS-based amorphous formulations.

Here, we report the stability of amorphous acetaminophen in HPMC-AS ASDs at different drug loadings by identifying the presence of drug−polymer intramolecular interactions with multinuclear multidimensional NMR experiments. Acetaminophen (**Figures 4.1**) is one of the most widely used API and its chemical−physical data, including melting point and solubility profiles, as well as crystalline data [53,54], NMR spectra[55], are largely known. The HPMC-AS polymer was chosen as excipient due to its excellent capacity to stabilise amorphous dispersion.[42,44] Moreover, the lack of overlap between acetaminophen and polymer signals in the ^{13}C NMR spectra allows monitoring of the changes in chemical shift and line width of the signals of both components to establish API−polymer interactions and crystalline/amorphous behaviour. Multidimensional multinuclear MAS NMR data enable access to structural information in the solid state, highlighting the presence of API−polymer intermolecular interactions for ASDs with drug loading <20 wt. % and providing useful indications of their stability. The approach also suggests the absence of API−polymer intermolecular interaction in the 40 wt. % ASD and rather identifies signals corresponding to crystalline acetaminophen interacting with itself.

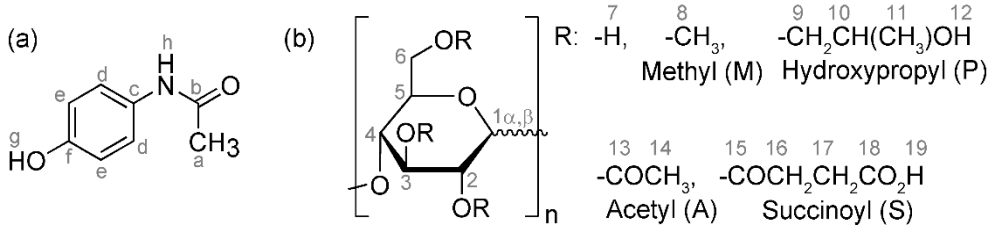

Figure 4.1. Chemical structures of (a) acetaminophen and (b) HPMC-AS polymer. HPMC-AS consist of a cellulose ring bonded with various R groups that include hydrogen, methyl (M), hydroxypropyl (P), acetyl (A), and succinoyl (S) groups. The wavy bond in the cellulose ring indicates that the cellulose ring can exist in two different cyclic hemiacetal configurations, called α- and β-glucopyranose, distinguishable from the different configurations of the anomeric carbon C1. The lettering and numbering are used for all NMR spectral assignments throughout.

4.4 Experimental section

4.4.1 Materials

ASDs were prepared using acetaminophen form I (99.5%) purchased from Spectrum Chemical Company and HPMC-AS polymer M grade obtained from Shin-Etsu Chemical Co. (lot # 6033060, M content = 23.4%, P content = 7.3%, A content = 8.8%, and S content = 11.2%). Sigma - Aldrich's acetaminophen form I was used to carry out the PXRD analysis. The dipeptide β-AspAla was obtained from Bachem. All materials were used as received.

4.4.2 Synthesis of ASDs

General procedure of the preparation of ASDs: Gram-scale batches formulated at 10, 20, and 40 wt. % of acetaminophen were manufactured using a custom-built small-scale spray dryer. Spray dry solution of acetaminophen and the polymer containing 2.5% solid (acetaminophen and HPMC-AS) were sprayed at 65−70 °C from acetone (80 mL) using heated nitrogen gas through a two-fluid spraying nozzle (2050 LC/64AC, Spraying Systems Co.). The ASD was then collected by filtration from the spray dryer and dried overnight in vacuo. ASDs were stored in a freezer kept at low temperature (−80 °C) to prevent API recrystallisation.

Synthesis of 10 wt. % acetaminophen in HPMC-AS ASD: This formulation was prepared according to the general procedure highlighted above using acetaminophen (0.2 g, 1.3 mmol) and HPMC-AS (1.7 g).

Synthesis of 20 wt. % acetaminophen in HPMC-AS ASD: This formulation was prepared according to the general procedure highlighted above using acetaminophen (0.4 g, 2.7 mmol) and HPMC-AS (1.6 g).

Synthesis of 40 wt. % acetaminophen in HPMC-AS ASD: This formulation was prepared according to the general procedure highlighted above using acetaminophen (0.8 g. 5.3 mmol) and HPMC-AS (1.2 g).

4.4.3 PXRD Measurements

Laboratory PXRD data were collected using a PANalytical Empyrean diffractometer equipped with a high throughput transmission geometry, focusing mirror, 1/2° divergence, and antiscatter slits, 4 mm beam mask, 0.04° soller slits, with Cu Kα of 1.541874 Å. PXRD patterns were measured over the 2θ range 2−40° over 1 h.

4.4.4 Standard and Modulated DSC Measurements

DSC experiments were performed using a DSC Q1000 (TA Instruments, DE) system using TA-Tzero aluminium pans loaded with an amount of around 10 mg of the sample. Standard DSC analyses were carried out using a cool−heat−cool cycle method in which the sample was cooled to −15 °C and heated up to 160 °C with a ramp of 10 °C min^{-1}, and then, after an isotherm of 5 min, a cool ramp of 20 °C min^{-1} was applied back down to −15 °C. mDSC experiments were carried out using a heating ramp of 2.5 °C min^{-1} with a modulation amplitude of 1.5 °C every 60 s.

4.4.5 Solid-State NMR Experiments

^{1}H NMR spectra were recorded on a Bruker 800 MHz (18.8 T) Avance Neo NMR spectrometer using a Bruker 1.3 mm HX MAS probe or on a Bruker 850 MHz (20 T) Avance Neo spectrometer equipped with a Bruker 1.3 mm triple-resonance HXY MAS probe in the double resonance (DR) mode. All spectra were recorded under a MAS frequency of ν_r = 60 kHz. ^{1}H pulses were carried out at a radio frequency (rf) field amplitude of 100 kHz. ASDs *1*H spin-lattice relaxation times T_1 were recorded at 18.8 T from saturation recovery experiments and fitted to a stretch exponential function of the form $1 - \exp[-(\tau/T_1)^{\alpha}]$ in which τ is the variable delay and α the stretch factor ranging from 0.5 and 1.

All ^{13}C/^{15}N cross-polarisation (CP) and 2D ^{1}H−^{13}C/^{15}N CP heteronuclear correlation (HECTOR) experiments were performed on a Bruker 400 MHz (9.4 T) Avance III HD NMR spectrometer equipped with a Bruker 4 mm triple-resonance HXY MAS probe in the DR mode tuned to ^{1}H and ^{13}C or ^{15}N at Larmor frequencies of 400.1, 100.6, and 40.5 MHz. ^{1}H pulses and SPINAL-64 heteronuclear

Decouplingduring ^{13}C/^{15}N detection were carried out with an rf field amplitude of 83 kHz.[56] All experiments were performed under a MAS frequency of ν_r = 12.5 kHz for ^{13}C and 10 kHz for ^{15}N and using a recycle delay of 1.3 × ^{1}H T_1s obtained as above (data at 9.4 T, not given). The Hartmann−Hahn conditions[57] for ^{13}C CP were achieved using a ^{13}C rf amplitude of around 45 kHz ramped to obtain maximum signal at a ^{1}H rf field of 60 kHz, and for ^{15}N CP, a ^{15}N rf amplitude of 28 kHz ramped to obtain maximum signal at a ^{1}H rf field of 50 kHz was used. A 2 ms contact time during ^{13}C CP and optimised CP contact times of 1 ms for the amorphous material and 6 ms for the crystalline sample during ^{15}N CP were used. ASD's ^{1}H spin-lattice relaxation times in the rotating frame ($T_{1\rho}$) were obtained at

9.4 T, using a spin-lock pulse sequence through ^{13}C detection via CP, at ^{1}H frequencies of $\omega_1/2\pi$ of 40 and 83 kHz and fitted to a stretch exponential function of the form exp $[-(\tau/T_{1\rho})^{\beta}]$ (with β ranging between 0.2 and 1). ^{13}C T_1s were obtained at 9.4 T from ^{13}C inversion recovery via CP experiments and fitted to an expression of the form exp $[-(\tau/T_1)^{\gamma}]$ (with γ ranging from 0.4 to 1). Frequency switched Lee−Goldberg (FSLG) homonuclear decoupling[58] during the ^{1}H t_1 evolution time in the 2D CP HETCOR spectra was obtained at an rf amplitude of 83 kHz and an offset of 60 kHz. Experimentally determined ^{1}H scaling factors λ_{exp} for FSLG (as measured on L-alanine using the experimental conditions given above) were used to recover the full ^{1}H chemical shifts $\delta(^{1}H)^{MAS}$ from the scaled down apparent chemical shifts $\delta(^{1}H)^{APP}$ according to $\delta(^{1}H)^{APP} = \lambda_{exp}\,\delta(^{1}H)^{MAS}$ that result from this decoupling.

$^{14}N-^{1}H$ HMQC experiments were carried out using a Bruker 800 MHz (18.8 T) Avance Neo NMR spectrometer equipped with a Bruker 1.3 mm HX MAS probe tuned to ^{1}H and ^{14}N at 800.3 and 58.7 MHz, respectively, or using a Bruker 850 MHz (20.0 T) Avance Neo NMR spectrometer equipped with a Bruker 1.3 mm triple-resonance HXY MAS probe operating in the DR mode tuned to ^{1}H and ^{14}N at 850.2 and 61.4 MHz, respectively. Experiments were performed under a MAS frequency ν_r = 60 kHz. In the $^{14}N-^{1}H$ HMQC pulse sequence used, heteronuclear dipolar couplings were reintroduced via rotary resonance recoupling, R^3[59], on the n = 2 resonance condition[48], using an x, $-x$ phase inversion[60] of individual block lengths of one rotor period of 16.7 μs at an rf amplitude of 120 kHz (2 × MAS frequency). ^{1}H and ^{14}N pulses were performed at an rf amplitude of 100 and 72 kHz, respectively. HMQC spectra were processed after removal of the first few points in the free induction decay (FID) using a home-built macro running on TopSpin to reduce baseline distortion and residual t_1 noise from the spectrum.

^{1}H, ^{13}C, and ^{15}N spectra were externally referenced to the NH proton of the dipeptide β-AspAla at 8.0 ppm[50], the tertiary carbon of adamantane at 29.45 ppm[61], and to glycine at −347.2 ppm[62], respectively. ^{14}N shifts were referenced to solid NH_4Cl at −341.3 ppm[62], which has a cubic ^{14}N site.[63] Magic angle calibrations were achieved by maximizing either the separation of NH_3 and NH resonances of the dipeptide β-AspAla in the ^{14}N−^{1}H HMQC spectrum or the number of rotational resonances in the time domain of the ^{79}Br FID of KBr. The errors associated with ^{1}H, ^{13}C, and ^{15}N chemical shifts and ^{14}N parameters are given in the respective tables. ^{1}H $T_{1\rho}$ and ^{13}C T_1 fitting data were carried out using MATLAB R2017a. Deconvolution of the experimental spectra was carried out in TopSpin 4.0.5 using the solid line shape analysis routine.

4.5 Result and discussions

4.5.1 PXRD Characterization.

Acetaminophen exists in three polymorphic forms[53,64,65]: monoclinic form I (space group $P2_1/a$ and the number of asymmetric units in the cell, $Z' = 1$), which is the most thermodynamically stable form; orthorhombic form II (space group *Pcab*, $Z' = 1$) polymorph, and a highly metastable form III (space group $Pca2_1$, $Z' = 2$). Time-dependent PXRD pattern measurements (**Figure 4.2**) on acetaminophen−HPMC-AS ASDs at 10 wt. % (in dark blue), 20 wt. % (in orange), and 40 wt. % (in red) loadings were carried out over a 1-year period of exposure at room temperature (RT, around 20 °C) and ambient relative humidity (RH, ranging from 30 to 50%) to monitor the chemical stability of the systems and potential recrystallisation phenomena. The diffraction patterns of the 10 wt. % (in dark blue) ASD exhibit the typical broad signal of an amorphous material and the absence of Bragg peaks up to 1 year, indicating a strong tendency of this system to remain in the amorphous state. The 20 wt. % ASD shows a typical broad signal of an amorphous material only up to 4 weeks at RT and ambient RH after which reflections from acetaminophen form I start to appear. This is in sharp contrast with the PXRD data in 40 wt. % ASD that shows recrystallisation after only 1 week and, interestingly, to a mixture of both acetaminophen form I and II polymorphs.

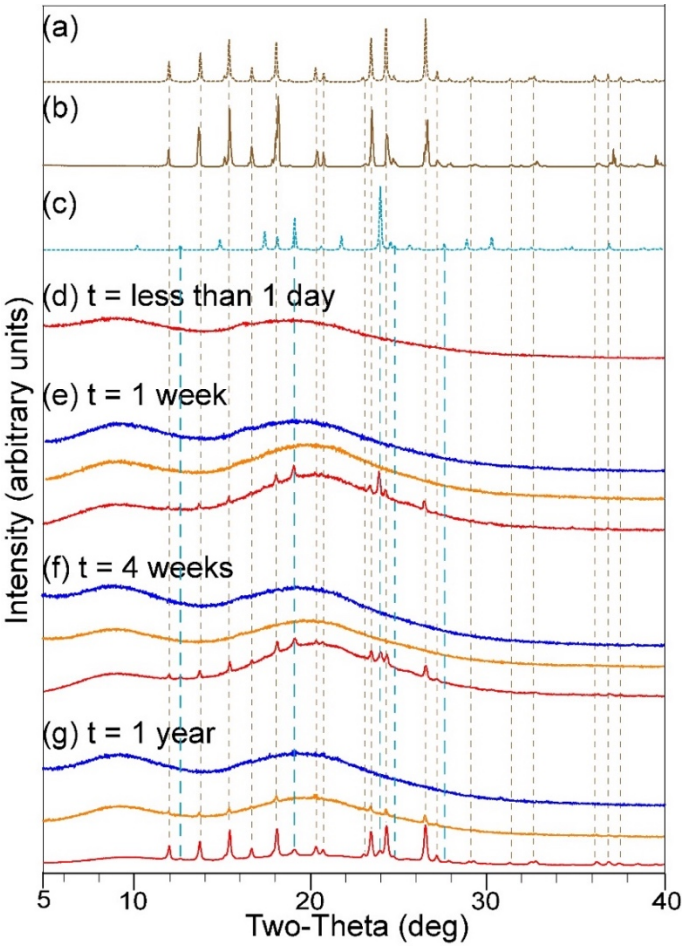

Figure 4.2. PXRD patterns of (a) simulated acetaminophen form I from CSD (refcode HXACAN01, brown dotted lines)[64], (b) experimental acetaminophen form I (brown full lines), and (c) simulated acetaminophen form II from CSD (refcode HXACAN23, light blue dotted lines).[64] Comparison of PXRD patterns of 10 wt. % (dark blue), 20 wt. % (orange), and 40 wt. % (red) for the acetaminophen−HPMC-AS ASDs at times of (d) less than 1 day, (e) 1 week, (f) 4 weeks, and (g) 1 year at RT (around 20 °C) and ambient RH (ranging from 30 to 50%). After 1 year, the 10 wt. % ASD still shows an amorphous state, while in the 20 wt. % traces of recrystallisation to acetaminophen I is observed and further confirmed by the ^{13}C CP HETCOR spectra (**Figure 4.3**). In 40 wt. % ASD, acetaminophen forms I and II are detected after only 1 week.

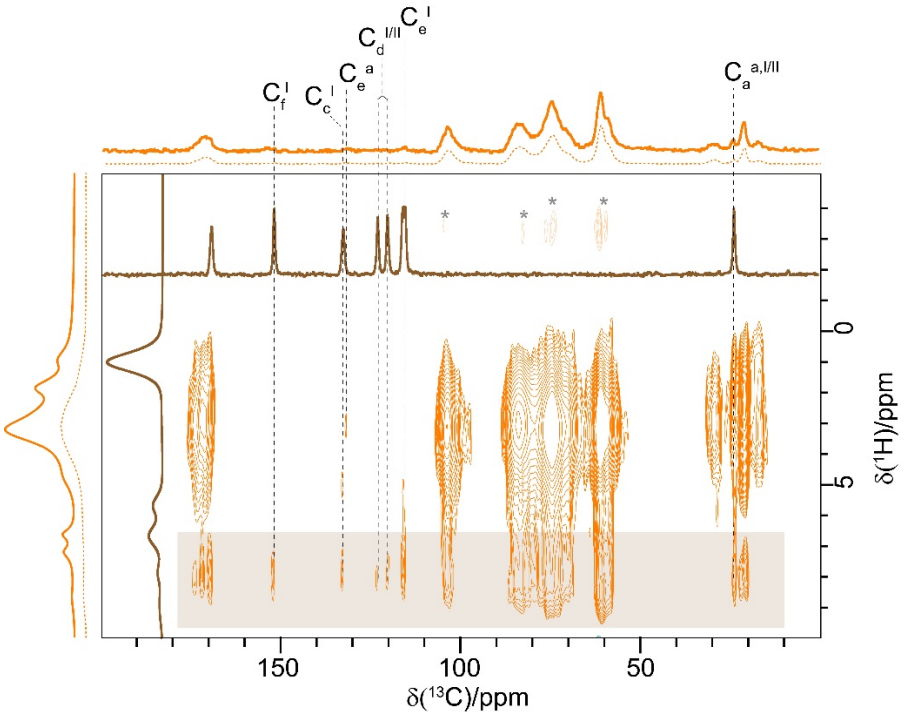

Figure 4.3. ^{13}C CP HETCOR recorded at contact time of 2 ms for the 20% wt. acetaminophen HPMC-AS solid dispersion after 1 year at room temperature (RT) and ambient room humidity (RH). The shaded section denotates drug-drug correlations from presence of acetaminophen form I in the sample, confirming the PXRD data (**Figure 4.2**, panel **(g)**). Top: ^{13}C CP MAS spectrum. Left: ^{1}H MAS NMR spectrum recorded at high magnetic field. The dashed spectra are internal projections. ^{1}H and ^{13}C CP spectra of acetaminophen form I are given in brown. The notation 'I' indicates the characteristic resonances for the acetaminophen form I, while the notation 'a' indicates resonances that can be attributed to amorphous acetaminophen. Asterisks denotate speed sidebands.

4.5.2 Thermal Characterization

The GT model was used to estimate the predicted Tgmix values of the acetaminophen− HPMC-AS dispersion at different drug loading wt % from **Equation 4.1**.

$$Tg = \frac{w_{acetaminophen}\, Tg_{acetaminophen} + k\, w_{HPMC\text{-}AS}\, Tg_{HPMC\text{-}AS}}{w_{acetaminophen} + k\, w_{HPMC\text{-}AS}} \qquad \textbf{Eq. 4.1}$$

where w and Tg are the weight fractions and glass transition temperature of each component, respectively, and k a constant related to the density ρ (ρacetaminophen = 1.29 g cm^{-3}, $\rho_{HPMC\text{-}AS}$ = 1.28 g cm^{-3})[33] and given by **Equation 4.2**

$$k = \frac{\rho_{acetaminophen}\, Tg_{acetaminophen}}{\rho_{HPMC\text{-}AS}\, Tg_{HPMC\text{-}AS}} \qquad \textbf{Eq. 4.2}$$

Table 4.1 summarises Tgs for the individual components as well as the predicted and experimental Tg_{mix} values obtained for the 10, 20, and 40 wt. % ASDs with negative deviations from predicted Tgs represented in **Figure 4.4**.

Table 4.1. Tg values obtained for the acetaminophen HPMC-AS ASDs.

Acetaminophen (w/w%)	Predicted Tgmix /°C	Experimental Tg /°C	(Tg – Tgmix) /°C
HPMC-AS	n.a.	120 (ref 2)	n.a.
10	103	76[a]	-27
20	105	74[a]	-31
40	88	45[b]	-43
Acetaminophen	n.a.	25 (ref 2)	n.a.

[a] Experimental values carried out using a standard DSC analysis. [b] Experimental values carried out using mDSC experiment. n.a.: not applicable.

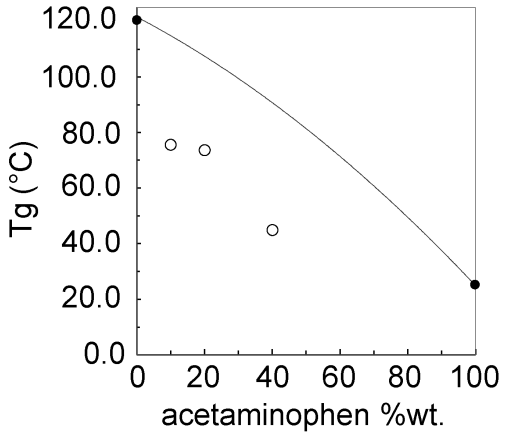

Figure 4.4. Tg values of acetaminophen−HPMC-AS dispersions obtained at different acetaminophen loadings in HPMC-AS polymer-based ASDs. Experimentally obtained values for the ASDs, individual component, and predicted values from the GT model based on **Equation 4.1** are given in empty circles (○), filled circles (●), and solid line, respectively.

This demonstrates the nonideal drug−polymer mixture,[7] the negative deviations suggesting that intramolecular interactions between like species (drug−drug or

polymer−polymer) dominate. However, importantly, this does not exclude the presence, to a lesser extent, of intramolecular drug−polymer interactions (see below).[66] Additionally, negative deviations can also be interpreted as being indicative of nonideal additivity of volume for the two components and points out of a likelihood of phase separation of the system.[67] The largest deviation is found for the 40 wt % solid dispersion and suggests that at, among the ASDs studied, recrystallisation phenomena and phase separation occur more quickly in this formulation.

4.5.3 Solid-State NMR Data

Figure 4.5(a) compares the ^{13}C CP MAS spectra of acetaminophen form I, HPMC-AS polymer, 10, 20, and 40 wt % ASDs. The spectrum of acetaminophen form I presents resonances at around 170 ppm for the carbonyl (C_b^I), 152−116 ppm for the aromatic carbons (C_f^I, C_c^I, C_d^I, C_e^I), and 24 ppm for the methyl carbon (C_a^I) (see **Figure 4.1(a)** and **Table 4.2**) ("I" indicates characteristic resonances for the acetaminophen form I) based on the previous literature.[68] The four peaks in the region 105−60 ppm in the spectrum of the HPMC-AS polymer (**Figure 4.1(b)**) can be attributed to the anomeric C_1, C_4, $C_{2,3}$, and $C_{5,10}$ carbons, while the shoulders at around 70 and 58 ppm correspond to $C_{6,9}$ (CH_2s) and C_8 (methoxy group), and the three peaks in the aliphatic region to $C_{16,17}$ (CH_2 of the S group), C_{14} (CH_3 of the A group), and C_{11} (methyl group of the P moiety). Deconvolution in the carbonyl region of the HPMC-AS polymer reveals two signals assigned to $C_{15,18}$ (most shifted peak, S substituent the Cos) and C_{13} (A's CO).[69] The knowledge of the C assignment of both the drug and HPMC-AS polymer plays an important role in the identification of drug−polymer interactions in ASDs as this is largely based on the change in chemical shifts.[4,43] The ^{13}C assignments for the ^{13}C CP MAS NMR spectra of all ASDs, recorded at less than 1 day at RT/ambient RH, are based on the known spectra of HPMC-AS[69] and acetaminophen form I and form II[68] (**Table 4.2**). In the spectra of the ASDs, signals assignable to the amorphous acetaminophen generally appear broader than in the crystalline form as expected from amorphization as the loss of crystallinity brings a range of chemical environments present that are randomly distributed in the sample resulting in severe inhomogeneous line broadening.[43] The decreased resolution is evident from the absence of split signals of the aromatic carbons of acetaminophen (C_d^I

and C_e^I), due to the lack of crystal packing, indicating the presence of amorphous acetaminophen. This is further confirmed by a significant shortening of ^{13}C T_1 values by up to 2 orders of magnitude from acetaminophen form I to the amorphous acetaminophen in the ASD (**Table 4.3**). Meanwhile, the ^{13}C T_1 values for HPMC-AS in the ASDs are slightly increased, presumably indicating an increase in rigidity when formulated and suggesting its co-binding in API−polymer interactions (see below). In addition, ^{13}C NMR signals for C_d^I/C_e^I and quaternary carbons C_f^a show a small difference in chemical shifts of 2−3 ppm *vs* acetaminophen form I (**Table 4.2**). This suggests a structural change in the amorphous systems[43,45,70] attributed to crystalline API conversion to its amorphous form[71] and results from the absence of long-range 3D interactions (e.g., hydrogen bonding, π−π interactions) in the crystalline sample, resulting in variation of local electronic environments.

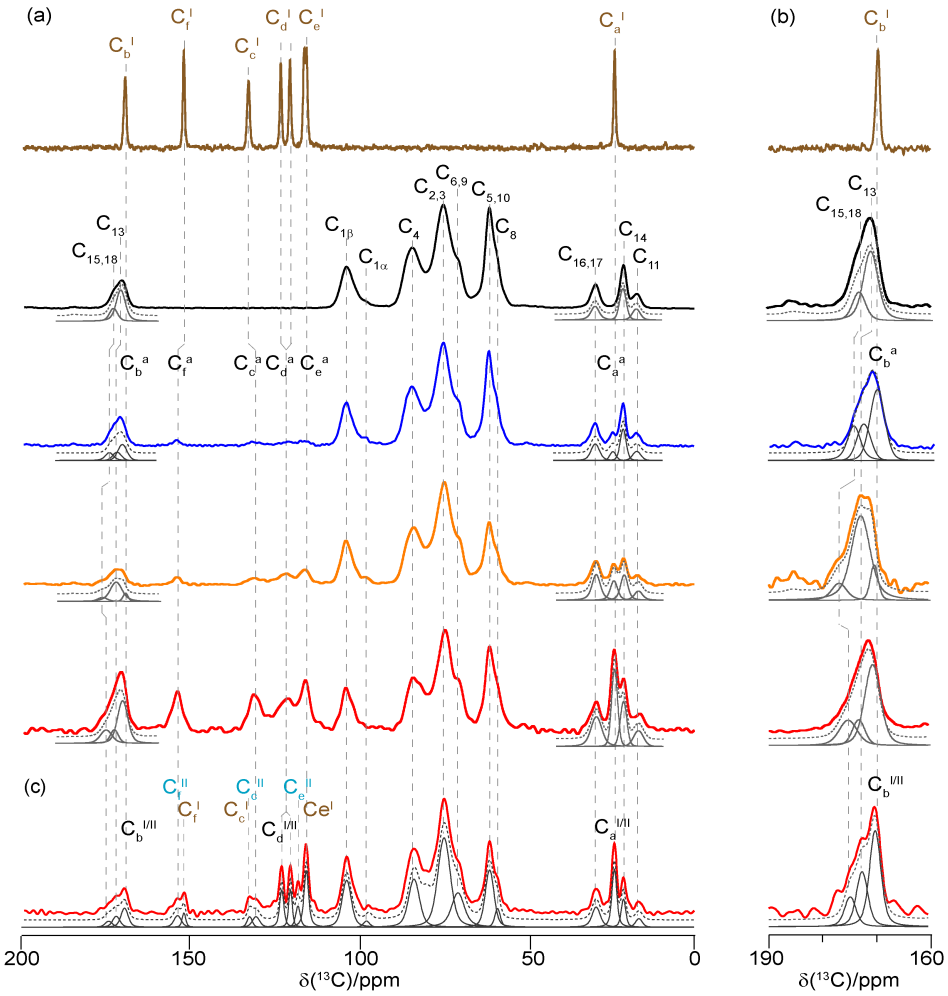

Figure 4.5. (a) ^{13}C CP MAS spectra of crystalline acetaminophen form I (brown), HPMC-AS (black)[69], 10 wt % (dark blue), 20 wt % (orange), and 40 wt % acetaminophen−HPMC-AS ASDs (red) recorded at less than 1 day at RT/ambient RH. (b) Magnified view of the 190−160 ppm (carbonyl region) of all of the spectra. (c) ^{13}C CP spectrum of the 40 wt % dispersion toward recrystallisation after 1 week at RT/ambient RH. A magnified view of the aromatic region of this spectrum is given in **Figure 4.6.** For spectral identification, simulated spectra (dashed gray lines) and spectral deconvolution (gray lines) are also shown. The notations “I” and “II” indicate the characteristic resonances for the acetaminophen forms I and II, respectively, while the notation “a” indicates resonance that can be attributed to amorphous acetaminophen.

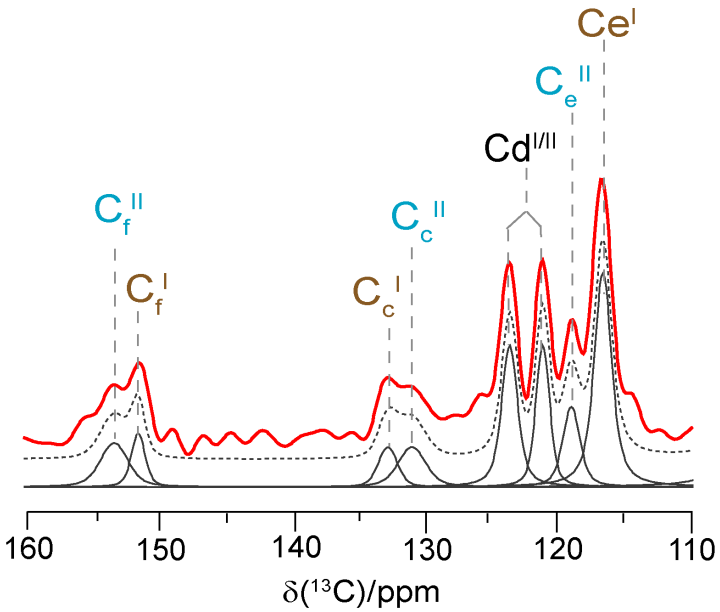

Figure 4.6. Magnified view of the 160–110 ppm ^{13}C region for the ^{13}C CP spectrum of 40% wt. acetaminophen in HPMC-AS solid dispersion after 1 week at RT and ambient RH. Simulated spectra (dashed grey lines) and spectral deconvolution (grey lines) are given and allowed assignment of all the resonances in paracetamol forms I and II based on literature data [68].

Table 4.2. A comprehensive list of ^{13}C chemical shifts[a]

Signal	Acetaminophen form I	HPMC-AS	10% wt. ASD	20% wt. ASD	40% wt. ASD	Recrystallised 40% wt. ASD
C15,18	n.a.	174	174	177	176	174.9
C13	n.a.	171	172	173	173	172.4
Cb	169.7	n.a.	171	171	171	169.8 (I/II)
Cf	152.2	n.a.	154	154	154	153.8 (II), 152.2 (I)
Cc	132.9	n.a.	131	131	131	132.9 (I), 130.76 (II)
Cd	123.3, 120.5	n.a.	121	121	121	123.3 (I), 120.5 (I/II)
Ce	116.3, 115.6	n.a.	116	116	116	118.3 (II), 115.7 (I)
C1α	n.a.	104	104	104	104	104
C1β	n.a.	100	100	100	100	100
C4	n.a.	84	84	84	84	84
C2,3	n.a.	75	75	75	75	75
C6,9	n.a.	70	70	70	70	70
C5,10	n.a.	61	61	61	61	61
C8	n.a.	58	58	58	58	58
C16,17	n.a.	29	29	29	29	29
Ca	23.6	n.a.	24.2	24.1	24.0	23.6 (I/II)
C14	n.a.	21	21	21	21	21.1
C11	n.a.	17	17	17	17	16.9

[a]Values are given in ppm. The ^{13}C chemical shifts of all assigned resonances are quoted within an accuracy of ±1 ppm due to the broad line widths associated with amorphous samples, except for the crystalline species where they are quoted at ±0.5 ppm. “I” and “II” indicate resonances belonging to acetaminophen form I and II, respectively.

Table 4.3. ^{13}C T_1 relaxation times values measured at 9.4 T.[a]

Signal	Acetaminophen form I	HPMC-AS	10% wt. ASD	20% wt. ASD	40% wt. ASD
C15,18	n.a.	20 (3)	22 (10)	25 (25)	20 (20)
C13	n.a.	27 (4)	n.d.	34 (3)	67 (48)
Cb	2220 (260)	n.a.	33 (7)	34 (4)	44 (17)
Cf	1050 (200)	n.a.	n.d.	24 (5)	38 (26)
Cc	1450 (280)	n.a.	n.d.	40 (13)	38 (30)
Cd	1440 (230)	n.a.	n.d.	5 (4)	23 (28)
Ce	1480 (250)	n.a.	n.d.	4 (1)	8 (22)
C1	n.a.	27 (2)	35 (10)	40 (3)	35 (4)
C4	n.a.	21 (1)	26 (2)	35 (2)	30 (4)
C2,3	n.a.	17 (0.7)	22 (0.9)	28 (1)	23 (2)
C6,9	n.a.	6 (0.5)	10 (0.9)	11 (1)	7 (2)
C5,10	n.a.	7 (0.3)	7 (0.9)	14 (3)	8 (0.8)
C8	n.a.	4 (0.3)	5 (0.8)	5 (0.4)	5 (0.7)
C16,17	n.a.	1 (0.2)	3 (0.9)	3 (0.4)	2 (0.9)
Ca	50 (10)	n.a.	9 (7.3)	11 (1.3)	11 (1)
C14	n.a.	10 (0.6)	11 (1.5)	12 (0.9)	9 (2)
C11	n.a.	1 (0.2)	1 (0.2)	1 (0.2)	1 (0.7)

[a] Values are given in seconds. Numbers in parenthesis indicate the standard error associated with the fit (e.g., ^{13}C T_1 for signal C_b in the acetaminophen form I reads 2220 ± 260 s). In some cases, the signal to noise ratio was too poor to reliably extract T_1 values which have therefore not been determined (n.d.). n.a.: not applicable.

Furthermore, and more importantly, the carbonyl carbons of the A and S units ($C_{15,18}$ and C_{13}) in the ASDs appear to be sensitive to the amount of amorphous acetaminophen in the ASDs as a slight change in chemical shifts *vs* HPMC-AS to a higher frequency is observed (**Figure 4.5(b)** and **Table 4.2**), as shown by the deconvoluted signals for the 190−160 ppm region of the spectra that assumed the presence of three carbonyl signals C_b, $C_{13,15}$, and C_{18} "three signals model" and supported by residual spectra (**Figure 4.7**). These shifts are ascribed to API−polymer intramolecular interaction in ASDs and detect molecular association via H-bonding in dispersions[31,72,73], as previously observed in the posaconazole (POSA) and HPMC-AS ASD.[44]

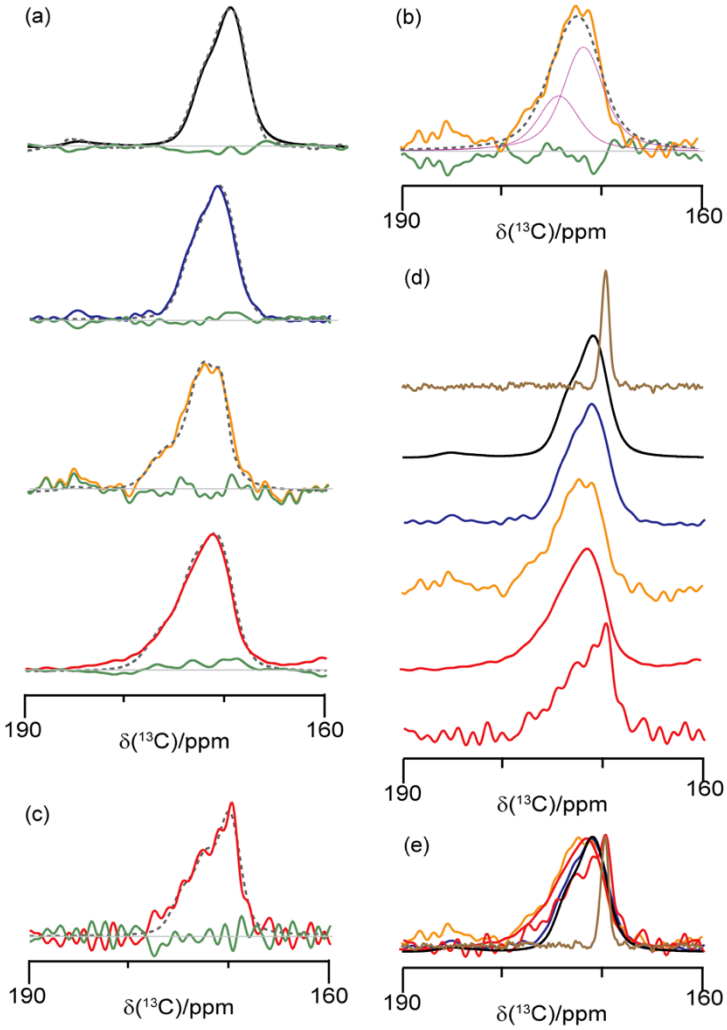

Figure 4.7. (a) Residual ^{13}C spectrum (in green) between experimental and simulated spectra using the “three signals model”. Experimental spectra for HPMC-AS, 10% wt., 20% wt., and 40% wt. acetaminophen dispersion are given in black, dark blue, orange, and red, respectively while simulated spectra are provided as dark grey dashed lines. The horizontal light grey lines mark the zero-intensity signal. (b) Residual ^{13}C spectrum (in green) between experimental and simulated spectra for the 20% wt. ASD using two peaks only (in violet) rather than the “three signals model" of (a). (c) Residual ^{13}C spectrum obtained for the 40% wt. dispersion towards recrystallisation. (d) Stacked and (e) Overlaid spectra overview in the 190–160 ppm (carbonyl) region. The crystalline acetaminophen form I ^{13}C CP spectrum is given in brown for comparison.

The ^{13}C CP MAS NMR spectrum of the 40 wt % ASD was also recorded after 1 week under ambient conditions (**Figure 4.5(c)**) and shows significant differences with the one obtained at less than 1 day at RT/ambient RH. The spectrum exhibits a number of additional and sharper peaks as well as a lengthening of the ^{1}H T_1's (**Table 4.4**), indicating the presence of crystalline acetaminophen arising from fast recrystallisation from the ASDs. The resonances observed in **Figure 4.5(c)** (a magnified view of the aromatic region of this spectrum is given in **Figure 4.6**) indicate the presence of signals that can be attributed to both acetaminophen form I (**Figure 4.5(a)**, brown) and II[68] as anticipated from the PXRD data (**Figure 4.2**). The presence of signals attributable to the two polymorphs of acetaminophen in 40 wt % ASD strongly indicates that instability of this dispersion toward recrystallisation and could be reasonably explained by the lack of any interaction between acetaminophen and HPMC-AS, as predicted by the significant negative deviation from the GT model (**Figure 4.4**).

Table 4.4. ^{1}H T_1 relaxation times values measured at 18.8 T.[a]

Signal	10% wt. ASD	20% wt. ASD	Recrystallised 40% wt. ASD
Hg,h	0.8 (0.2)	1.2 (0.3)	8.0 (2.0) (g), 5.5 (1.0) (h)
Hd	1.1 (0.2)	1.7 (0.2)	6.5 (0.7) (I), 4.3 (0.6) (II)
He	1.1 (0.3)	1.7 (0.3)	4.5 (0.7) (I), 6.5 (0.7) (II)
H1	1.6 (0.2)	1.9 (0.3)	1.9 (0.2)
H6,9	1.9 (0.2)	2.2 (0.3)	2.5 (0.2)
H2,3,5,10	2.1 (0.1)	2.5 (0.2)	3.0 (0.1)
H8	2.0 (0.1)	2.4 (0.2)	3.0 (0.1)
H4	1.9 (0.1)	2.3 (0.2)	2.8 (0.2)
H16,17	2.0 (0.2)	2.3 (0.3)	2.7 (0.1)
Ha	n.d.[b]	n.d. [b]	n.d. [b]
H11,14	n.d.[b]	n.d. [b]	n.d. [b]

[a] Values are given in seconds. [b] The ^{1}H T_1 for Ha and for the succinoyl CH_2s $H_{11,14}$ signals are not determined (n.d.) due to overlapping peaks. The number in parenthesis indicate the standard error associated with the fit.

Figure 4.8(a) compares the ^{15}N CP MAS NMR spectra of acetaminophen form I, 10 and 20 wt % amorphous acetaminophen in HPMC-AS solid dispersion, which show one signal assignable to the acetaminophen NH amide group (**Figure 4.1(a)**). This peak resonates at −243 ppm and is fairly narrow (full-width-at-half maximum, FWHM of 26 Hz), which is consistent with the literature data for acetaminophen form I,68 while the signal appears at −247 ppm for both 10 and 20 wt % ASDs and is significantly broader (FWHM of 240−260 Hz). The change in the ^{15}N chemical shift and broadening of the ^{15}N spectra observed between crystalline and amorphous species suggests a different hydrogen-bonding network and

intramolecular interactions (**Table 4.5**).[42,45,74] The ^{15}N CP spectrum of the 40 wt % ASD shows a single resonance at −243 ppm (FWHM of 24 Hz) at the same chemical shift for crystalline form I and likely arises from acetaminophen that underwent recrystallisation during data acquisition. Although acetaminophen forms I and II in the 40 wt % ASD have been observed in both PXRD and ^{13}C NMR data, the two expected ^{15}N signals are not resolved at 9.4 T, likely due to their very similar chemical shift values only separated by 0.4 ppm.[68] The ^{1}H MAS NMR spectrum (**Figure 4.8(b)**) of acetaminophen form I, obtained under a high magnetic field (>18.8 T) and very fast MAS frequency (>50 kHz), shows fairly resolved resonances at around 9.0, 7.9, 6.7, 5.7, and 1.1 ppm assigned to −NH and −OH groups, aromatic protons (H_d^I and H_e^I), and methyl groups, respectively. In the HPMC-AS spectrum, the three main peaks and the peak at 1.1 ppm can be assigned to H_1, $H_{2,3,5,10}$, $H_{16,17}$, and $H_{11,14}$, respectively, while spectral deconvolution reveals additional signals at 3.9, 3.0, and 2.5 ppm that are assigned to $H_{6,9}$, H_8, and H_4, respectively. Due to possible exchange phenomena, the H_7, −O*H* (hydroxypropyl substituent group), and the $-CO_2H$ (succinoyl moiety) proton signals (**Figure 4.1**) are not observed in the 1D and ^{13}C CP HETCOR spectra.

The ^{1}H spectra of HPMC-AS and all three ASDs (**Figure 4.8(b)**) are assigned from correlations observed in the ^{13}C CP HETCOR spectra recorded at a short contact time (**Figure 4.12(a)**), ^{15}N CP HETCOR spectrum of the 20 wt % (**Figure 4.9**), and known ^{1}H chemical shifts. The ^{1}H spectra of the ASDs (**Figure 4.8(b)**) show a cluster of signals around 5 and 1 ppm, corresponding to HPMC-AS, as well as additional resonances for the acetaminophen. As summarised in **Table 4.6**, in the 10 and 20 wt % ASDs, the aromatic proton signals (H_d^a and H_e^a) are deshielded with respect to the crystalline counterpart, the small difference observed being typical of amorphization processes.[71] Finally, the H_g^a and H_h^a signals merged into a single broad signal centered at 8.5 ppm, which correlates strongly with the ^{15}N

signal as revealed by the ^{15}N CP HETCOR spectrum (**Figure 4.9**), potentially confirming the absence of deprotonation. It has been demonstrated that the deprotonation effect, promoted by the solvent during the spray dry process, might impact API−polymer interactions.[45] It is well known that evaluation of the length scale of spin diffusion allows the degree of mixture miscibility to be determined by recording the ^{1}H relaxation times of all components.[75−78] ^{1}H T_1 and $T_{1\rho}$ values have therefore been measured for the API and polymer in the ASD (**Tables 4.4** and **4.7**) and revealed that, for the 20 wt % formulation, they are similar (e.g., ^{1}H T_1 values for H_d^a and H_1 are 1.7 ± 0.2 and 1.9 ± 0.3 s, respectively, and ^{1}H $T_{1\rho}$ (H_d^a) = 3.8 ± 1.1 ms ≈ ^{1}H $T_{1\rho}$ (H_1) = 4.4 ± 0.3 ms at a spin-lock frequency of 40 kHz), indicating that in the 2−5 nm length scale,[79] there is miscibility in the acetaminophen−HPMC-AS ASD. In contrast, significantly different ^{1}H T_1 and $T_{1\rho}$ values are obtained for the recrystallised 40 wt % dispersion (**Table 4.7**), suggesting that phase separation phenomena occur in a domain size larger than 20−50 nm.[79]

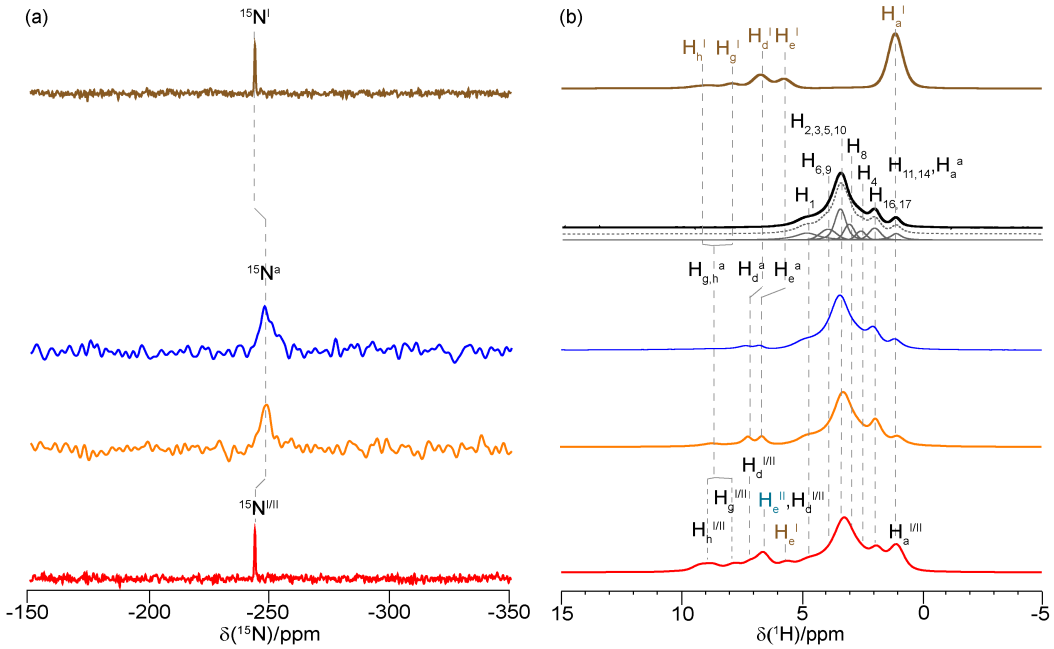

Figure 4.8. (a) ^{15}N CP MAS spectra of crystalline acetaminophen form I (brown), 10 wt % (dark blue), 20 wt % (orange), and 40 wt % (red) acetaminophen−HPMC-AS ASDs. (b) Quantitative ^{1}H spectra of crystalline acetaminophen form I (brown), HPMC-AS (black), 10 wt % (dark blue), 20 wt % (orange), and 40 wt % (red) acetaminophen HPMC-AS ASDs after recrystallisation. ^{1}H signal assignment is based on the ^{13}C and ^{15}N CP HETCOR experiments in **Figures 4.12(a)** and **4.9**, respectively. Magnified views of both ^{15}N CP and ^{1}H spectra can be found in **Figures 4.10** and **4.11**, respectively.

Table 4.5. Experimental ^{15}N Isotropic Chemical Shifts $\delta_{iso}(^{15}N)$, ^{14}N Shifts $\delta_{iso}(^{14}N)$ ^{14}N Quadrupolar-Induced Shift $\delta^{Q}_{iso}(^{14}N)$, and Quadrupolar Products P_Q

Sample	$\delta_{iso}(^{15}N)$[a]	$\delta_{iso}(^{14}N)$[a]	$\delta^{Q}_{iso}(^{14}N)$[a]	P_Q[b]
Acetaminophen form I[51],[c]	-244	-125	119	2.5
10% wt. ASD [c]	-247	-75	172	2.9
20% wt. ASD [d]	-247	-57	190	2.9
20% wt. ASD [e]	-247	-80	167	2.9
Recrystallised 40% wt. ASD [c]	-243	-67	176	2.9

[a] Shifts are given in ppm. $\delta_{iso}(^{15}N)$ values are obtained from the peak positions in the ^{15}N CP MAS spectra (with an associated error of ± 1 ppm) while $\delta_{iso}(^{14}N)$ values represent the centre of gravity of the ^{14}N line shape extracted from the ^{14}N-^{1}H HMQC spectra (with an associated error of ± 5 ppm). Magnetic field dependent ^{14}N shifts quoted in the table are given for 20 T. [b] P_Q values are given in MHz, with an estimated error of ± 0.1 MHz, and obtained from Eq. 4.5. [c] Experimental data obtained at 20 T. [d] Experimental data recorded at 18.8 T. [e] Experimental data obtained at 18.8 T (as in d) and quoted at 20 T.

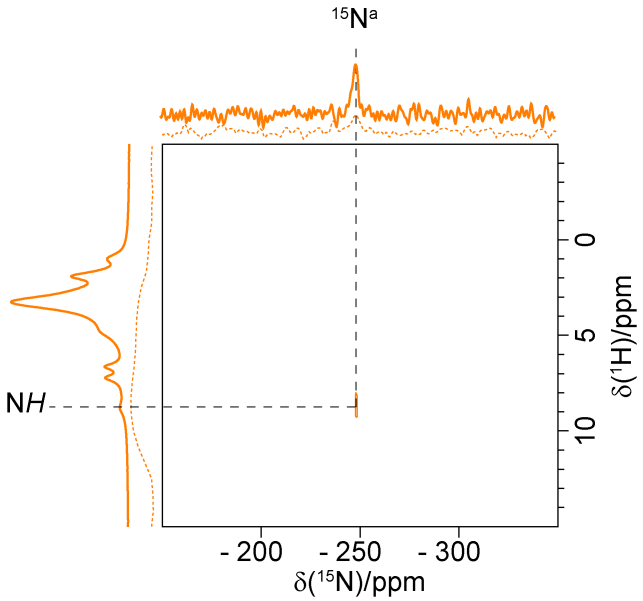

Figure 4.9. ^{15}N CP HETCOR of the 20% acetaminophen HPMC-AS solid dispersion recorded with an optimised contact time of 1 ms. On top: ^{15}N CP spectrum. On the left: ^{1}H spectrum. Dashed spectra are the HETCOR internal projections. The 2D spectra shown only one resonance at $\delta(^{1}H)$ = 8.5 ppm confirming the proposed ^{1}H assignment for acetaminophen's NH in amorphous samples. Notation 'a' indicates resonance that can be attributed to amorphous acetaminophen.

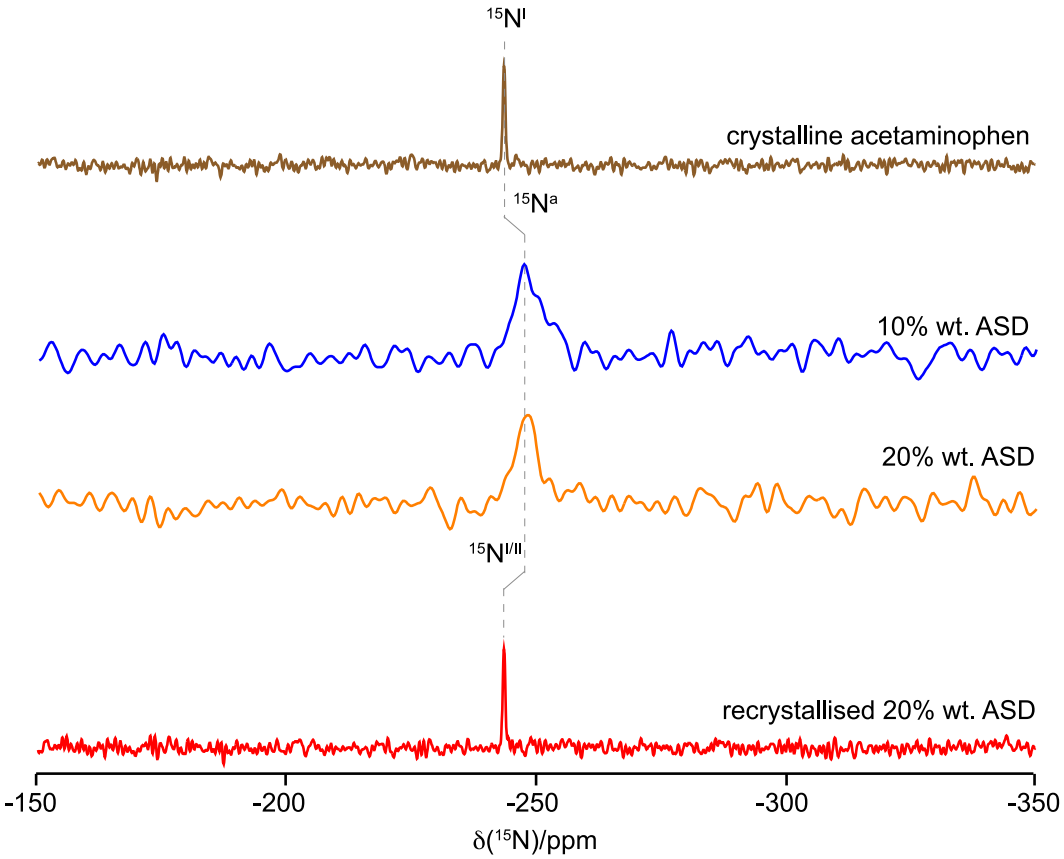

Figure 4.10. Magnified view of the ^{15}N CP spectra. From the top to the bottom: crystalline acetaminophen form I, 10% wt., 20% wt., and recrystallised 40% wt. ASDs.

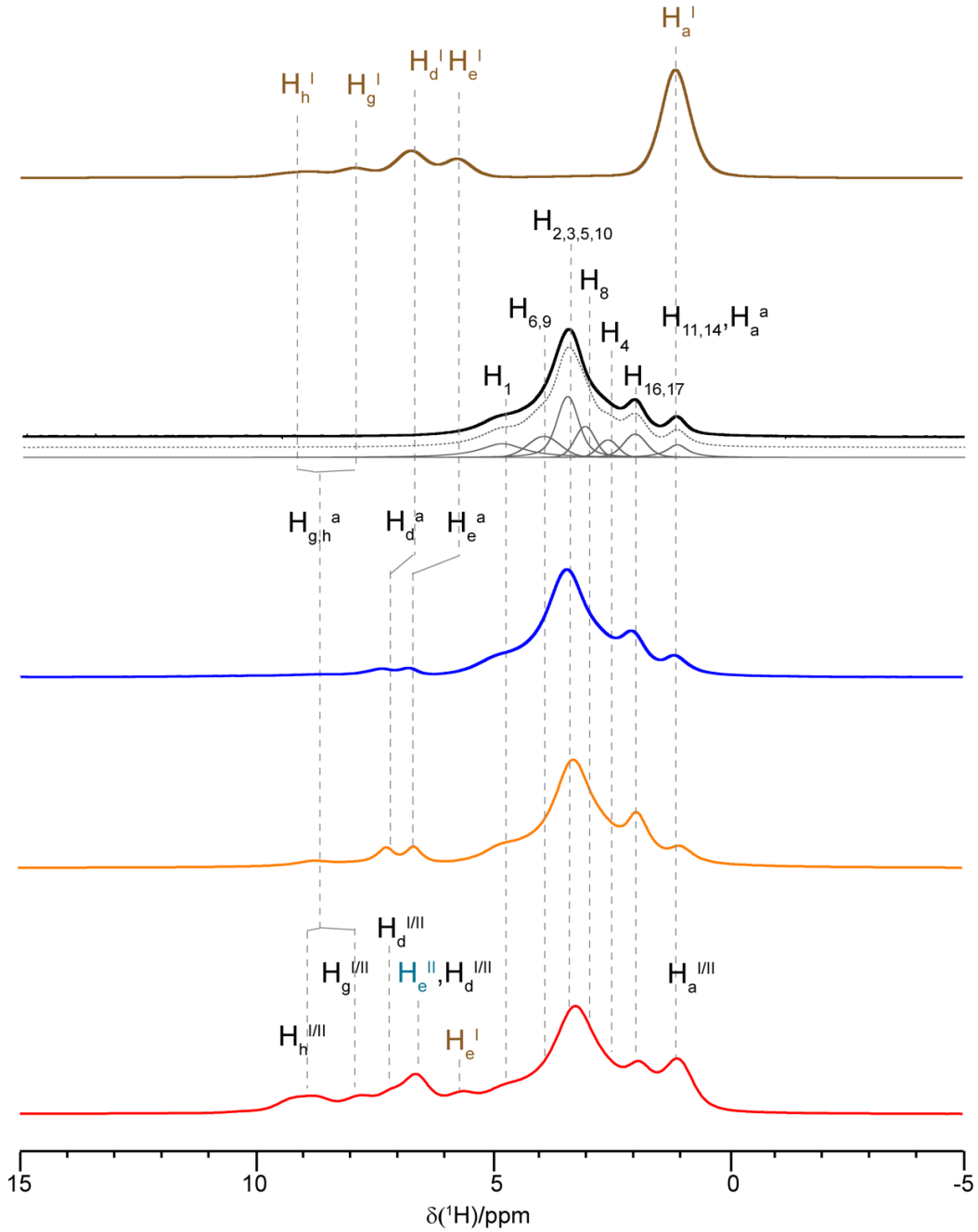

Figure 4.11. Magnified view of the quantitative ^{1}H spectra recorded at high magnetic field and high MAS frequency. From the top to the bottom: crystalline acetaminophen form I, HPMC-AS polymer, 10% wt., 20% wt., and recrystallised 40% wt. ASDs

Table 4.6. ^{1}H chemical shifts.[a]

Signal	Acetaminophen form I	HPMC-AS	10% wt. ASD	20% wt. ASD	Recrystalised 40% wt. ASD
Hh	9.0	n.a.	8.5	8.5	9.0 (I/II)
Hg	7.9	n.a.	8.5	8.5	7.9 (I/II)
Hd	6.7	n.a.	7.4	7.4	7.2 (I/II), 5.7 (I/II)
He	5.7	n.a.	6.8	6.8	6.8 (II), 5.7 (I)
H1	n.a.	4.8	4.8	4.8	4.8
H6,9	n.a.	3.9	3.9	3.9	3.9
H2,3,5,10	n.a.	3.4	3.4	3.4	3.4
H8	n.a.	3.0	3.0	3.0	3.0
H4	n.a.	2.5	2.5	2.5	2.5
H16,17	n.a.	2.0	2.0	2.0	2.0
H14	n.a.	1.1	1.1	1.1	1.1
Ha	1.1	n.a.	1.1	1.1	1.1

[a] Values are given in ppm. The associated error with the chemical shift values is ± 0.2 ppm. n.a.: not applicable.

Table 4.7. ^{1}H $T_{1\rho}$, ^{13}C detected via CP, values for the 10% wt., 20% wt. and recrystallised 40% wt. at 9.4 T recorded at two different spin locks magnitude (83 and 40 kHz).[a]

Signal	20% wt. dispersion		Recrystallised 40% wt. dispersion	
	83 kHz	40 kHz	83 kHz	40 kHz
HdI	n.a.	n.a.	> 96b	> 50b
HdII	n.a.	n.a.	13.3 (7.6)	> 12b
Hda	7.3 (2.0)	3.8 (1.1)	n.a.	n.a.
HeI	n.a.	n.a.	7.8 (2.2)	> 11[b]
HeII	n.a.	n.a.	30.8 (13.1)	3.4 (4.5)b
Hea	8.9 (1.2)	4.1 (0.8)	n.a.	n.a.
H1	9.2 (0.5)	4.4 (0.3)	5.3 (0.5)	2.4 (0.3)
H2,3	9.2 (0.3)	4.2 (0.1)	5.4 (0.3)	2.4 (0.1)
H4	9.2 (0.3)	4.2 (0.1)	5.3 (0.4)	2.4 (0.2)
H5,10	10.5 (0.7)	4.7 (0.1)	5.8 (0.4)	2.6 (0.1)
H8	10.8 (0.7)	4.4 (0.4)	5.6 (0.7)	2.4 (0.3)
H6,9	8.9 (0.3)	4.6 (0.2)	5.6 (0.4)	2.3 (0.2)
H16,17	8.6 (0.6)	4.4 (0.6)	4.8 (1.4)	1.9 (1.1)
HaI/II	n.a.	n.a.	6.5 (2.3)	1.5 (1.4)
Haa	9.6 (0.6)	3.2 (0.4)	n.a.	n.a.
H14	11.1 (1.0)	4.8 (0.5)	5.4 (0.6)	2.5 (0.4)
H11	9.1 (1.7)	5.7 (1.6)	4.5 (1.8)	1.8 (0.5)

[a] Values are given in ms. The number in parenthesis indicate the standard error associated with the fit. [b] Shortest values given as these challenge the detection of the full exponential decays of the signals due to NMR probe limitation on spin-lock pulse duration. n.a.: not applicable.

Through-space ^{13}C CP HETCOR experiments recorded at a longer contact time (in the range of ms) allow observation of acetaminophen−polymer interactions with correlation signals providing direct evidence of intermolecular drug polymer interactions. The corresponding ^{13}C CP HETCOR spectra of both 10 and 20 wt % ASD identified correlation signals between peaks in ^{13}C at 120−150 ppm corresponding to acetaminophen with ^{1}H at 3 ppm (shaded signals in **Figure 4.12(b)**).

These spatial correlations, detected via the strong $^{13}C-^{1}H$ heteronuclear dipolar coupling due to the rigid protons on the cellulose ring, cannot be ascribed to intramolecular correlations within acetaminophen due to the absence of ^{1}H signals at this shift (**Figure 4.8(b)**) but rather an intermolecular acetaminophen−HPMC-AS interaction involving the aromatic carbons of acetaminophen with the backbone cellulose ring's protons of the polymer.

In sharp contrast, the ^{13}C CP HETCOR spectrum of 40 wt % ASD identifies correlated signals corresponding to crystalline acetaminophen interacting with itself, as shown by the shaded signals in **Figure 4.12(b)** (no 2D correlation is observed for the broader shoulders of the 1D spectrum likely due to the poor signal-to-noise ratio in the HETCOR of the minor amorphous acetaminophen species). This suggests the absence of acetaminophen−HPMC-AS intramolecular interaction and indicates a two- phase immiscible system in which API−API interactions dominate, in good agreement with GT predictions, the presence of acetaminophen recrystallisation and validating ^{1}H relaxation data (see above), thereby confirming the instability of this ASD at the atomic level.

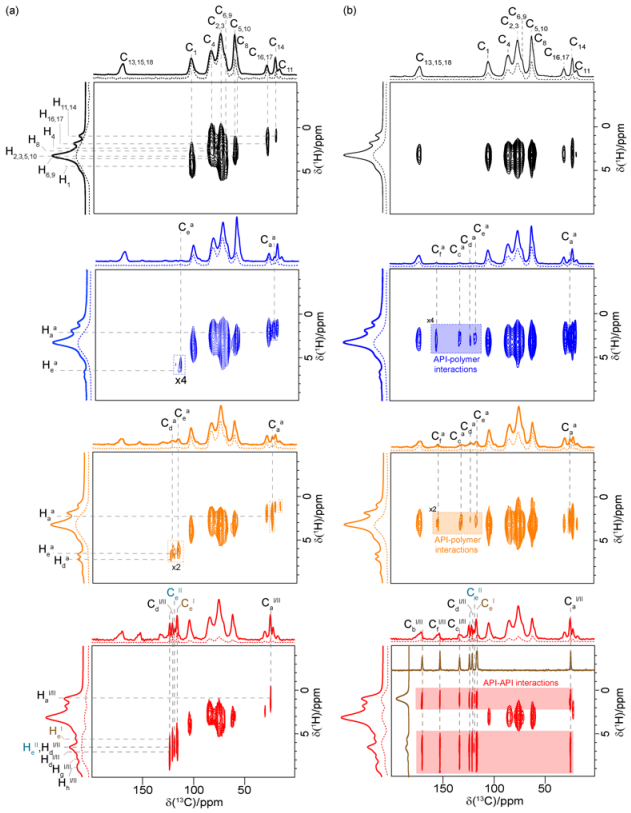

Figure 4.12 ^{13}C CP HETCOR spectra of HPMC-AS (black), 10 wt % (dark blue), 20 wt % (orange), and 40 wt % (red) acetaminophen HPMC-AS ASD recorded with a contact time of (a) 50 μs and (b) 2 ms. Correlations were used for ^{1}H spectral assignments. Top: ^{13}C CP MAS spectra at a contact time of 2 ms. Left: ^{1}H MAS NMR spectra. Internal projections are shown in dotted lines. The ^{13}C CP MAS NMR spectrum of acetaminophen form I is also given (brown). In panel (a), the dashed lines are used to highlight correlations used for ^{1}H assignment. For clarity, the correlation peaks for the polymer are only highlighted for the polymer's HETCOR in panel ((a), black). In panel (b), the dashed lines denote the carbon signal involved in API−polymer interaction or API−API interaction for the 40 wt % dispersion, while the shaded sections in the spectra mark the cross-correlation peaks that show the API−polymer interactions. **Figure 4.13** shows a magnified view of the ^{13}C region at around 110−200 ppm, highlighting the API−polymer interactions.

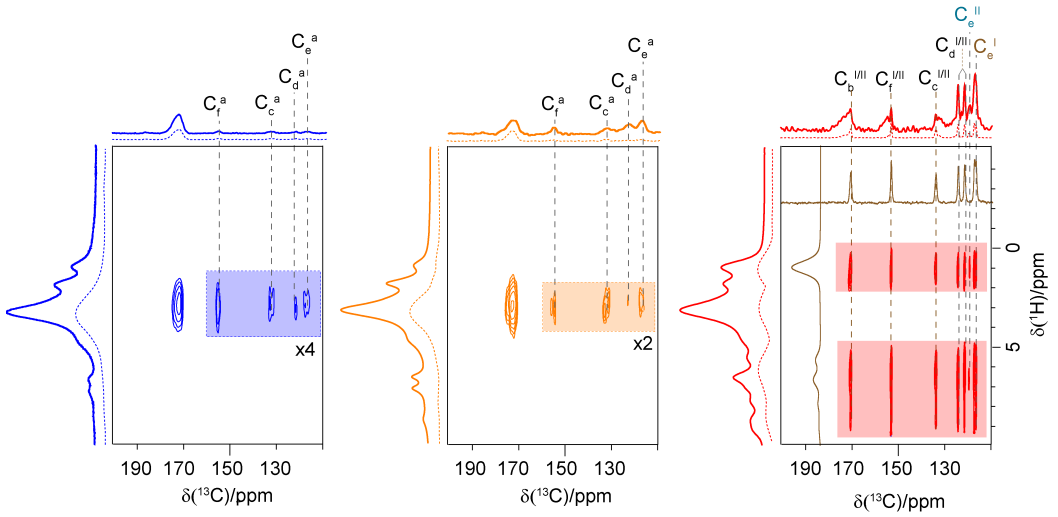

Figure 4.13. Magnified view of the 200-110 ppm ^{13}C region of the ^{13}C CP HETCOR spectra recorded at long contact time (2 ms) showing the API-polymer spatial correlations. The 2D HETCORs for the 10% wt., 20% wt. and 40% wt. dispersions are given in dark blue, yellow and red, respectively. The signals reported in the shaded area are involved in the spatial correlations. The dashed lines denotate the carbon signal involved in API-polymer interaction, or the API-API interaction for the 40% wt. dispersion.

$^{14}N-^{1}H$ HMQC experiments were then deployed under optima conditions of high magnetic field and very fast MAS frequency to establish the involvement of the amide nitrogen in the intermolecular interactions in these ASDs. ^{14}N is a high abundance spin (99.6%) but due to its low gyromagnetic ratio (1.93×10^7 rad T^{-1} s^{-1}) and spin quantum number I = 1, ^{14}N has low sensitivity and exhibits quadrupole interaction, leading to a significant signal broadening. For these reasons, the direct detection of the ^{14}N signal in the solid-state represents a challenge. The development of indirectly detected ^{14}N via ^{1}H as for example via 2D $^{14}N-^{1}H$ HMQC experiments at high magnetic field and very fast MAS frequency has enabled the

solving of this challenge, establishing this approach as a promising methodology for identifying H-bonding between components in pharmaceutical systems.[51.52.80] The corresponding $^{14}N-^{1}H$ HMQC experiments for the 10 and 20 wt % ASDs (**Figure 4.14**) identify the presence of correlation between the acetaminophen $^{14}N^{a}$ signal with the $-OCH_3$ methoxy group (H_8) of the polymer at 3 ppm and highlight H-bonding between this amide donor and oxygen acceptor. In the spectra, no correlation between the NH group of acetaminophen and the protons of the substituent groups P, A, and S (**Figure 4.1**) was identified, thus excluding the involvement of these groups in the formation of the H-bond between API and the polymer.

Importantly, this ^{14}N signal correlating with H_8 does not correspond to the same proton (H_h^{a}) identified via ^{15}N CP HECTOR that established the NH correlation within acetaminophen (**Figure 4.9**) and suggests longer-range interactions. We note that this interaction for the 10 and 20 wt % amorphous dispersions was identified using short recoupling times of 133.6 and 66.8 μs, respectively, suggesting a closer contact between acetaminophen and HPMC-AS in those systems than in crystalline acetaminophen, which is consistent with the previous work in the amorphous formulation.[52] It is proposed that this H-bonding interaction is dominant to stabilise acetaminophen in its amorphous form in these ASDs.

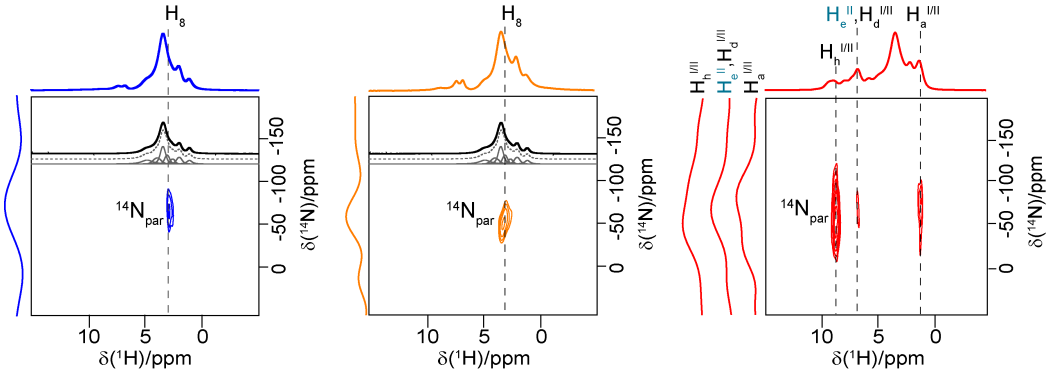

Figure 4.13. $^{14}N-^{1}H$ HMQC experiments of 10 wt % (dark blue), 20 wt % (orange), and 40 wt % (red) acetaminophen HPMC-AS ASDs obtained at a MAS frequency of 60 kHz. Data for 10/40% and 20 wt % were collected at 20 and 18.8 T, respectively. Spectra were recorded with recoupling times of 133.6 μs (10 wt % ASD, 8 rotor periods), 66.8 μs (20 wt % ASD, 4 rotor periods), and 801.6 μs (40 wt % ASD, 48 rotor periods). The deconvoluted ^{1}H spectra of HPMC-AS under the same condition are also given in black. Spectra on the left of the 2D HMQC are the ^{14}N slices extracted at the indicated ^{1}H chemical shifts in dashed black lines.

In contrast to the 10 and 20 wt % ASDs, the $^{14}N-^{1}H$ HMQC spectrum for the 40 wt % ASD clearly exhibits correlations between the ^{14}N and ^{1}H ($H_h^{I/II}$, $H_e^{II}/H_d^{I/II}$, and $H_a^{I/II}$) signals within acetaminophen and no correlation to the HPMC-AS polymer, confirming the absence of acetaminophen−HPMC-AS interactions at this high drug loading. The API−API H-bonding interaction was found at significantly longer recoupling times, reasonably indicating a longer distance between the packed acetaminophen molecules in the crystal structure compared to the API−polymer distance in amorphous systems, as illustrated previously.[50] For both the 10 and 20 wt % amorphous dispersions, the correlation signals in the ^{13}C CP HETCOR experiments carried out at long contact times (**Figure 4.12(b)**) and $^{14}N-^{1}H$ HMQC spectra at short recoupling times (**Figure 4.14**) highlight intermolecular amorphous drug−polymer H-bonding interactions (**Figure 4.15**).

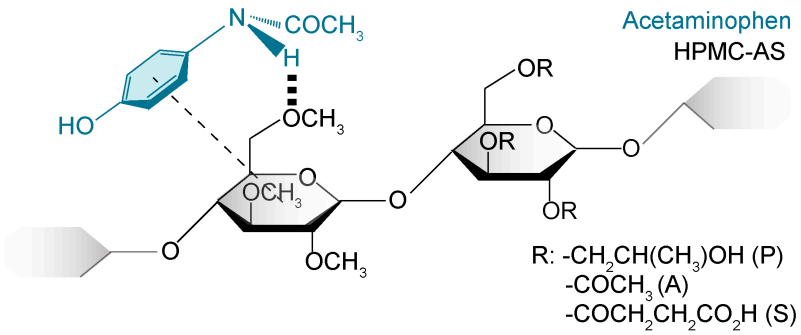

Figure 4.15. Schematic representation of the interactions that have been experimentally identified in this work. For dispersions with a drug loading of <20 wt %, spatial proximity (---) and H-bond (≡) were identified between the API and the polymer. The acetaminophen and HPMC-AS molecules are given in light blue and black, respectively.

The experimental ^{14}N shifts for the observed signals in **Figure 4.14** and the ^{15}N isotropic chemical shifts obtained in the ^{15}N CP experiments (**Figure 4.8(a)**) for the 10% wt. and 20% wt. ASDs are listed in **Table 4.5**. The differences in shifts between ^{14}N and ^{15}N are due to the ^{14}N isotropic second-order quadrupolar shift which is given by **Equation 4.3**:

$$\delta_{iso}^{Q}(^{14}N) = \delta_{iso}(^{14}N) - \delta_{iso}(^{15}N) \qquad \textbf{Eq. 4.3}$$

and allows the determination of the quadrupolar product P_Q from **Equation 4.4**[50]:

$$\delta_{iso}^{Q}(^{14}N) = \left(\frac{3}{40}\right)\left(\frac{P_Q}{v_0}\right) \times 10^6 \qquad \textbf{Eq 4.4}$$

where v_0 is the ^{14}N Larmor frequency. P_Q depends on the quadrupolar coupling constant C_Q and asymmetry parameter η_Q, as expressed by **Equation 4.5**:

$$P_Q = C_Q\sqrt{1+\frac{\eta_Q^2}{3}} \qquad \textbf{Eq 4.5}$$

A significant difference of around 180−190 ppm between ^{15}N isotropic chemical shift and ^{14}N shift is observed (**Table 4.5**) in the acetaminophen HPMC-AS ASD. This is attributed to the isotropic second-order quadrupolar shift being sensitive to the presence of the H-bond, as previously observed in the 50 wt % acetaminophen−PVP solid dispersion that extracted a $\delta_{iso}^{Q}(^{14}N)$ value of around 184 ppm.[51] This data further supports the presence of acetaminophen HPMC-AS H-bond in the dispersions with drug loading <20% wt and acetaminophen−acetaminophen H-bond interaction in the recrystallised 40% ASD. These are stabilising interactions that can be imputed in the understanding of the stability of the amorphous acetaminophen−HPMC-AS solid dispersions. Interestingly, the main stabilizing interaction that has been identified in this work is H-bonding between the acetaminophen's amide group with the OCH_3 proton (H_8) of the HPMC-AS methyl substituent (M), likely due to the small steric hindrance of this substituent vs the others (**Figure 4.1**). This is an unexpected finding given that the acetyl and succinoyl groups in HPMC-AS have been previously suggested to be responsible for the formation of API−polymer H-bonding and contribute to the formation of stabilizing interactions.[42]

4.6 Conclusions

Molecular interactions in acetaminophen−HPMC-AS solid dispersion at 10, 20, and 40 wt % drug loadings were identified by combining time-dependent PXRD with multidimensional multinuclear NMR experiments. The presence of chemical shift differences in 1D ^{1}H, ^{13}C, and ^{15}N CP MAS NMR spectra between crystalline and amorphous acetaminophen suggests a strong structural perturbation in the amorphous species and can be potentially rationalised by the presence of H-bonding interactions between acetaminophen and the polymer. ^{13}C CP HETCOR exploiting strong $^{13}C-^{1}H$ dipolar coupling highlighted spatial interaction between the acetaminophen's aromatic protons with the polymer's cellulose ring protons in the 10 and 20 wt % ASDs. This interaction was further unequivocally confirmed by $^{14}N-^{1}H$ HMQC experiments that identify H-bond interactions between the NH of acetaminophen and the OCH_3 proton of the HPMC-AS methyl substituent. The presence of this type of drug/polymer interaction in amorphous systems is of crucial importance as it stabilises the amorphous dispersions. No acetaminophen−HPMC-AS interactions were found in the 40 wt % dispersion, further validated from ^{1}H relaxation data, indicating the instability of this system and its tendency to recrystallise on a short timescale.

4.7 References

[1] G. L. Amidon, H. Lennernäs, V.P. Shah, J.R. Crison, *Pharm. Res.* **1995**, *12*, 413.

[2] M. Rams-Baron, R, Jachowicz, E. Boldyreva, D. Zhou, W. Jamroz, M. Paluch (Eds), *Amorphous Drug*; Springer International Publishing AG, Switzerland, **2018**.

[3] M. Savolainen, K. Kogermann, A. Heinz, J. Aaltonen, L. Peltonen, C. Strachan, J. Yliruusi, *Eur. J. Pharm. Biopharm*. **2009**, *71*, 71.

[4] A. Newman (Ed), *Pharmaceutical Amorphous Solid Dispersion*; John Wiley & Sons: Hoboken, New Jersey, **2015**.

[5] C. Leuner, J. Dressman, *Eur. J. Pharm. Biopharm.* **2000**, *50*, 47.

[6] G. Van den Mooter, *Drug Discovery Today: Technol.* **2012**, *9*, 79

[7] S. Baghel, H. Cathcart, N. J. O'Reilly, *J. Pharm. Sci.* **2016**, *105*, 2527.

[8] W. L. Chiou, S. Riegelman, *J. Pharm. Sci.* **1971**, *60*, 1281.

[9] T. Vasconcelos, S. Marques, J. das Neves, B. Sarmento, *Drug Delivery Rev*. **2016**, *100*, 85.

[10] A. Singh, G. Van den Mooter, *Adv. Drug Delivery Rev*. **2016**, *100*, 27.

[11] S. Wanning, R. Süverkrüp, A. Lamprecht, *Int. J. Pharm.* **2015**, *488*, 136.

[12] Z. Dong, A. Chatterji, H. Sandhu, D. S. Choi, H. Chokshi, N. Shah, *Int. J. Pharm.* **2008**, *355*, 141.

[13] D. Law, E. A. Schmitt, K. C. Marsh, E. A. Everitt, W. Wang, J. J. Fort, S. L. Krill, Y. Qiu, *J. Pharm. Sci.* **2004**, *93*, 563.

[14] D. S. Jones, Y. Tian, S. Li, T. Yu, O. A. Abu-Diak, G. P. Andrews, *J. Pharm. Sci.* **2016**, *105*, 3064.

[15] P. Gupta, V. K. Kakumanu, A. K. Bansal, *Pharm. Res.* **2004**, *21*, 1762.

[16] K. Lehmkemper, S. O. Kyerematen, O. Heinzerling, M. Degenhardt, G. Sadowski, *Mol. Pharmaceutics* **2017**, *14*, 157.

[17] J. C. Dinunzio, J. R. Hughey, C. Brough, D. A. Miller, R. O. Williams, J. W. McGinity, *Drug Dev. Ind. Pharm.* **2010**, *36*, 1064.

[18] F. Tanno, Y. Nishiyama, H. Kokubo, S. Obara, *Drug Dev. Ind. Pharm.* **2004**, *30*, 9.

[19] D. T. Friesen, R. Shanker, M. Crew, D. T. Smithey, W. J. Curatolo, J. A. S. Nightingale, *Mol. Pharmaceutics* **2008**, *5*, 1003.

[20] K. Lehmkemper, S. O Kyerematen, O. Heinzerling, M. Degenhardt, G. Sadowski, *Mol. Pharmaceutics* **2017**, *14*, 4374.

[21] T. Van Duong, G. Van den Mooter, *Expert Opin. Drug Delivery* **2016**, *13*, 1681.

[22] S. Janssens, G. Van den Mooter, *J. Pharm. Pharmacol.* **2010**, *61*, 1571.

[23] W. K. Miller, D. K. Lyon, D. T. Friesen, W. B. Caldwell, D. T. Vodak, D. E. Dobry, *Patent* EP2579896A1, **2016**.

[24] Y. Qiu, Y. Chen, G. Zhang, L. Yu, R. V. Mantri (Eds), *Developing Solid Oral Dosage Forms-Pharmaceutical Theory and Practice*, 2nd ed.; Elsevier, **2017**.

[25] M. Tobyn, J. Brown, A. B. Dennis, M. Fakes, Q. Gao, J. Gamble, Y. Z. Khimyak, G. McGeorge, C. Patel, W. Sinclair, P. Timmins, S. Yin, *J. Pharm. Sci.* **2009**, *98*, 3456.

[26] D. McNamara, S. Yin, D. Pan, G. Crull, P. Timmins, B. Vig, *Mol. Pharmaceutics* **2017**, *14*, 377.

[27] M. M. De Villiers, D. E. Wurster, J. G. Van Der Watt, A. Ketkar, *Int. J. Pharm*. **1998**, *163*, 219.

[28] J. A. Baird, L. S. Taylor, *Adv. Drug Delivery Rev.* **2012**, *64*, 396.

[29] G. Smith, A. Hussain, N. I. Bukhari, I. Ermolina, *Eur. J. Pharm. Biopharm.* **2015**, *92*, 180.

[30] G. Van den Mooter, J. Van den Brande, P. Augustijns, R. Kinget, *J. Therm. Anal. Calorim.* **1999**, *57*, 493.

[31] A. Paudel, J. Van Humbeeck, G. Van den Mooter, *Mol. Pharmaceutics* **2010**, *7*, 1133.

[32] M. Gordon, J. S. Taylor, *Rubber Chem. Technol*. **1953**, *26*, 323.

[33] K. Lehmkemper, S. O. Kyerematenga, M. Bartels, M. Degenhardt, G. Sadowski, *Eur. J. Pharm. Biopharm.* **2018**, *124*, 147.

[34] F. Tres, J. D. Patient, P. M. Williams, K. Treacher, J. Booth, L. P. Hughes, S. A. C. Wren, J. W. Aylott, J. C. Burley, *Mol. Pharmaceutics* **2015**, *12*, 1512.

[35] N. Furuyama, S. Hasegawa, T. Hamaura, S. Yada, H. Nakagami, E. Yonemochi, K. Terada, *Int. J. Pharm.* **2008**, *361*, 12.

[36] L. S. Taylor, G. Zografi, *Pharm. Res.* **1997**, *14*, 1691.

[37] T. T. D. Tran, P. H. L. Tran, *Pharmaceutics* **2020**, *12*, 745.

[38] U. Holzgrabe, I. Wawer, B. Diehl, B. (Eds), *NMR Spectroscopy in Pharmaceutical Analysis*, Elsevier Science, Oxford, **2008**.

[39] J. R. Everett, R. K. Harris, J. C. Lindon, I. D. Wilson (Eds), *NMR in Pharmaceutical Science*, Wilson Wiley, **2015**.

[40] M. Pellecchia, I. Bertini, D. Cowburn, C. Dalvit, E. Giralt, W. Jahnke, T. L. James, S. W. Homans, H. Kessler, C. Luchinat, B. Meyer, H. Oschkinat, J. Peng, H. Schwalbe, G. Siegal, *Nat. Rev. Drug Discovery* **2008**, *7*, 738.

[41] D. M. Sperger, E. J. Munson, *AAPS PharmSciTech* **2011**, *12*, 821.

[42] Y. Ishizuka, K. Ueda, H. Okada, J. Takeda, M. Karashima, K. Yazawa, K. Higashi, K. Kawakami, Y. Ikeda, K. Moribe, *Mol. Pharmaceutics* **2019**, *16*, 2785.

[43] A. Paudel, M. Geppi, G. Van Den Mooter, *J. Pharm. Sci.* **2014**, *103*, 2635.

[44] X. Lu, C. Huang, M. B. Lowinger, F. Yang, W. Xu, C. D. Brown, D. Hesk, A. Koynov, L. Schenck, Y. Su, *Mol. Pharmaceutics* **2019**, *16*, 2579.

[45] M. Li, F. Meng, Y. Tsutsumi, J. P. Amoureux, W. Xu, X. Lu, F. Zhang, Y. Su, Mol. *Pharmaceutics* **2020**, *17*, 2196.

[46] J. Struppe, C. M. Quinn, S. Sarkar, A. M. Gronenborn, T. Polenova, *Mol. Pharmaceutics* **2020**, 17, 674.

[47] D. A. Hirsh, A. V. Wijesekara, S. L. Carnahan, I. Hung, J. W. Lubach, K. Nagapudi, A. J. Rossini, *Mol. Pharmaceutics* **2019**, *16*, 3121.

[48] Z. Gan, J. Paul, J. Tre, *Chem. Phys. Lett.* **2007**, *435*, 163.

[49] A. S. Tatton, T. N. Pham, F. G. Vogt, D. Iuga, A. J. Edwards, S. P. Brown, *CrystEngComm* **2012**, *14*, 2654.

[50] A. S. Tatton, J. P. Bradley, D. Iuga, S. P. Brown, *Z. Phys. Chem*. **2012**, *226*, 1187.

[51] A. S. Tatton, T. N. Pham, F. G. Vogt, D. Iuga, A. J. Edwards, S. P. Brown, *Mol. Pharmaceutics* **2013**, *10*, 999.

[52] M. Grüne, R. Luxenhofer, D. Iuga, S. P. Brown, A. C. Pöppler, *J. Mater. Chem. B* **2020**, *8*, 6827.

[53] D. A. Druzhbin, T. N. Drebushchak, V. S. Min'kov, E. V. Boldyreva, *J. Struct. Chem*. **2015**, *56*, 317.

[54] Y. Nguyen Thi, K. Rademann, F. Emmerling, *CrystEngComm* **2015**, *17*, 9029.

[55] E. Pisa, L. P. Hughes, S. A. C. Wren, J. Booth, J. F. McCabe, D. T. E. Whittaker, M. D. Mantle, *Mol. Pharmaceutics* **2020**, 17, 2021.

[56] T. Bräuniger, P. Wormald, P. Hodgkinson. *Monats. Chem.* **2002**, *133*, 1549.

[57] S. R. Hartmann, E. L. Hahn, *Phys. Rev.* **1962**, *128*, 2042.

[58] B. J. Van Rossum, H. Förster, H. J. M. De Groot, *J. Magn. Reson.* **1997**, *124*, 516.

[59] T. G. Oas, R. G. Griffin, M. H. Levitt, *J. Chem. Phys.* **1988**, *89*, 692.

[60] P. R. Costa, J. D. Gross, M. Hong, R. G. Griffin, *Chem. Phys. Lett.* **1997**, *280*, 95.

[61] C. R. Morcombe, K. W. Zilm, *J. Magn. Reson.* **2003**, *162*, 479.

[62] P. Bertani, J. Raya, B. Bechinger, *Solid State Nucl. Magn. Reson*. 2014, 61−62, 15.

[63] H. J. Jakobsen, A. R. Hove, R. G. Hazell, H. Bildsøe, J. Skibsted, *Magn. Reson. Chem*. **2006**, *44*, 348.

[64] M. A. Perrin, M. A. Neumann, H. Elmaleh, L. Zaske, *Chem. Commun*. **2009**, *22*, 3181.

[65] R. Telford, C. C. Seaton, A. Clout, A. Buanz, S. Gaisford, G. R. Williams, T. J. Prior, C. H. Okoye, T. Munshi, I. J. Scowen, *Chem. Commun.* **2016**, *52*, 12028.

[66] Y. Li, H. Pang, Z. Guo, L. Lin, Y. Dong, G. Li, M. Lu, C. Wu, *J. Pharm. Pharmacol.* 2014, *66*, 148.

[67] M. Maldonado-Santoyo, S. M. Nuño-Donlucas, L. C. Cesteros, I. Katime, *J. Appl. Polym. Sci.* **2004**, *91*, 1887.

[68] J. C. Burley, M. J. Duer, R. S. Stein, R. M. Vrcelj, *J. Pharm. Sci.* **2007**, *31*, 271.

[69] A. Pugliese, L. E. Hawarden, A. Abraham, M. Tobyn, F. Blanc, *Magn. Reson. Chem*. **2020**, *58*, 1036.

[70] P. Hodgkinson, *Prog. Nucl. Magn. Reson. Spectrosc.* **2020**, *118*, 10.

[71] X. Lu, W. Xu, M. Hanada, S. V. Jermain, R. O. Williams, Y. Su, *J. Pharm. Biomed. Anal.* **2019**, *165*, 47.

[72] X. Yuan, T. X. Xiang, B. D. Anderson, E. J. Munson, *Mol. Pharmaceutics* **2015**, *12*, 4518.

[73] H. Nie, Y. Su, M. Zhang, Y. Song, A. Leone, L. S. Taylor, P. J. Marsac, T. Li, S. R. Byrn, *Mol. Pharmaceutics* **2016**, *13*, 3964.

[74] Y. Song, X. Yang, X. Chen, H. Nie, S. Byrn, J. W. Lubach, *Mol. Pharmaceutics* **2015**, *12*, 857.

[75] P. Duan, M. S. Lamm, F. Yang, W. Xu, D. Skomski, Y. Su, K. Schmidt-Rohr, *Mol. Pharmaceutics* **2020**, *17*, 3567.

[76] T. N. Pham, S. J. Watson, A. J. Edwards, M. Chavda, J. S. Clawson, M. Strohmeier, F. G. Vogt, *Mol. Pharmaceutics* **2010**, *7*, 1667.

[77] L. C. Dickinson, H. Yang, C. W. Chu, R. S. Stein, J. C. W. Chien, *Macromolecules* **1987**, *20*, 1757.

[78] F. A. Bovey, P. A. Mirau, (Eds), *NMR of Polymers,* 1st ed.; Academic Press: San Diego, CA, **1996**.

[79] X. Yuan, D. Sperger, E. J. Munson, *Mol. Pharmaceutics* **2014**, *11*, 329.

[80] K. Maruyoshi, D. Iuga, O. N. Antzutkin, A. Alhalaweh, S. P. Velaga, S. P. Brown. *Chem. Commun.* **2012**, *48*, 10844.

Chapter 5: Quantification of amorphous or crystalline API and amorphous polymer mixtures Species Ratio in Pharmaceutical Amorphous Solid Dispersions using Time Domain ^{19}F Saturation Recovery Curves (qSRC).

5.1 Overview

Lucy E. Hawarden and Michael Tobyn (M.T.) from Bristol-Myers Squibb (BMS) devised the project. This work has been funded by the EPSRC NPIF Innovation Placement Award - placement with BMS. Quantitative analyses were hence obtained at the BMS facility. A.P. prepared the samples for the quantification and carried out data analysis and interpretation. A.P. wrote the manuscript receiving feedback from Frédéric Blanc, and M.T.

5.2 Abstract

Monitoring the amorphous state of the active pharmaceutical ingredient (API) and miscibility in amorphous solidi dispersions (ASDs) is essential to understand their stability. Alongside the common and consolidated analytical techniques based on the spectrophotometry, solid-state nuclear magnetic resonance (NMR) has an important role. Recently, due to its relative ease of use, wide versatility, portable dimension, the time domain (TD) NMR methodology has spread in the study of ASDs to the pharmaceutical industry, where it could be implemented in the production line.

Here we have tested the suitability of a recently developed TD NMR-based method (Bruker ® FormCheck) relying on the measurement of the saturation recovery curves (SRCs) of the components (amorphous and crystalline) of a reference mixture which are then compared with the SRC of a mixture (SRCmix) allowing the quantification the amorphous/crystalline species in amorphous or crystalline API and amorphous polymer mixtures. Targeted samples designed to simulate real scenarios of samples of pharmaceutical interest (e.g., API recrystallised by ASD) were analysed with this technique. The method is based on the collection of the saturation recovery curves (SRCs) of the two single components and compared with the SRC obtained from the mixture (SRCmix). As the SRCmix is the linear combination of the single components SRCs, the approach allows quantification of the ratio of the components in the mixture. Accurate amorphous/crystalline ratio quantification have been carried out under specific condition and lead to establish this method has a quick and useful analytic tool in the quantification of amorphous/crystalline species ratio in pharmaceutical amorphous solid dispersions.

5.3 Introduction

As already discussed in the previous chapters, amorphous solid dispersions (ASDs)[1,2] represents a promising technique to prepare bioavailable, kinetically stable, amorphous and fully miscible drug-polymer system. In these formulations, the active pharmaceutical ingredient (API) is dispersed in a carrier matrix, generally a polymer. It has also been demonstrated the extraordinary role of solid state nuclear magnetic resonance (NMR)[3-5] when applied in the study of ASD, ranging from the study of API-polymer miscibility, structural characterization of polymer commonly used as excipients (chapter 3)[6], and in the identification of the presence of drug-polymer interactions (chapters 2, 3, and 4).

However, the metastable nature of the ASD and external factors like moisture[7], water[8], and condition of storage[9] can inhibit the polymer stabilising effect promoting API recrystallisation[10], hence API-polymer mixture phase separation leads to an undesirable and instable system compromising the product in terms of drug delivery performance. Therefore, the monitoring of these recrystallisation phenomena, the degree of phase separation and the understanding of API-polymer miscibility play an important role and represents an exciting field of research.

Many strategies and methods have been employed to characterise ASD phase behaviour. Differential scanning calorimetry (DSC) technique led us to investigate the ASD heterogeneity comparing the glass Tgs of the final dispersion and the single mixture components. However, for an ASD, while two different Tgs clearly indicate phase separation, a single Tg does not reliably indicate an intimate API-polymer blend.[11] High resolution image based methods such as atomic force and transmission electron microscopies have been also used to elucidate ASD phase

separation from spatial resolution but some limitations exist and include the preparation method of the model film sample which does not represent well the materials produced in industrial setting.[12-17]

Phase separation phenomena, and consequent recrystallisation of the API in ASDs have been successfully highlighted using solid state nuclear magnetic resonance (NMR). It has been widely demonstrated that relaxometry measurements of spin-lattice relaxation time in the laboratory frame (T_1) and the rotating frame ($T_{1\rho}$) give access to important information about the molecular mobility of the species present in ASDs, reflecting the degree of separation and API-polymer miscibility as well as the presence of crystalline phases or crystalline API.[18-24] It is founded that due to the ordered rigid three dimensional crystalline structure, the T_1 of the crystals is long. On the contrary, the amorphous samples exhibit shorter T_1 likely because the disorder structure allows more significant molecular motion. For example, direct comparison of ^{1}H T_1 and $T_{1\rho}$ relaxation times evaluates the miscibility of nifedipine (NIF) – poly(vinyl pyrrolidone) (PVP) ASDs at different drug loadings.[19] While for ASDs with a high drug load ($\geq$ 90 wt %), different $T_{1\rho}$ values for NIF and PVP indicating the non-miscibility of these systems, resulting in clear phase separation, comparable T_1 (NIF)/(PVP) relaxation times, and $T_{1\rho}$(NIF) $\approx$ $T_{1\rho}$ (PVP) values indicate an excellent NIF-PVP miscibility for ASDs with drug load $\leq$ 75 wt %.

The application of a mono- or biexponential model used to fit raw relaxation dataset recorded by NMR allows to exploit the miscibility of API-polymer through ^{1}H $T_{1\rho}$ measurements. It has been reported for the NIF dispersed in PVP, α,β-poly(*N*-5-hydroxylpentyl)-L-aspartamide (PHPA), and hydroxypropylmethylcellulose (HPMC). The monoexponentially fitted $T_{1\rho}$ decays found for both the NIF-PVP and NIF-HPMC ASDs indicate that the size domain of API-polymer in these dispersions are less than several nm, hence indicating a good miscibility on the length scale of

NIF in PVP and HPMC. On the contrary, the $T_{1\rho}$ extrapolated by a bi-exponential model for the NIF-PHPA denotes a not ideal miscibility.[25]

Despite the undoubted potential of the high-field NMR technique and in the pharmaceutical field, some limitation such as high cost, low sensitivity, have pushed the pharmaceutical industry to explore alternative and cheap experimental set-ups to study amorphous APIs behaviour and ASDs. In this scenario, the relative cheap and portable superconducting magnetic free bench top time domain (TD) NMR methodology has been recently employed as routine technique in the production line for its high versatility, low operational cost, ease of sample handling, and automated use.

The usefulness of TD NMR has been demonstrated to characterise APIs, and monitoring API containing a solid dispersion, using ^{1}H T_1 relaxation time measurement. For example, amorphous carbamazepine (CBZ) was discriminate from its crystalline form III (^{1}H T_1s of 3 s and 45 s, respectively), as well as amorphous indomethacin (IMC) vs. IMC γ-form (^{1}H T_1 = 1.3 s vs. 4.0 s).[26] Moreover, it has been reported that the ^{1}H T_1 relaxation behaviour of IMC-PVP ASDs at different API contents follows a trend of extending the T_1 values with increasing IMC content, and that the change in T_1 values of the IMC in the ASD during thermal stress test, is an effective method in evaluating the crystalline state of API incorporated into solid dispersions.[27]

Recently, a novel and proficient protocol (FormCheck) to quantify the relative amounts of components in solid mixture based on the measurement and fit of T_1 obtained via saturation recovery curve (qSRC) using TD NMR has been proposed.[28] The method relying on the fact that the T_1 value of the mixture is a linear combination of the T_1 of the individual components. To test and optimised this method, several binary blended of model systems with various composition

were prepared and studied. qSRC analysis were carried out on the crystalline ibuprofen (IBU)/IMC and IBU/intraconazole (ITR) blends lead to interesting results. While quantifying the percentage of IBU in the IBU/ IMC mixtures validates this approach, the qSRC method has been shown to fail for the IBU/ITR system. This can be rationalised by taking into account the effects of differences in T_1 values between the mixture components. In fact, from the best fits of SRCs for IBU to IMC the two obtained values of ^{1}H T_1 differ by a factor of about 6, while the values of T_1^{ITR} and T_1^{IBU} were found to be identical. This shows that small differences in T_1 relaxation time of the components will lead to corresponding small differences in SRCs, and at the limit of equal relaxation times, the qSRC method might fail.

The aim of this work is to exploit the potential of this new method to quantify crystalline vs. amorphous specie ratio in mixture based on avagacestat (API)-HPMC-AS (polymer) (**Figure 5.1(a)**) ASDs using an implemented FormCheck software tool designed by Bruker® that allows the automatic quantification of specie in binary based on the fit of the ^{19}F SRC resulting from the mixture (SRCmix) *vs* ^{19}F SRCs of the single components. The use of ^{19}F as a probe nucleus allows to monitory only the API, as the polymer does not contain any fluorinated species. Hence, the polymer is NMR invisible during the experiments. To the best of our knowledge, at today in literature, no examples of amorphous or crystalline API and amorphous polymer mixtures specie ratio in mixture based on ASDs, via ^{19}F spectroscopy have yet been reported.

The structural characterisation of avagacestat in its crystalline and amorphous forms have been previously exploited and published by our team.[29] Top **Figure 5.1(b)** depicts the 1D ^{1}H-^{13}C cross-polarisation (CP) magic angle spinning spectrum of the crystalline avagacestat and reports the tentative carbon assignment. The assignment is supported by the ^{13}C CP spectrum obtained without ^{19}F decoupling during the acquisition time (**Figure 5.1(b)**, middle) and the ^{13}C CP

phase inversion (CPPI) NMR spectrum[30] (**Figure 5.1(b)**, bottom) which was useful in identify carbon atoms directly bounded with fluorine and to distinguish between CH_3, CH_2, CH, and ternary carbons, respectively. **Figure 5.1(c)** reports the ^{13}C spectra of the HPMC-AS polymer, 25 wt % avagacestat-HPMC-AS dispersion and amorphous API. The comparison between these spectra allows to unambiguously identify the position polymer's CO signals and the CO of the API amide in the dispersion's spectrum, confirming that the correlation peak highlighted in the 2D ^{19}F-^{13}C CP heteronuclear correlation (HETCOR) spectrum (**Figure 5.1(d)**) indicates a correlation between the polymer's CO and the CF_3 group of the API. This result suggests that the polymer may be hydrogen bonded to the NH_2 group of the API which is spatially close to the CF_3 group.

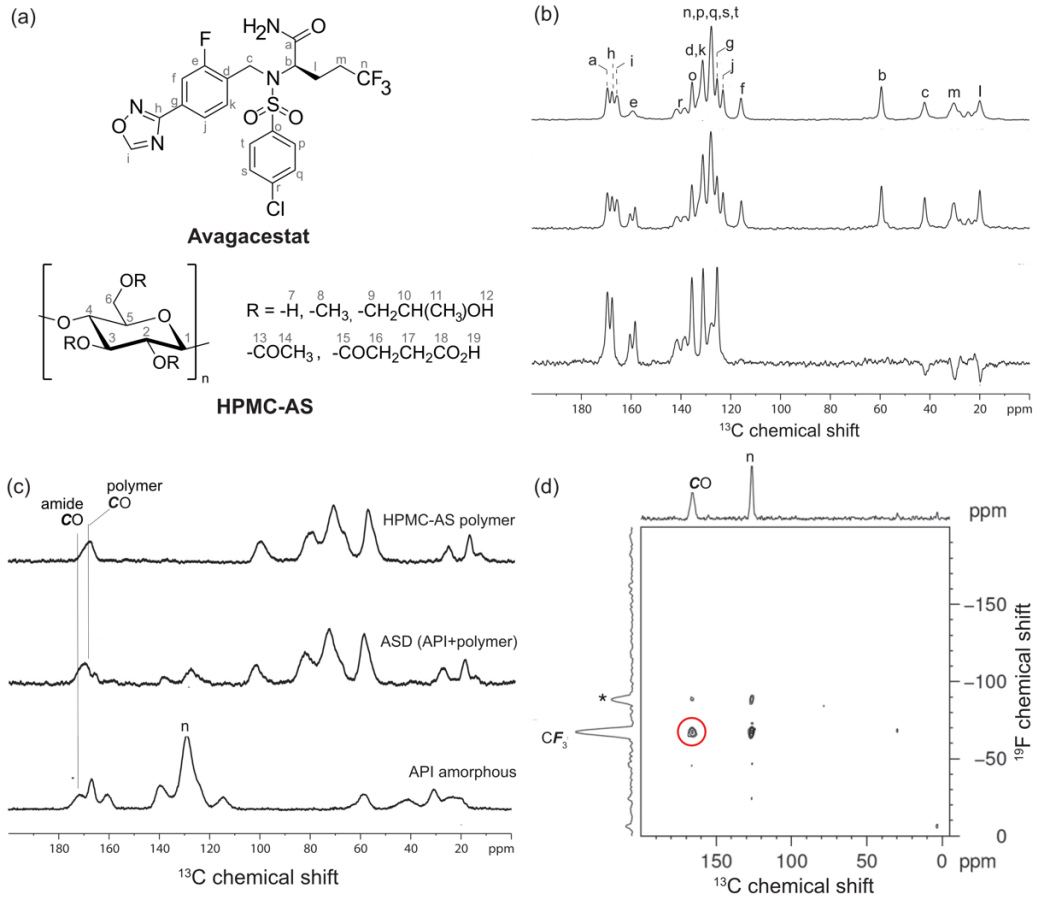

Figure 5.1. (a) Chemical structure of avagacestat (API) and HPMC-AS polymer. The structure of the polymer consists in a cellulose ring backbone randomly substituted with the R groups reported. (b) 1D ^{1}H-^{13}C CP spectra carried out with (top) and without (middle) ^{19}F decoupling and ^{19}F decoupled ^{1}H-^{13}C CPPI spectrum (bottom) of crystalline avagacestat. (c) Comparison of the ^{1}H-^{13}C CP spectra of HPMC-AS, 25 wt % avagacestat-HPMC-AS ASD and amorphous API. (d) ^{19}F-^{13}C CP HETCOR spectrum of 25 wt % ASD. The signal highlighted by the red circle indicates a spatial correlation between the fluorine atoms of the CF_3 group of the API to the carbonyl groups of the polymer. ^{19}F-^{13}C CP and ^{19}F spectra of the 25 wt. % ASD are reported on the top and on the left of the 2D spectrum. respectively. The signal labelled with the asterisk (*) is a spinning side band. Spectra report the proposed assignment. Figure adapted from[29].

5.4 Materials

Crystalline avagacestat (BMS 708163) was prepared by Bristol-Myer Squibb[31,32] while HPMC-AS polymer M grade was purchased from Shin-Etsu Chemical Co. (lot # 6033060).

Gram-scale batches of neat amorphous avagacestat and dispersions formulated at 25 and 75 wt % of avagacestat were prepared using a custom-built small-scale spray dryer (**Figure 5.2**). Feed solution of avagacestat or avagacestat and HPMC-AS containing 2.5% solid were sprayed at 65 – 70 ºC from acetone using heated nitrogen gas through a two-fluid spraying nozzle (2050 LC/64AC, spraying Systems Co.). The resulting amorphous material was then collected by filtration from the spray dryer and dried in vacuo overnight. ASDs were stored in a fridge (at around +5 ºC) to prevent API recrystallisation.

Neat amorphous API was prepared according to the general procedure reported above using avagacestat (4.0 g, 7.7 mmol) dissolved in acetone (160 mL). The 25 wt % avagacestat in HPMC-AS ASD was prepared from an avagacestat (1.0 g, 1.9 mmol) and HPMC-AS (3.0 g) dissolved in acetone (160 mL) feed solution while the 75 wt % ASD was prepared from an avagacestat (1.9 g, 3.6 mmol) and HPMC-AS (0.7 g) dissolved in acetone (100 mL) solution.

A detailed list of the samples used for the quantification of amorphous/crystalline species ratio is given in **Table 5.3.**

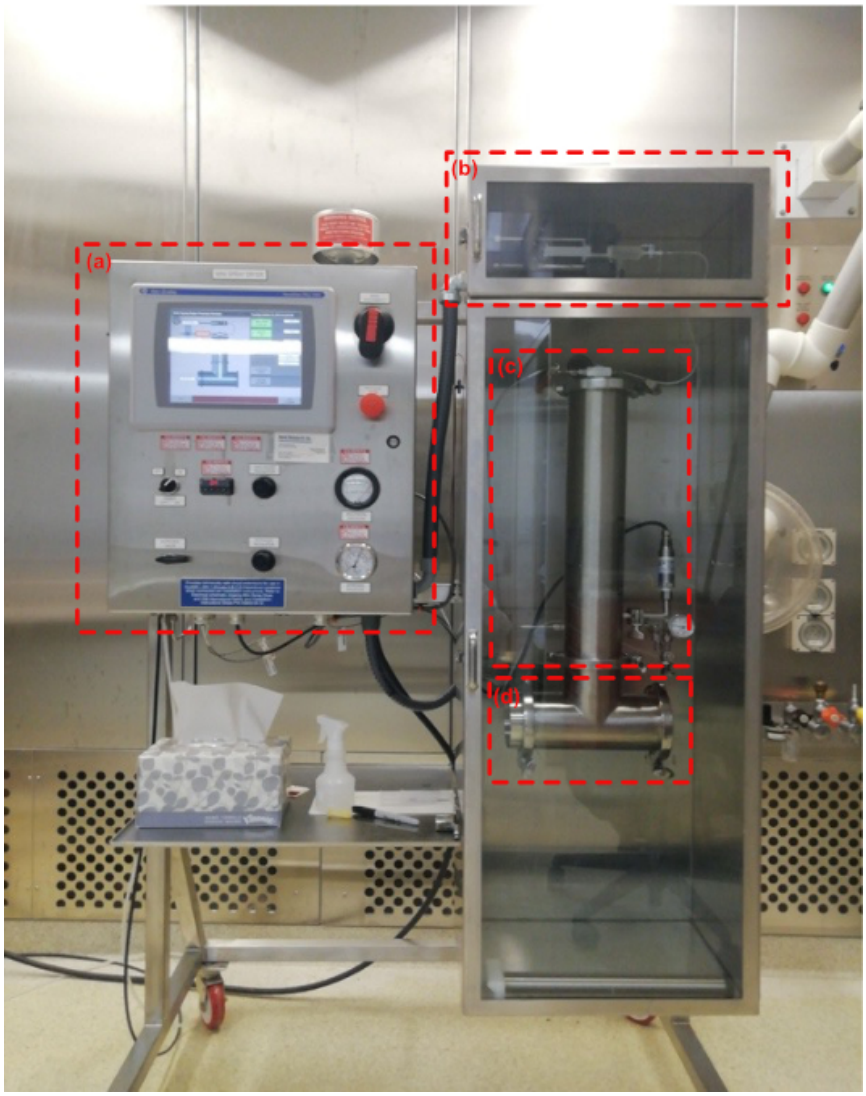

Figure 5.2. Custom-built small-scale spray dryer apparatus. The equipment consists of (a) controller panel, (b) solution feed injects system, and (c) the atomiser column. (d) The final amorphous sample is collected at the bottom of the column.

5.5 Methods

5.5.1 PXRD

Powder X-ray diffraction (PXRD) patterns of spray dried materials were recorded on a Bruker D4 Endeavor/Lynxeye (Bruker, Germany) X-ray powder diffractometer with Cu Kα radiation (λ = 1.541 Å), equipped with a ceramic tube which was set at the power level of 40 kV and 40 mA (1.6 kW), and a position sensitive LynxEye detector. Incident optics consisted of a 0.6° divergence slit. Diffracted optics consisted of a Ni−K−beta filter and a 3° opening on detector window. Data were collected in reflectance geometry, while spinning, over a 2θ range of 2−40°, with a step size of 0.03°, and counting time of 1 s/step in continuous mode.

5.5.2 High filed NMR

Quantitative ^{1}H and ^{19}F direct excitation experiments were conduct using a Bruker 850 MHz (20.0 T) Avance Neo NMR spectrometer equipped with a Bruker 1.3 mm triple-resonance HXY magic angle spinning (MAS) probe (operating in double resonance (DR) mode). H channel was tuned to ^{1}H or ^{19}F at 850.2 and 800.0 MHz, respectively.

^{14}N–^{1}H Heteronuclear multiple quantum coherence (HMQC) experiments were carried out using a Bruker 850 MHz Avance Neo NMR spectrometer equipped with a Bruker 1.3 mm triple-resonance HXY MAS probe operating in DR mode tuned to ^{1}H and ^{14}N at 850.2 and 61.4 MHz, respectively. All the HMQC experiments were performed under a MAS frequency ν_r= 60 kHz. Heteronuclear dipolar couplings were reintroduced via rotary resonance recoupling, R3[33], on the n = 2 resonance condition[34], using an x, −x phase inversion[35] of individual block lengths of one rotor period of 16.7 μs at an radio frequency (rf) amplitude of 120 kHz (2 × MAS frequency). ^{1}H and ^{19}F pulses were performed at rf amplitude of 100 kHz, while a rf amplitude of 42 kHz was applied for ^{14}N pulse. ^{1}H and ^{19}F spectra were externally referenced to the NH proton of the β-AspAla dipeptide at 8.0 ppm[36], and polyvinylidene difluoride to the main amorphous peak at -92 ppm[37], respectively while ^{14}N shift were referred to solid $NHCl_4$ at -341.3 ppm[38], which has a cubic ^{14}N site.[39]

5.5.3 Time Domain NMR

^{19}F spin-lattice relaxation time T_1s were measured using a 20 MHz permanent magnet (0.47 T) bench-top TD NMR minispec mq20-Series Bruker spectrometer. The magnetic field of the magnet was kept constant by controlling the magnet temperature at 40 ± 0.01 ºC, equipped with a 3 cm prototype ^{19}F probe. For the analysis, 2 cm of samples (in height) were putted in 1 cm wide NMR tube coaxial to a 3 cm diameter NMR tube to fit the probe. T_1 data were extrapolated from saturation recovery pulse experiments fitting the raw dataset with a stretch exponential function as in **Equation 5.1**, where τ is the variable delay and α the stretch factor ranging from 0.6 and 0.9 ^{19}F T_1 fitting data were carried out using MATLAB R2021b.

$$1 - \exp\left[-\left(\frac{\tau}{T_1}\right)^{\alpha}\right] \qquad \textbf{Eq. 5.1}$$

5.5.4 qSRC Method via Bruker FormCheck application

To quantify fraction of component (c_n) in the mixture of n solid components, the Bruker Form Check application uses the SRC. In a mixture of n solid components, the corresponding SRC can be considered as the linear combination of the individual SRCs of each component (SRC_i^{pure}), according to **Equation 5.2 i**n which c_i is proportional to the fraction of the component i in the mixture and b is an offset for experimental imperfections.

$$SRC = \sum_{i=1}^{n} c_1 \cdot SRC_i^{pure} + b \qquad \textbf{Eq. 5.2}$$

However, the term SRC_i^{pure} cannot be used as it is into Eq. 5.2, as it depends on several instruments settings and amount of sample, hence it is necessary to normalise them by the respective masses (m_i), and to make the measurement instrument-independent by the instrument response per mole of observed nuclei X (S_0), as **Equation5.3**. (In this work X = ^{19}F).

$$SRC_i^{norm} = \frac{SRC_i}{m_i \cdot S_0} \qquad \textbf{Eq. 5.3}$$

Any residual instrument influences from the SRC curves can be removed use the intensity of the curve at the plateau (S_i) (achieved at the $\tau > 5 \cdot T_1$), that can be expressed as a function of the number of moles of the observable X nuclei: $S_i = n_X \cdot S_0$ (**Equation 5.4**).

$$SRC_i^{norm} = \frac{SRC_i \cdot n_X}{m_i \cdot S_i} \qquad \textbf{Eq. 5.4}$$

Finally, from the definition of mole, the sample mass m_i can be expressed as a function of moles of the molecule n_i and that the ratio molecular mass M_i **Eq. 5.4** can be rewritten as the following:

$$SRC_i^{norm} = \frac{SRC_i}{m_i \cdot S_i} \frac{N_X}{M_i} \qquad \textbf{Eq 5.5}$$

SRCs were recorded with 128 scans per recovery increment, 24 logarithmically distributed recovery points raging from 0 to 15 s. Each SRC dataset have been fitted with a monoexponentially curve allowing the determination of the ^{19}F T_1 vale for each samples.

qSRC data processing, analysis have been carried out with minispec Form Check by Bruker Dynamic Center software.

5.6 Results and Discussions

5.6.1 PXRD characterisation

The amorphous behaviour of the fresh prepared sample has been probed by PXRD. **Figure 5.3** shown the PXRD pattern of the amorphous avagacestat (black), 25 (red) and 75 wt % (violet) avagecestat HPMC-AS ASDs. All the patterns exhibit the typical broad signal of amorphous materials with no sign of Bragg peaks from crystalline avagacestat.

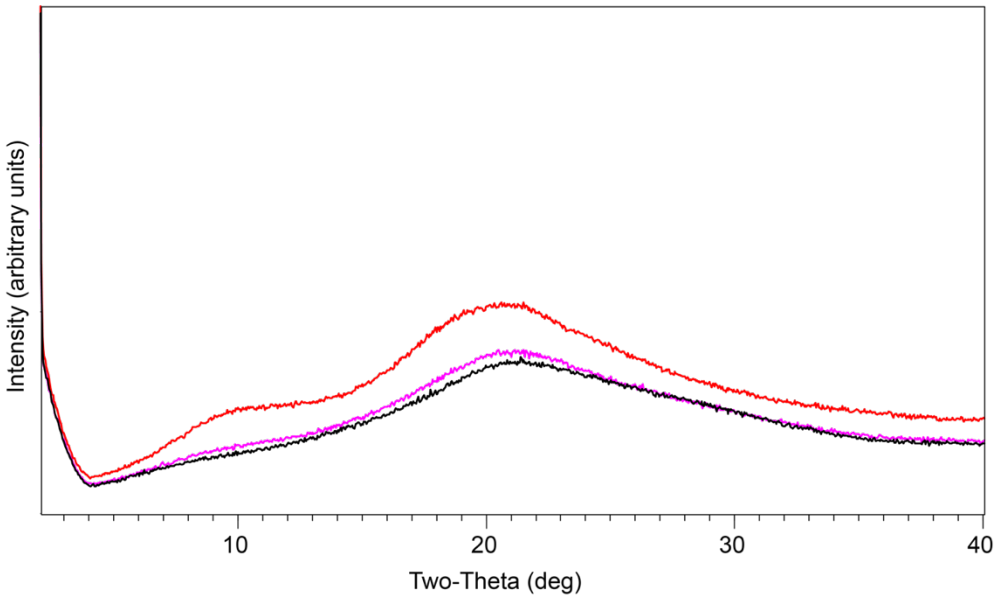

Figure 5.3. PXRD of patterns of net amorphous avagacestat (black), 25 (red) and 75 wt % (violet) avagecestat HPMC-AS ASDs.

5.6.2 High field NMR characterization

Figures 5.4 shows the 1D ^{19}F and ^{1}H NMR spectra of the crystalline avagacestat and of the 25 wt. % avagacestat ASD. As expected, the ^{19}F spectrum of the crystalline API clearly exhibits two fluorine environments. The signals at -66 and -118 ppm that can be attributed to the aliphatic CF_3 and aromatic CF atoms, respectively. The particular shape of the CF peak can be either due to a dynamic disorder in the aryl ring or due to a small conformational change in aryl fluorine atom.[29] Two broad peaks are founded in the ^{19}F spectrum of the 25 wt. % ASD. (FWHM of CF_3 and CF are ~8800 Hz and ~2400 HZ, respectively). The ^{1}H spectrum of crystalline avagacestat (**Figure 5.4(b)**, blue) shows fairly resolved resonances at 7.6, 6.8, 4.0, 2.0, and 0.7 ppm tentatively assigned to aromatic protons, H_b, H_c, H_m, and H_l, respectively. In the HPMC-AS polymer spectrum (**Figure 5.4(b)**, green), three main peaks and a peak at 1.1 ppm that can be assigned to H_1, $H_{2,3,5,10}$, $H_{16,17}$ and $H_{11,14}$, respectively, while spectral deconvolution reveals addition signals at 3.9, 3.0, and 2.5 ppm attributable to $H_{6,9}$, H_8, and H_4, respectively. H_7 and H_{12} signals are not detectable in the spectrum reasonably due to possible exchange phenomena.[40] Finally, the spectrum of the 25 wt % ASD (**Figure 5.4(b)**, red) show a cluster of signals in the 5 – 1 ppm region resulting from the overlapping of the polymer protons backbone with the protons of the API. The peak at around 8 ppm could be tentatively the proton aromatic signals of the API in the ASD.

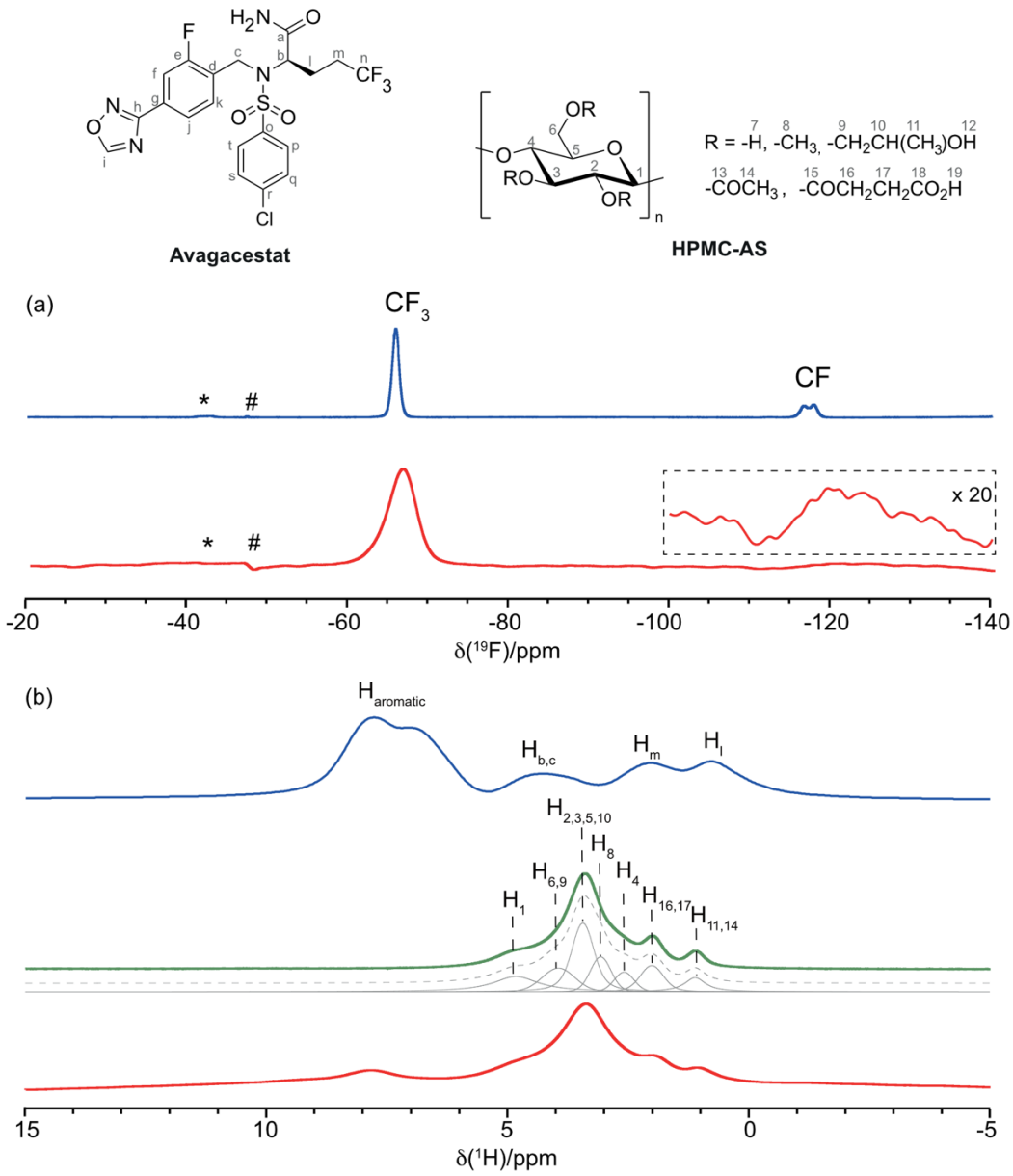

Figure 5.4. Quantitative (a) ^{19}F and (b) ^{1}H spectra of crystalline avagacestat (in blue), and 25 wt % avagacestat-HPMC-AS ASD (in red), recorded at 20.0 T under MAS condition of 60 kHz. ^{1}H HPMC-AS spectrum is given in green with, for spectral identification, simulated spectrum (dashed gray line) and spectral deconvolution (gray lines) are given. The insert shows a magnified view (x 20) of the spectrum from - 100 to -140 ppm. Asterisks (*) and the symbol (#) denote spinning sidebands and instrumental artifact, respectively. Avagacestat and HPMC-AS chemical structures are given on top.

As reported in the literature, the stability of the 25 wt. % ASD could be due to the presence of hydrogen bond (H-bond) between the avagacestat and HPMC-AS as reveled by ^{19}F-^{13}C HETCOR experiments.[29] Detailed information regarding API-API and API-polymer inter and/or intramolecular interactions in ASDs can be achieved from HMQC experiments. The ^{14}N-^{1}H HMQC spectra of the crystalline API and 25 wt. % ASD recorded at a recoupling time of 133.6 μs (8 rotor periods) are given in **Figure 5.5**. The spectroscopic data for the crystalline API (in **panel (a)**) shows a correlation between the avagacestat amide ^{14}N spectra with the CH_2 group (H_m) adjacent to the CF_3 of the API, suggesting a contact between the amide and the CF_3 groups. We note that this spectrum was recorded at a short recoupling time, generally indicating a close contact between those groups hence. Therefore, the correlation founded in this spectrum could reasonably suggests an intramolecular contact between H_m and the API's CF_3 or, alternatively, an intermolecular contact between the same group. One of these hypotheses could be confirmed by further investigations, such HMQC experiments carried out at different longer recoupling times. The 2D spectrum for the 25 wt. % ASD (**Figure 5.5(b)**) shows the presence of correlation between the avagacestat ^{14}N aromatic signal with the -OCH_3 (H_8) of the polymer at 3 ppm, indicating intermolecular interaction between the ^{14}N atoms of the API's oxadiazol moiety with the polymer. This exciting result is added to the previously highlighted H-bond identified between the CO's polymer groups and API's NH_2[29], providing a further important input for understanding the stability of this formulation.

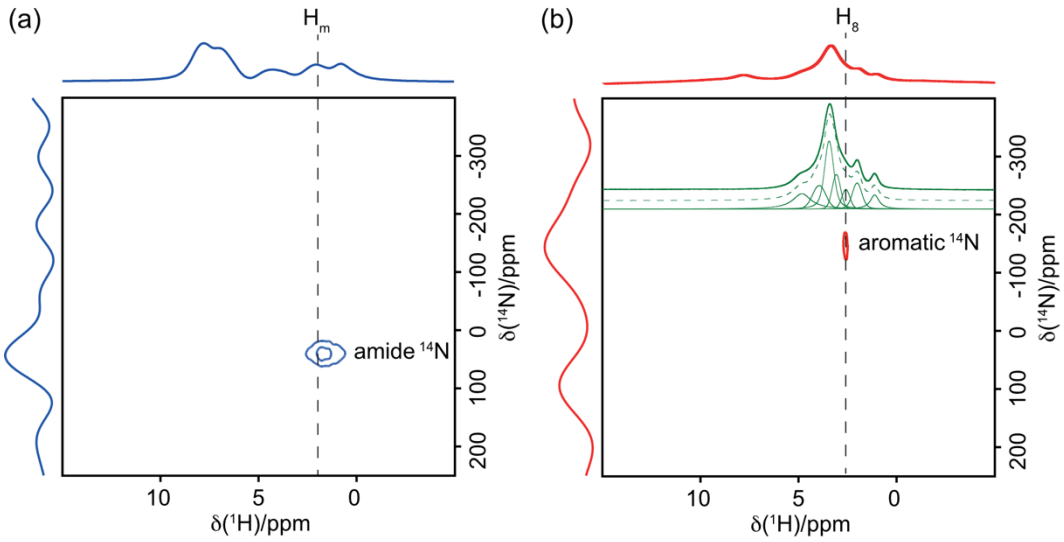

Figure 5.5. ^{14}N-^{1}H HMQC spectra of (a) crystalline avagacestat and (b) 25 wt % avagacestat HPMC-AS ASD (in red). The spectra of the deconvoluted ^{1}H spectrum of the polymer is given in green[6] (simulated spectra, and spectral deconvolution are in dashed green line and light green lines, respectively). Spectra on the left of the HMQC are the ^{14}N slices extracted at the indicated ^{1}H chemical shift in dashed black lines.

5.6.3 Relaxation measurement by TD NMR

Figure 5.6 shows the ^{19}F SRCs for the neat amorphous API (black circle), crystalline API (blue square), 25 wt. % (red circle) and 75 wt. % ASDs (magenta diamond). The ^{19}F T_1 results obtained clearly indicate that amorphous vs. crystalline species can be distinguish by the TD NMR technique. In particular, as expected, the crystalline API presents longer T_1 value with respect the amorphous samples, and the values of crystalline and amorphous species differ by a factor of approximatively 3.

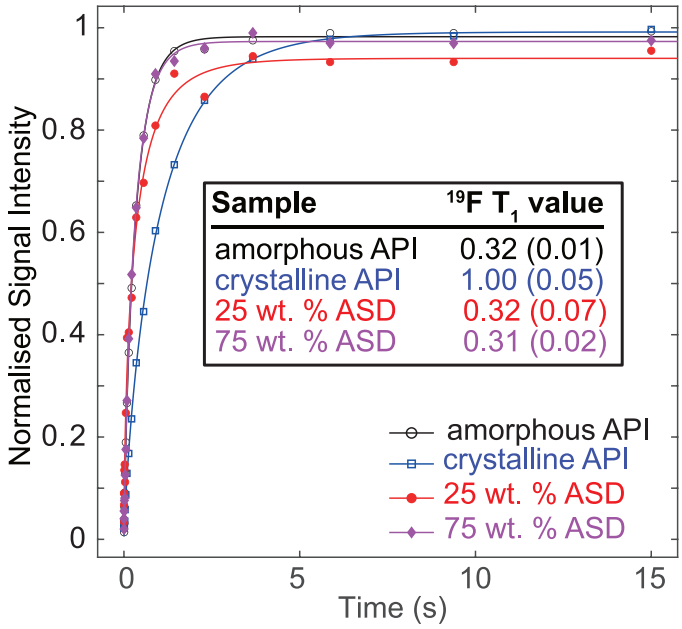

Figure 5.6. Raw ^{19}F SRCs recorded by TD NMR for neat amorphous and crystalline API (black and blue, respectively), 25 wt. % ASD (red) and 75 wt. % ASD (magenta). The best fit for each SRC dataset is reported (continue lines). Inset: ^{19}F T_1 values for the amorphous and crystalline API, 25 wt. % and 75 wt. % ASD obtained from the fit of the raw ^{19}F SRCs dataset. Values are given in seconds. The number in parenthesis indicate the standard error associated with the fit.

5.6.5 Crystalline/amorphous specie ratio quantification by FormCheck

The FormCheck method permits the quantification of the fraction in wt. % of components in the mixture of n solid components by recording the SRC of the mixture (SRCmix) and then compared it with the SRC of the single components, as the SRCmix can be considered as the linear combination of the individual SRCs of each component. In the context of this work, the quantification of the amorphous/crystalline specie ratio in the binary mixture have been obtained by measuring the SRC curves of the mixture, amorphous component, c_1, and crystalline component, c_2, used as reference (ref. pair) to quantify the ratio of c_1:c_2

in the mixture. The value of c_1:c_2 were extrapolated by the SRC curve recorded for the mixture (SRCmix) as it results to be the linear combination of the c_1 and c_2 SRCs (**Figure 5.7**).

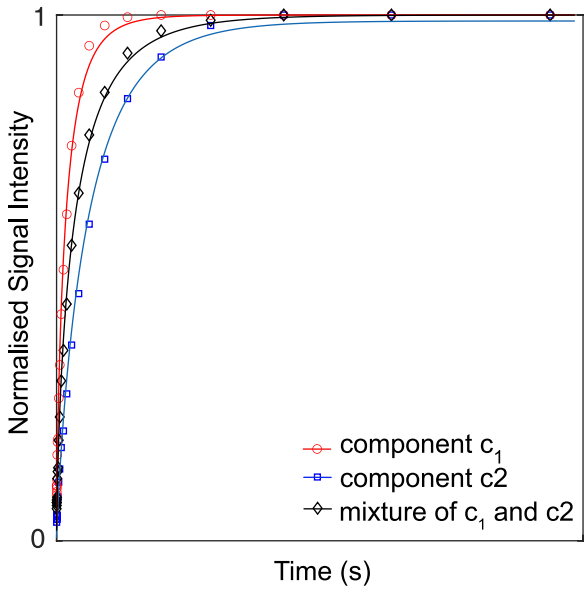

Figure 5.7. SRCs of a hypothetical 2-component system. The SRCs for the amorphous (c_1) and crystalline (c_2) components used in the reference mixture are label with a (o) and a (□), respectively. Continue lines represent the best fit for the respective data set and allow the estimation of T_1 for each components. The diamond black (◊) trace represents a 0.5:0.5 mixture of c_1 and c_2 components. The SRCmix can be represented as a linear combination of the component SRCs.

Hence, to proceed with the quantification of mixture of crystalline-amorphous species, a range of SRCs of pair of single components that could be used as reference mixture to build up calibration curve for the quantification have been recorded. The list of the reference sample we prepared and mixed to make ref. pairs is reported in **Table 5.1**. The choice of amorphous and crystalline components for the ref. pairs 1 and 2 were taken in order to simulate systems in which some API has recrystallised from the amorphous dispersions. While the use of amorphous API and crystalline API as amorphous and crystalline components, respectively in ref. pair 3 bring to a reference system to test the methodology in identify the API in its two different possible state, ref. pairs 4 and 5 were made to

pick out ASDs from physical mixtures (PMs). The raw ^{19}F SRCs obtained for c_1 and c_2 for each ref. pairs are reported in **Figure 5.8.** All the datasets of SRC were fitted with a monoexponentially curve allowing the determination of the ^{19}F T_1 vale for each sample, summarised in **Table 5.1**. The values obtained clearly show that there is a significative difference between the relaxation behavior for crystalline and amorphous species.

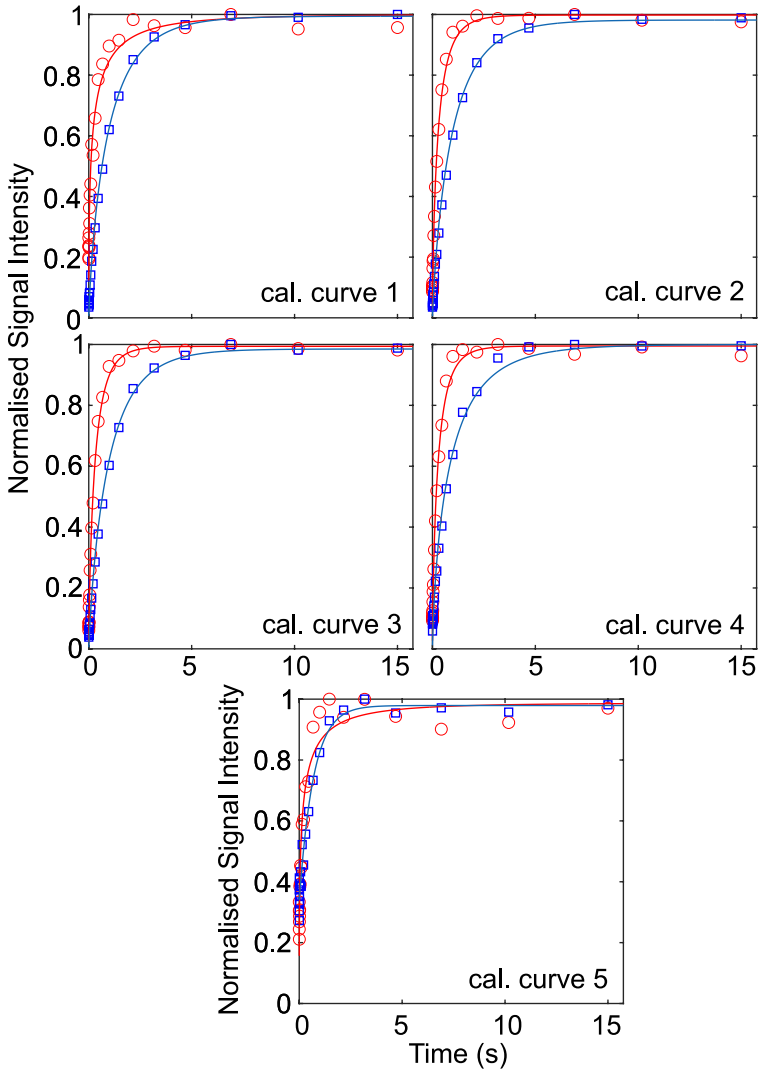

Figure 5.8. The all five ref. pairs that have been recorded to allow the quantification of amorphous/crystalline specie in binary mixtures. Every ref. pair consists of a couple of ^{19}F SRCs, one for each of the two components c_1 and c_2 present in the sample. SRC of the amorphous component, c_1, is identify by a circle (o), while the SRC of crystalline, c_2, is highlighted by a square (□). Continue lines are the best fit for the dataset.

Table 5.1. List of the amorphous (c_1) and crystalline (c_2) components used as ref. pair., and ^{19}F T_1 values for c_1 and c_2.

Ref. pair	c_1, amorphous component	c_2, crystalline component	c_1, ^{19}F T_1 value[a]	c_2, ^{19}F T_1 value[a]
1	25 wt. % ASD	Crystalline API	0.23 (0.10)	1.06 (0.10)
2	75 wt. % ASD	Crystalline API	0.30 (0.04)	1.10 (0.11)
3	Amorphous API	Crystalline API	0.32 (0.03)	1.08 (0.11)
4	75 wt. % ASD	75:25 wt. % physical mixture of crystalline API:HPMC-AS	0.29 (0.05)	1.00 (0.20)
5	25 wt. % ASD	25:75 wt. % physical mixture of crystalline API:HPMC-AS	0.16 (0.10)	0.70 (0.13)

[a] Values come from the best fitting curve of the relative dataset and are given in seconds. The number in parenthesis indicate the standard error associated with the fit.

Table 5.2. Composition of the binary mixtures prepared, and the c1:c2 ratio of the different components, and ^{19}F T_1 values for each mixtures.

Mixture	c1, amorphous component	c2, crystalline component	c1:c2 wt. % ratio in the sample	^{19}F T_1 value[a]
A	25 wt. % ASD	25:75 wt. % physical mixture of crystalline API:HMPC-AS	50:50	0.38 (0.25)
B	Amorphous API	Crystalline API	50:50	0.51 (0.27)
C	75 wt. % ASD	75: 25 wt. % physical mixture of crystalline API:HMPC-AS	50:50	0.39 (0.19)
D	HPMC-AS	Crystalline API	75:25	0.99 (0.20)
E	HPMC-AS	Crystalline API	25:75	0.75 (0.24)
F	25 wt. % ASD	None	100:0	0.21 (0.08)
G	75 wt. % ASD	none	100:0	0.30 (0.04)

[a] Values come from the best fitting curve of the relative dataset and are given in s. The number in parenthesis indicate the standard error associated with the fit.

Finally, binary mixtures of amorphous and crystalline components were prepared at different c_1:c_2 ratio as listed **Table 5.2**. The ^{19}F T_1 values for each mixture were extracted by the fit of the relative SRC dataset.

Table 5.3 lists the results that have been carried out from the ^{19}F qSRC quantification using the FormCheck application, and compare the expected c_1:c_2 ratio, based on the nominal composition, while **Figure 5.9** graphically shows the SRCs obtained for the mixture and compared with the SRCs of the ref. pairs components.

The components of mixtures A, B and C were specifically chosen so that they could be analysed using the ref. pairs 5, 4 and 3, respectively. Excellent quantification results are expected from the FormCheck methodology, when the components of the calibration curve are the same as the components of the mixture being analysed. Indeed, the experimental c_1:c_2 ratio quantification for mixture A *vs*. ref. pair 5, B *vs*. ref. pair 3 and C *vs* ref. pair 4, totally match the expected ratio (**Table 5.3** and **Figure 5.9(a), (b), and (c)**), also demonstrating that the system can distinguish between PM and amorphous dispersion (A *vs*. 5, and C *vs*. 4). The successful quantifications of the components ratio in mixture A and C using ref. pairs 5 and 4 represent an interesting result, indicating that the FormCheck method can be applied to quantify amount of recrystallised API from ASD.

On the contrary, the quantification of the ratio between c_1 and c_2 in mixtures A, C and E using the ref. pairs 1 and 2 failed (results highlighted in red in **Table 5.3** and **Figure 5.9(d)**, **(e)**, and **(g)**). This is not surprising and indeed support the assumptions that the method does not work when the reference components do not match the mixture's components or when the components are intimately interconnected by the presence of chemical interactions.[28] (**Table 5.2**).

Very interestingly, accurate experimentally estimation in the sample F and G have been achieved when analysed using ref. pairs 1 and 2, respectively, despite no crystalline components are present in the mixture. This could indicate that the qSRC methodology can be successfully applied directly on amorphous sample itself, without the need to prepare complex mixture, making it easy to use this technique as a well implemented production line routine investigation method for checking the state of recrystallisation from ASDs (**Figure 5.9(g**) and **(h)**).

Because of the components of the mixture D are different from the components of the ref. pair 4, it would be expected that the quantification of the components of its mixture through the ref. pair 4 failed. Instead, surprisingly, the FormCheck method bring to results similar to those expected (**Table 5.3**). This unexpected output is difficult to explain and could be due to errors during sample preparation (less likely) or software problems (**Figure 5.9(i)**). Confirmation regarding this result could come from further investigations, by performing quantification analyses c_1: c_2 ratio, for example involving the mixture E vs. ref. pair 5.

Table 5.3. Expected and experimental ^{19}F qSRC results obtained from the FormCheck application.[a]

Experiment	Expected c_1:c_2	Experimental c_1:c_2 quantification
A vs. 5	0.5:0.5	0.55 (0.22):0.45 (0.20)
B vs. 3	0.5:0.5	0.56 (0.09):0.44 (0.10)
C vs. 4	0.5:0.5	0.56 (0.06):0.44 (0.07)
A vs. 1	0.5:0.5	0.73 (0.13):0.27 (0.11) [b]
C vs. 2	0.5:0.5	0.61 (0.10):0.39 (0.10) [b]
E vs. 1	0.0:1.0	0.46 (0.20):0.54 (0.18) [b]
F vs. 1	1.0:0.0	1.00 (0.11):0.0 (0.10)
G vs. 2	1.0:0.0	0.99 (0.03):0.01 (0.03)
D vs. 4	0.0:1.0	0.04 (0.03):0.96 (0.03)

[a] The number in parenthesis indicate the standard error associated with the fit.

[b] Experimental results in disagreement with the expected c_1:c_2 ratio are given in red.

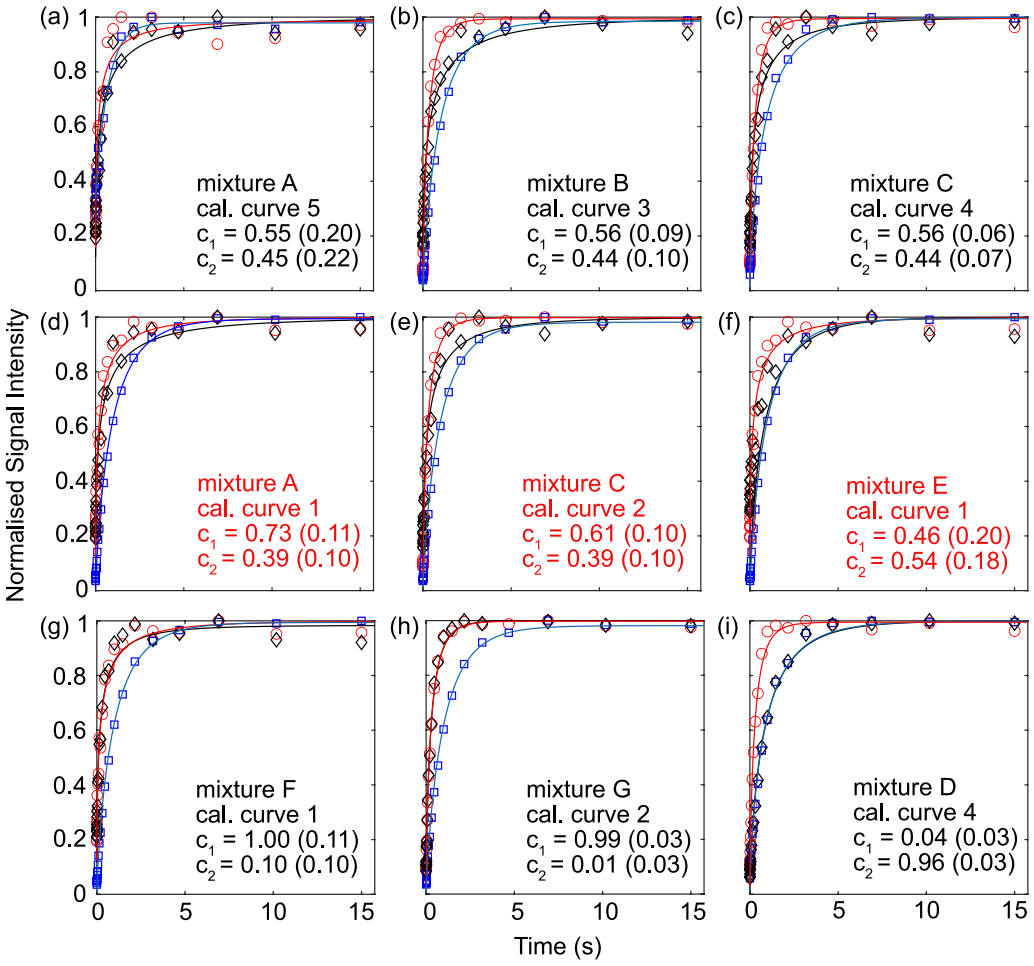

Figure 5.9. FormCheck analysis results reported as SRCmix vs SRCs of the references components used in the ref. pair. The datapoints of the SRCs for the amorphous, c_1, and crystalline, c_2, components are labelled respectively with a (o) and a (□), while the datapoints of the SCR for the mixture (SRCmix) are highlighted by diamonds. Continue lines are the best fit for each datapoints. The experimental values obtained from the FormCheck methods are also reported, and the results in disagreement with the expected ones are highlighted in red.

5.6 Conclusions

Here, we tested the ability of the emerging FormCheck method to determine the composition of binary mixtures composed of crystalline and amorphous components of pharmaceutical interest. The specific mixtures designed and prepared for this purpose have led to interesting results that allow to judge the goodness of this method. The FormCheck method is based on the measurement of the SRCs of the components of a reference mixture which are then compared with the SRC of a mixture (SRCmix) of which one wants to measure the unknown ratio between the constituent components, as the SRCmix results to be the linear combination of the SRCs of the component in the reference sample. From the experiments carried out, it emerged that the best quantitative measurements occur when either the components of the reference mixture exactly match the components of the mixture under analysis, or interestingly, even using a single reference component. On the contrary, the method fails when the components nature of the reference mixture does not coincide with those of the mixture under analysis. Considering the results obtained, the FormCheck method can be used effectively for quick and easy analyses in the pharmaceutical industry, to determine the presence, for example, of crystalline species in ASD, providing useful information to monitor ASD phase separation phenomena with relative formation of crystalline API, and therefore giving evidence on the stability of the formulation.

5.7 Reference

[1] Newman, A., *Pharmaceutical Amorphous Solid Dispersions*. Wiley, Hobken, New Jersey, USA: **2015**.

[2] Baghel, S.; Cathcart, H.; O'Reilly, N. J. *J .Pharm. Sci.* **2016**, *105*, 2527.

[3] Laws, D. D.; Bitter, H. L.; Jerschow, A. *Angew. Chem. Int. Ed*. **2002**, *41*, 3096.

[4] Duer, M., *Introduction to Solid-State NMR Spectroscopy*. Blackwell Publishing, Oxford, England: **2005**.

[5] Reif, B.; Ashbrook, S. E.; Emsley, L.; Hong, M. *Nat. Rev. Methods Primers* **2021**, *1*, 1.

[6] Pugliese, A.; Toresco, M.; McNamara, D.; Iuga, D.; Abraham, A.; Tobyn, M.; Hawarden, L. E.; Blanc, F. *Mol. Pharmaceutics* **2021**, *18*, 3519.

[7] Chen, H.; Pui, Y.; Liu, C.; Chen, Z.; Su, C. C.; Hageman, M.; Hussain, M.; Haskell, R.; Stefanski, K.; Foster, K.; Gudmundsson, O.; Qian, F. *J. Pharm. Sci.* **2018**, *107*, 317.

[8] Li, N.; Cape, J. L.; Mankani, B. R.; Zemlyanov, D. Y.; Shepard, K. B.; Morgen, M. M.; Taylor, L. S. *Mol. Pharmaceutics* 2020, *17*, 4004.

[9] Rumondor, A. C.; Wikstrom, H.; Van Eerdenbrugh, B.; Taylor, L. S. *AAPS PharmSciTech* **2011**, *12*, 1209.

[10] Liu, B.; Theil, F.; Lehmkemper, K.; Gessner, D.; Li, Y.; van Lishaut, H. *Mol. Pharmaceutics* **2021**, *18*, 2428.

[11] Qian, F.; Huang, J.; Zhu, Q.; Haddadin, R.; Gawel, J.; Garmise, R.; Hussain, M. *Int. J. Pharm.* **2010**, *395*, 232.

[12] Van Eerdenbrugh, B.; Lo, M.; Kjoller, K.; Marcott, C.; Taylor, L. S. *J. Pharm. Sci*. **2012**, *101*, 2066.

[13] Qi, S.; Moffat, J. G.; Yang, Z. *Mol Pharmaceutics* **2013**, *10*, 918.

[14] Purohit, H. S.; Taylor, L. S. *Mol. Pharmaceutics* **2015**, *12*, 4542.

[15] Li, N.; Taylor, L. S. *Mol. Pharmaceutics* **2016**, *13*, 1123.

[16] Li, N.; Gilpin, C. J.; Taylor, L. S. *Mol. Pharmaceutics* **2017**, *14*, 1691.

[17] Li, N.; Taylor, L. S. *Mol. Pharmaceutics* **2019**, *16*, 1751.

[18] Paudel, A.; Geppi, M.; Van den Mooter, G. *J. Pharm. Sci.* **2014**, *103*, 2635.

[19] Yuan, X.; Sperger, D.; Munson, E. J. *Mol. Pharmaceutics* **2014**, *11*, 329.

[20] Yuan, X.; Xiang, T. X.; Anderson, B. D.; Munson, E. J. *Mol. Pharmaceutics* **2015**, *12*, 4518.

[21] Calahan, J. L.; Azali, S. C.; Munson, E. J.; Nagapudi, K. *Mol. Pharmaceutics* **2015**, *12*, 4115.

[22] Sarpal, K.; Delaney, S.; Zhang, G. G. Z.; Munson, E. J. *Mol. Pharmaceutics* **2019**, *16*, 4836.

[23] Sarpal, K.; Tower, C. W.; Munson, E. J. *Mol. Pharmaceutics* **2020**, *17*, 787.

[24] Sarpal, K.; Munson, E. J. *J. Pharm. Sci*. **2021**, *110*, 145.

[25] Aso, Y.; Yoshioka, S.; Miyazaki, T.; Kawanishi, T.; Tanaka, K.; Kitamura, S.; Takakura, A.; Hayashi, T.; Muranushi, N. *Chem. Pharm. Bull*. **2007**, *8*, 1227.

[26] Okada, K.; Hirai, D.; Hayashi, Y.; Kumada, S.; Kosugi, A.; Onuki, Y. *Chem*. *Pharm. Bull*. **2019**, *67*, 265.

[27] Okada, K.; Hirai, D.; Kumada, S.; Kosugi, A.; Hayashi, Y.; Onuki, Y. *J. Pharm. Sci.* **2019**, *108*, 451.

[28] Stueber, D.; Jehle, S. *J. Pharm. Sci.* **2017**, *106*, 1828.

[29] Abraham, A.; Crull, G. *Mol. Pharmaceutics* **2014**, *11*, 3754.

[30] Wu, X.; Burns, S. T.; Zilm, K. W. *J. Magn. Reson., Ser. A* **1994**, *111*, 29.

[31] Starrett, J. E., Jr.; Gillman, K. W.; Olson, R. E. *Patent Application* 2009/0111858 A1, **2009**.

[32] Gillman, K. W.; Starrett, J. E., Jr.; Parker, M. F.; Xie, K.; Bronson, J. J.; Marcin, L. R.; McElhone, K. E.; Bergstrom, C. P.; Mate, R. A.; Williams, R.; Meredith, J.

E., Jr.; Burton, C. R.; Barten, D. M.; Toyn, J. H.; Roberts, S. B.; Lentz, K. A.; Houston, J. G.; Zaczek, R.; Albright, C. F.; Decicco, C. P.; Macor, J. E.; Olson, R. E. *ACS Med*. *Chem. Lett.* **2010**, *1*, 120.

[33] Oas, T. G.; Griffin, R. G.; Levitt, M. H. *J. Chem. Phys*. **1988**, *89*, 692.

[34] Gan, Z.; Amoureux, J. P.; Trébosc, *Chem. Phys. Lett.* **2007**, 435, 163.

[35] Costa, P. R.; Gross, J. D.; Hong, M.; Griffin, R. G. *Chem. Phys. Lett.* **1997**, *280*, 95.

[36] Tatton, A. S.; Bradley, J. P.; Iuga, D.; Brown, S. P. *Z. Phys. Chem.* **2012**, *226*, 1187.

[37] Ando, S.; Harris, R. K.; Reinsberg, S. A. *Magn. Reson. Chem*. **2002**, *40*, 97.

[38] Bertani, P.; Raya, J.; Bechinger, B. *Solid State Nucl. Magn. Reson*. **2014**, 61, 15.

[39] Jakobsen, H. J.; Hove, A. R.; Hazell, R. G.; Bildsoe, H.; Skibsted, *J. Magn. Reson. Chem*. **2006**, *44*, 348.

[40] Pugliese, A.; Hawarden, L. E.; Abraham, A.; Tobyn, M.; Blanc, F. *Magn. Reson. Chem*. **2020**, *58*, 1036.

Chapter 6: Conclusions and Further work

6.1 General conclusions

Within this thesis, the research presented in the previous chapters, solid-state NMR has proven to be a powerful and useful technique for studying the properties of solid pharmaceutical forms, and that it can be a widely usable toolkit in the pharmaceutical field.

Importantly, solid-state NMR technique is a nondestructive investigation method involving solids without any sample preparation procedure (e.g., dissolution in solvent). This allows for atomic-level information directly in the solid state and is a great advantage for samples such as ASDs. In fact, the dissolution of an ASD in solvent could destabilise the sample or alter API-polymer interactions.

In **Chapter 3,** it has been reported the structural elucidation of different grades of HPMC-AS polymer containing different A/S ratio as well as the ^{13}C NMR spectra assignment of its precursors, refined the previous published spectra assignments. The work was carried out using ^{13}C CP MAS NMR and ^{13}C-edited spectra. Moreover, this approach allowed to quantify the molar ratio of the A and S moieties of the polymer, complementing the method based on liquid chromatography widely used in the field.

The results reported here, allow the precise knowledge of ^{13}C chemical shifts as a function of structure and chemical environment in the polymer. This is of paramount importance and allows spatial interactions between this polymer and APIs to be detected and understood in ASDs.

In **Chapter 4** we focused on the detection of API-polymer interactions using NMR. It was demonstrated within this thesis, the role played by the polymer in effectively stabilise amorphous APIs in ASDs. This stabilisation mechanism is essentially based on inhibiting or slowing down the API recrystallisation process and can occur through the formation of specific API-polymer interactions. In some case, the understanding of these interactions still represents a challenge.

In the context of our research, NMR techniques have been applied on acetaminophen-HPMC-AS ASDs at different drug loadings (10, 20, and 40 wt. %) to identify the presence (or not) of acetaminophen-HPMC-AS interactions.

The comparison of API, polymer and some ASDs 1D ^{13}C and ^{15}N CP MAS NMR spectra showed the presence of chemical shift difference among this NMR data. This evidence can be rationalised by the occurrence of API-polymer interactions in the ASDs. ^{13}C CP HETCOR exploiting strong $^{13}C-^{1}H$ dipolar coupling highlighted spatial interaction between the acetaminophen's aromatic protons with the polymer for ASDs at drug loadings < 20 wt. %. This interaction was further unequivocally confirmed by $^{14}N-^{1}H$ HMQC experiments that identify H-bond interactions between the NH of acetaminophen and the -OCH_3 proton of the HPMC-AS methyl substituent. On the contrary, no acetaminophen−HPMC-AS interactions were found in the 40 wt % dispersion.

Finally, the versatility of the NMR methodology also at low magnetic field were demonstrated in **Chapter 5**. During this work it was tested the ability of an emerging method (FormCheck) that allow the quantification of the ratio of the components of binary mixture. Using a TD NMR spectrometer, this quantification is carried out by the measurement of the SRCs of the components of a reference mixture which are then compared with the SRC of a mixture (SRCmix), as the SRCmix results to be the linear combination of the SRCs of the component in the reference sample.

We judged the applicability of this method by design specific mixtures of amorphous and crystalline specie of pharmaceutical interest. The encouraging results obtained confirm the applicability of the FormCheck technique, and it emerged that the best quantitative measurements occurred when either the components of the reference mixture exactly matched the components of the mixture under analysis, or interestingly, even using a single reference component. This TD NMR based quantification methods is then a useful toolkit to determine the presence of crystalline species in ASD, providing useful information to monitor ASD phase separation phenomena with relative formation of crystalline API, and therefore giving evidence on the stability of the formulation.

6.2 Further work

To further expand on the research described here, it should move in the direction of the application of NMR on increasingly sophisticated methodologies that allow to enhance the sensitivity of the NMR technique, the real weakness of this technique in some cases. Indeed, a significant increase in sensitivity, would lead to a shorter acquisition time and extend the range of application of NMR in pharmaceutical research.

A method that shows an improved sensitivity compared to traditional NMR is the dynamic nuclear polarisation (DNP) technique. Some pioneerings works have already explored the applicability of the DNP in the study of API, excipients, and formulations, opening to new potential exciting adventure in the pharmaceutical field. [1,2]

In the context of this thesis, the research reported in **Chapters 3** and **4** would benefit from the use of the DNP technique. Useful information on the structural characterization of the polymer, and of the identification of the presence of API-polymer interactions would benefit from the increase in sensitivity that DNP represents, with the advantage also of a dramatic reduction of the acquisition time.

6.3 References

[1] Ni, Q. Z.; Yang, F.; Can, T. V.; Sergeyev, I. V.; D'Addio, S. M.; Jawla, S. K.; Li, Y.; Lipert, M. P.; Xu, W.; Williamson, R. T.; Leone, A.; Griffin, R. G.; Su, Y. *J. Phys. Chem. B* **2017**, *121,* 8132-8141.

[2] Zhao, L.; Pinon, A. C.; Emsley, L.; Rossini, A. J. *Magn. Reson. Chem.* **2018**, *56,* 583-609.